Particle Physics Instrumentation

Werner Riegler, CERN, werner.riegler@cern.ch

2013 CERN-Latin American School of High-Energy Physics: CLASHEP 2013
from 6-19 March 2013, Arequipa, Peru

Lecture3/3
Calorimetry, Particle ID,
Trigger, DAQ

Calorimetry

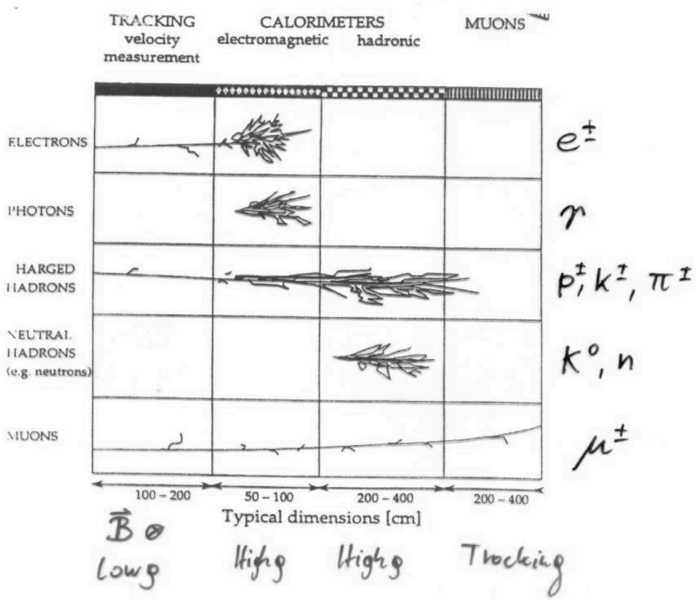

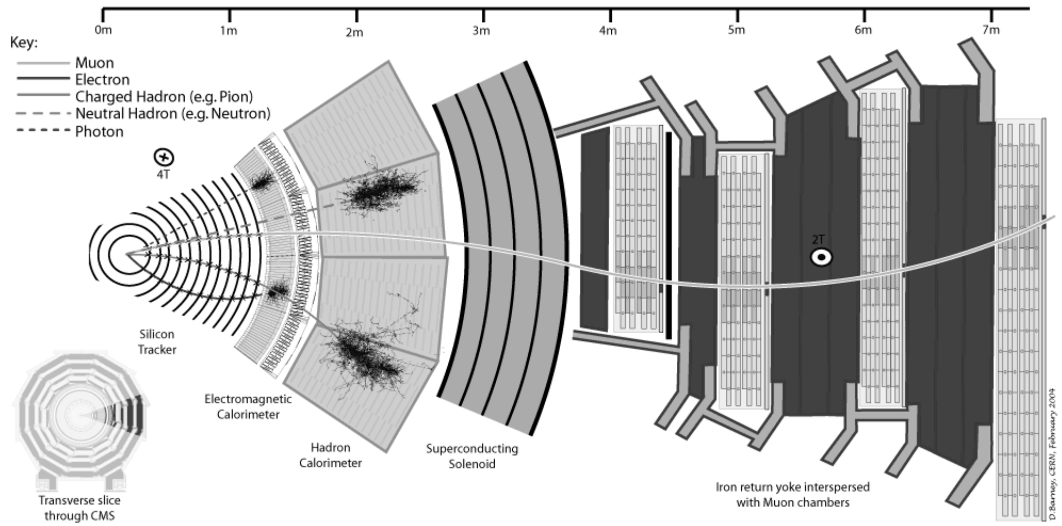

Bremsstrahlung

A charged particle of mass M and charge $q=Z_1e$ is deflected by a nucleus of charge Ze (which is partially 'shielded' by the electrons). During this deflection the charge is 'accelerated' and it therefore radiates → Bremsstrahlung.

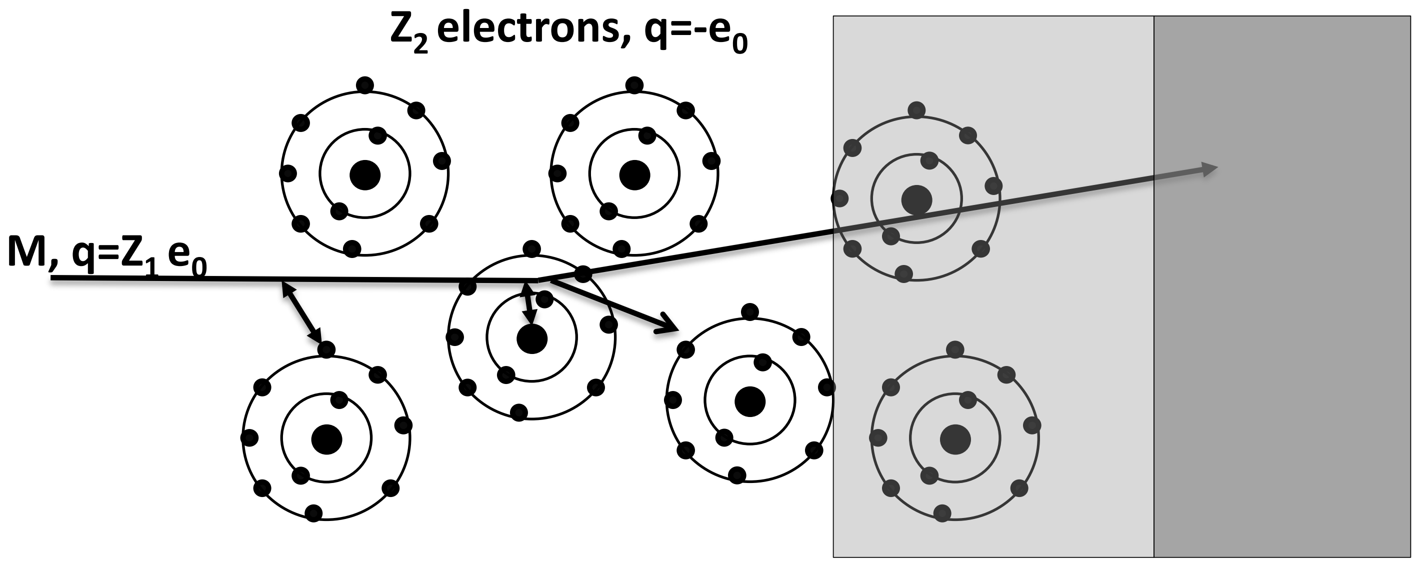

Bremsstrahlung + Pair Production → EM Shower

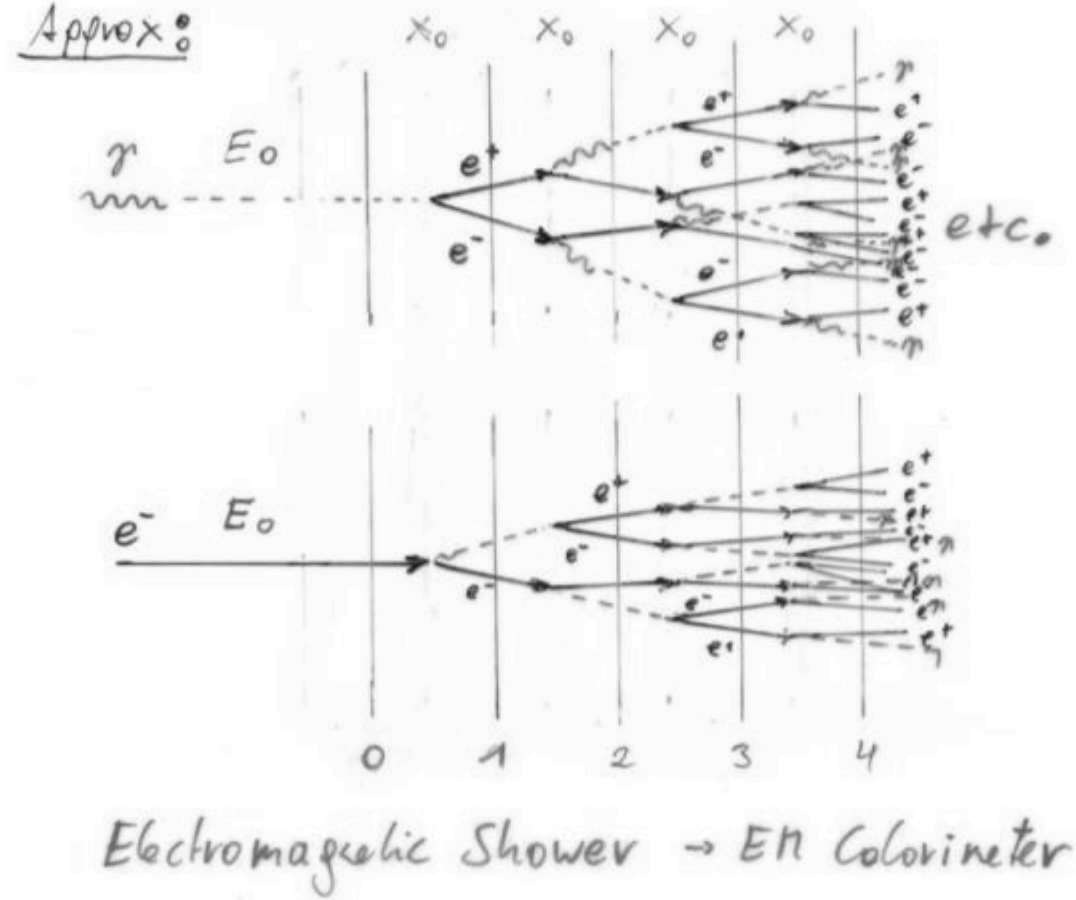

Electro-Magnetic Shower of High Energy Electrons and Photons

$N(n) = 2^n$ ..... Number of particles $(e^\pm, \gamma)$ after $n X_0$

$E(n) = \frac{E_0}{2^n}$ .... Average Energy of particles after $n X_0$

Shower stops if $E(n) = E_{critical}$

$\rightarrow n_{max} = \frac{1}{\ln 2} \ln \frac{E_0}{E_c}$ $\rightarrow$ Shower length rises with $\ln E_0$

Number of $e^\pm$ track segments (of length X_0) after $n X_0$:

$$N_{tr}(n) = 2^n$$

Total $e^\pm$ track length (after $n_{max} X_0$)

$$L = \sum_{n=0}^{n_{max}} 2^n X_0 = \left(2 \frac{E_0}{E_c} - 1\right) X_0 \sim 2 \frac{E_0}{E_c} X_0 = c_1 \cdot E_0$$

Total (charged) track length is proportional to the Energy of the Particle.

$\rightarrow$ Calorimeter Principle

Calorimetry: Energy Measurement by total Absorption of Particles

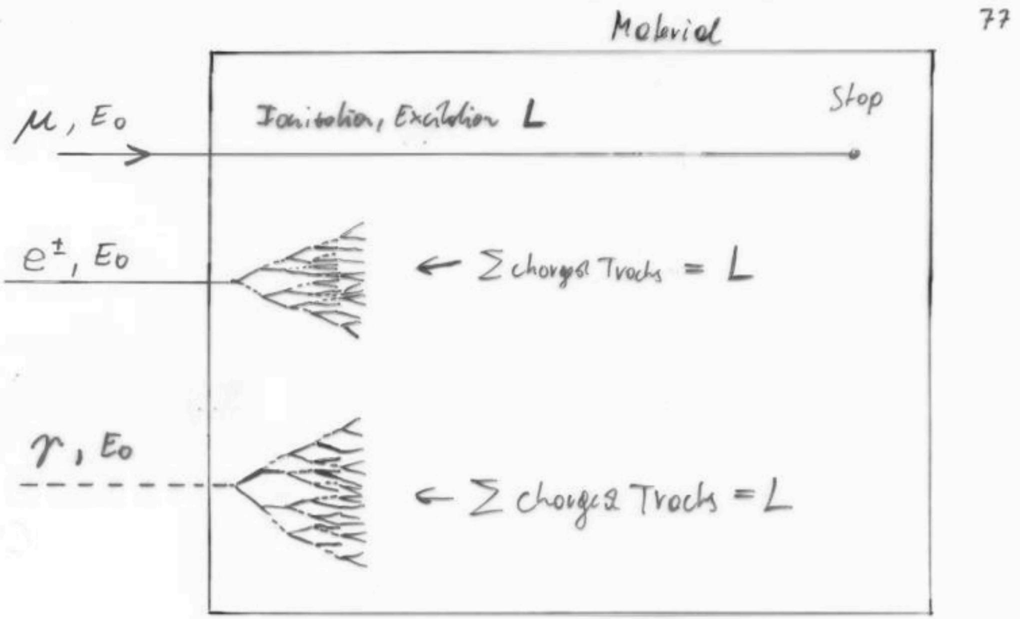

The $e^{\pm}$ in the Calorimeter ionize and excite the Material

Ionization: e^-, I^+ pairs in the Material

Excitation: Photons in the Material

Measuring the total Number of e^-, I^+ pairs or the total Number of Photons gives the particle Energy.

If N is the total Number of e^+, I^+ pairs or photons, or $N = c_1 E_0$:

$\Delta N = \sqrt{N}$ (Poisson Statistics)

$$\frac{\Delta E}{E} = \frac{\Delta N}{N} = \frac{1}{\sqrt{N}} = \frac{a}{\sqrt{E}} \rightarrow \text{Resolution}$$

Only Electrons and High Energy Photons show EM cascades at current GeV-TeV level Energies.

Strongly interacting particles like Pions, Kaons, produce hadonic showers in a similar fashion to the EM cascade →Hadronic calorimetry

Momentum Spectrometer: Δp/p α p

Calorimeter: Δ E/E α 1/ √ E

Energy measurement improves with higher particle energies – LHC !

Calorimetry: Energy Measurement by total Absorption of Particles

The Measurement is destructive. The particle can not be subject to further study.

Energy Measurement by

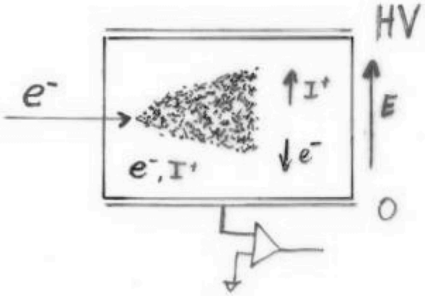

Collecting the produced Charge

Liquid Nobel Gases (Nobel Liquids)

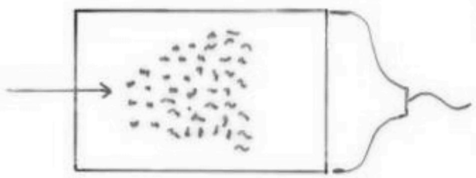

Measuring the Photons produced by the collision of the $e^\pm$ with Atom Electrons of the Material.

Scintillating Crystals, Plastic Scintillators

Total Amount of e^-, I^+ pairs or Photons is proportional to the total track length is proportional to the particle Energy.

Calorimetry

Calorimeters can be classified into:

Electromagnetic Calorimeters,
to measure electrons and photons through their EM interactions.

Hadron Calorimeters,
Used to measure hadrons through their strong and EM interactions.

The construction can be classified into:

Homogeneous Calorimeters,
that are built of only one type of material that performs both tasks, energy degradation and signal generation.

Sampling Calorimeters,
that consist of alternating layers of an absorber, a dense material used to degrade the energy of the incident particle, and an active medium that provides the detectable signal.

C.W. Fabjan and F. Gianotti, Rev. Mod. Phys., Vol. 75, N0. 4, October 2003

EM Calorimetry

Approximate longitudinal shower development

$N(n) = 2^n$ ..... Number of particles ($e^\pm, \gamma$) after $n X_0$

$E(n) = \frac{E_0}{2^n}$ .... Average Energy of particles after $n X_0$

Shower stops if $E(n) = E_{critical}$

$\Rightarrow n_{max} = \frac{1}{\ln 2} \ln \frac{E_0}{E_c}$ → Shower length rises with $\ln E_0$

Radiation Length X_0 and Moliere Radius are two key parameters for choice of calorimeter materials

Approximate transverse shower development

The transverse Shower Dimension is mainly related to the Multiple scattering of the low Energy Electrons.

$$\theta_0 \sim \frac{21\,[\text{MeV}]}{\beta p [\frac{\text{MeV}}{c}]} z_1 \cdot \sqrt{\frac{x}{X_0}}$$

Electrons E_c , $E \sim p \cdot c$

$$\theta_0 \sim \frac{21\,[\text{MeV}]}{\beta E_c [\text{MeV}]} \cdot z_1 \cdot \sqrt{\frac{x}{X_0}} \qquad z_1 = 1, \beta \sim 1$$

$$E_c \sim \frac{610}{Z + 1.24}\,\text{MeV} \sim \frac{610}{Z}\,\text{MeV}$$

$$\theta_0 = 0.0344 \cdot Z \cdot \sqrt{\frac{x}{X_0}}$$

Moliere Radius ρ_m = lateral Shower Radius after $1 X_0$:

$$\underline{\underline{\rho_m \approx 0.0344 \cdot Z \cdot X_0}}$$

95% of Energy are in a Cylinder of $2\rho_m$ Radius.

Simulated EM Shower Profiles in $PbWO_4$

Simulation of longitudinal shower profile **Simulation of transverse shower profile**

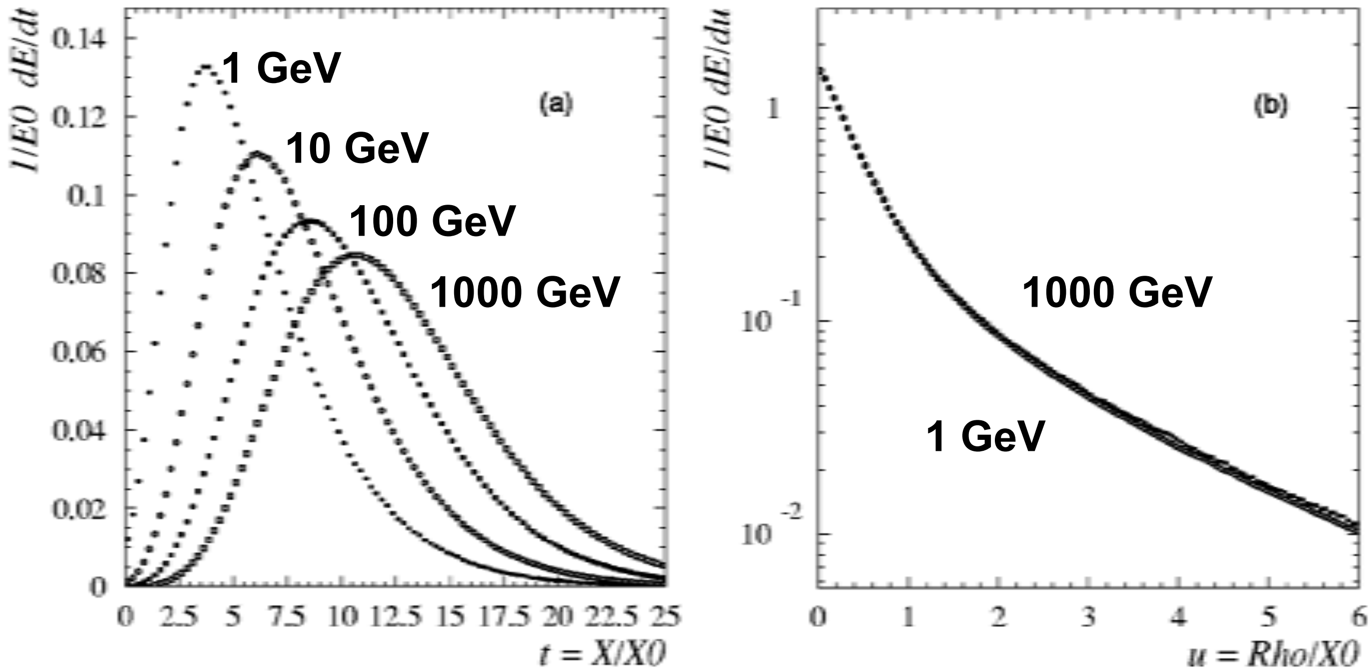

FIG. 2. (a) Simulated shower longitudinal profiles in $PbWO_4$, as a function of the material thickness (expressed in radiation lengths), for incident electrons of energy (from left to right) 1 GeV, 10 GeV, 100 GeV, 1 TeV. (b) Simulated radial shower profiles in $PbWO_4$, as a function of the radial distance from the shower axis (expressed in radiation lengths), for 1 GeV (closed circles) and 1 TeV (open circles) incident electrons. From Maire (2001).

In calorimeters with thickness ~ 25 X_0, the shower leakage beyond the end of the active detector is much less than 1% up to incident electron energies of ~ 300 GeV (LHC energies).

Crystals for Homogeneous EM Calorimetry

In crystals the light emission is related to the crystal structure of the material. Incident charged particles create electron-hole pairs and photons are emitted when electrons return to the valence band.

The incident electron or photon is completely absorbed and the produced amount of light, which is reflected through the transparent crystal, is measured by photomultipliers or solid state photon detectors.

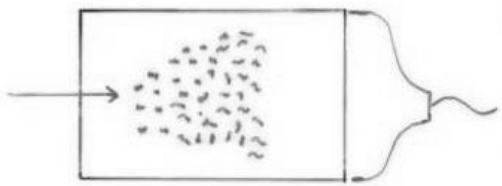

Measuring the Photons
produced by the collision
of the $e^{\pm}$ with Atom Electrons
of the Material.

Crystals for Homogeneous EM Calorimetry

	NaI(Tl)	CsI(Tl)	CsI	BGO	$PbWO_4$
Density (g/cm^3)	3.67	4.53	4.53	7.13	8.28
X_0 (cm)	2.59	1.85	1.85	1.12	0.89
R_M (cm)	4.5	3.8	3.8	2.4	2.2
Decay time (ns)	250	1000	10	300	5
slow component			36		15
Emission peak (nm)	410	565	305	410	440
slow component			480		
Light yield γ/MeV	4×10^4	5×10^4	4×10^4	8×10^3	1.5×10^2
Photoelectron yield (relative to NaI)	1	0.4	0.1	0.15	0.01
Rad. hardness (Gy)	1	10	10^3	1	10^5

Barbar@PEPII, 10ms interaction rate, good light yield, good S/N	**KTeV@Tevatron, High rate, Good resolution**	**L3@LEP, 25us bunch crossing, Low radiation dose**	**CMS@LHC, 25ns bunch crossing, high radiation dose**

Crystals for Homogeneous EM Calorimetry

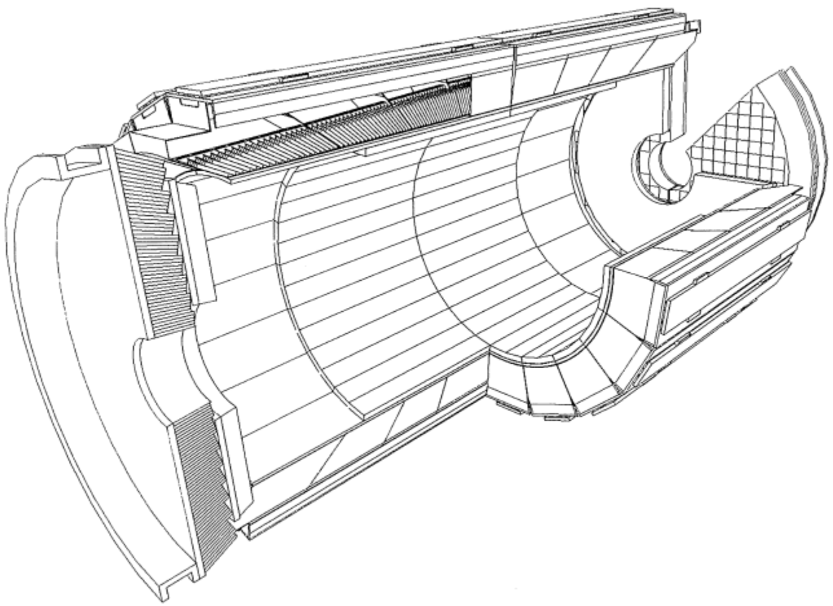

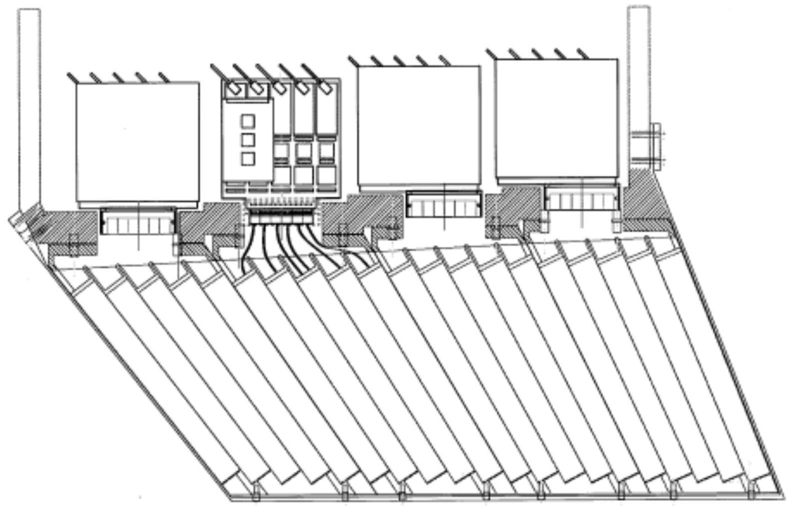

Fig. 2. Longitudinal drawing of module 2, showing the structure and the front-end electronics layout.

Noble Liquids for Homogeneous EM Calorimetry

	Ar	Kr	Xe
Z	18	36	58
A	40	84	131
X_0 (cm)	14	4.7	2.8
R_M (cm)	7.2	4.7	4.2
Density (g/cm^3)	1.4	2.5	3.0
Ionization energy (eV/pair)	23.3	20.5	15.6
Critical energy ϵ (MeV)	41.7	21.5	14.5
Drift velocity at saturation (mm/μs)	10	5	3

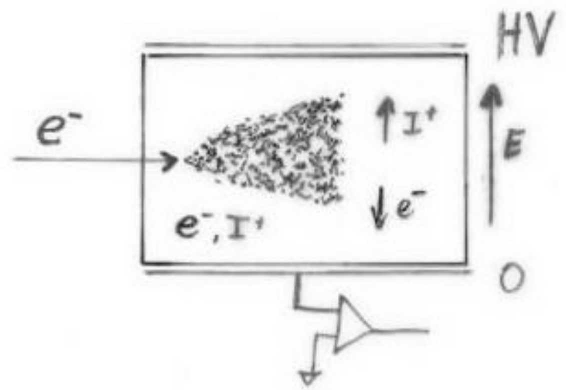

When a charge particle traverses these materials, about half the lost energy is converted into ionization and half into scintillation.

The best energy resolution would obviously be obtained by collecting both the charge and light signal. This is however rarely done because of the technical difficulties to extract light and charge in the same instrument.

Krypton is preferred in homogeneous detectors due to small radiation length and therefore compact detectors. Liquid Argon is frequently used due to low cost and high purity in sampling calorimeters (see later).

Noble Liquids for Homogeneous EM Calorimetry

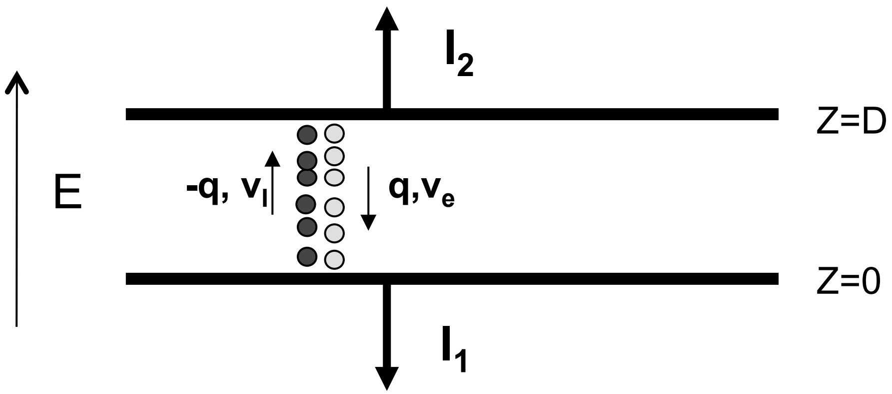

E.g. Liquid Argon, 5mm/ μs at 1kV/cm, 5mm gap →
1 μs for all electrons to reach the electrode.

The ion velocity is 10^3 to 10^5 times smaller →
doesn't contribute to the signal for electronics of
μs integration time.

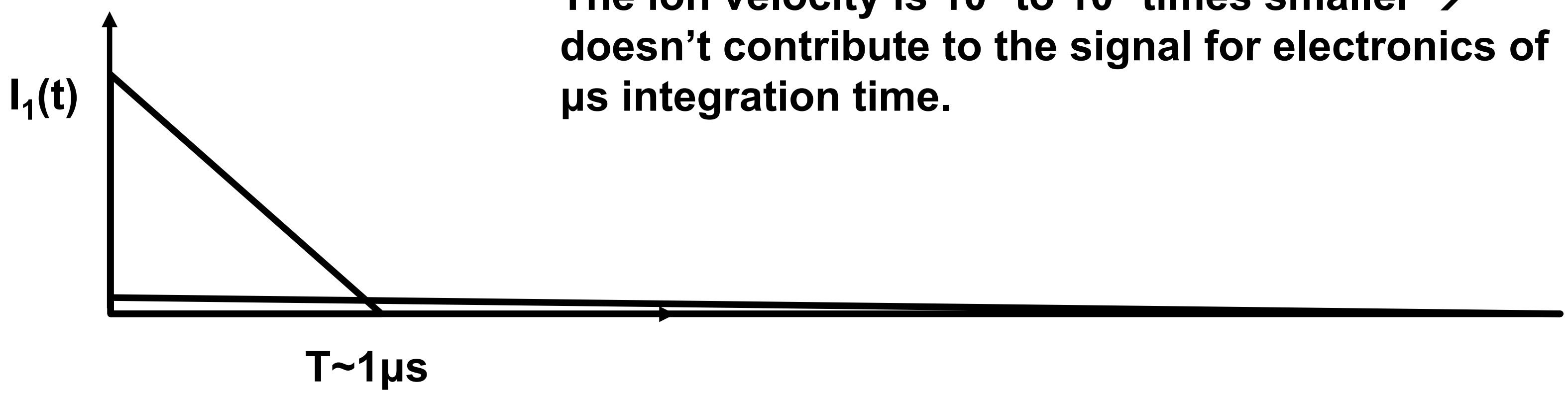

Homogeneous EM Calorimeters, Examples

NA48 Liquid Krypton
2cmx2cm cells
X_0 = 4.7cm
125cm length ($27X_0$)
ρ = 5.5cm

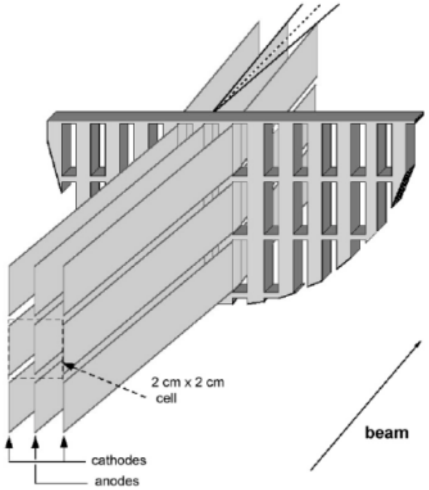

KTeV CsI
5cmx5cm and
X_0 = 1.85cm
2.5cmx2.5cm crystals
50cm length ($27X_0$)
ρ = 3.5cm

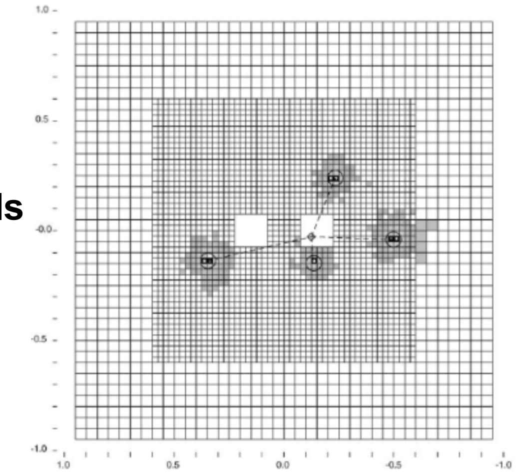

Fig. 1. Schematic of the KTeV CsI Calorimeter showing the cluster energy profiles due to four photons.

NA48 Experiment at CERN and KTeV Experiment at Fermilab, both built for measurement of direct CP violation. Homogenous calorimeters with Liquid Krypton (NA48) and CsI (KTeV). Excellent and very similar resolution.

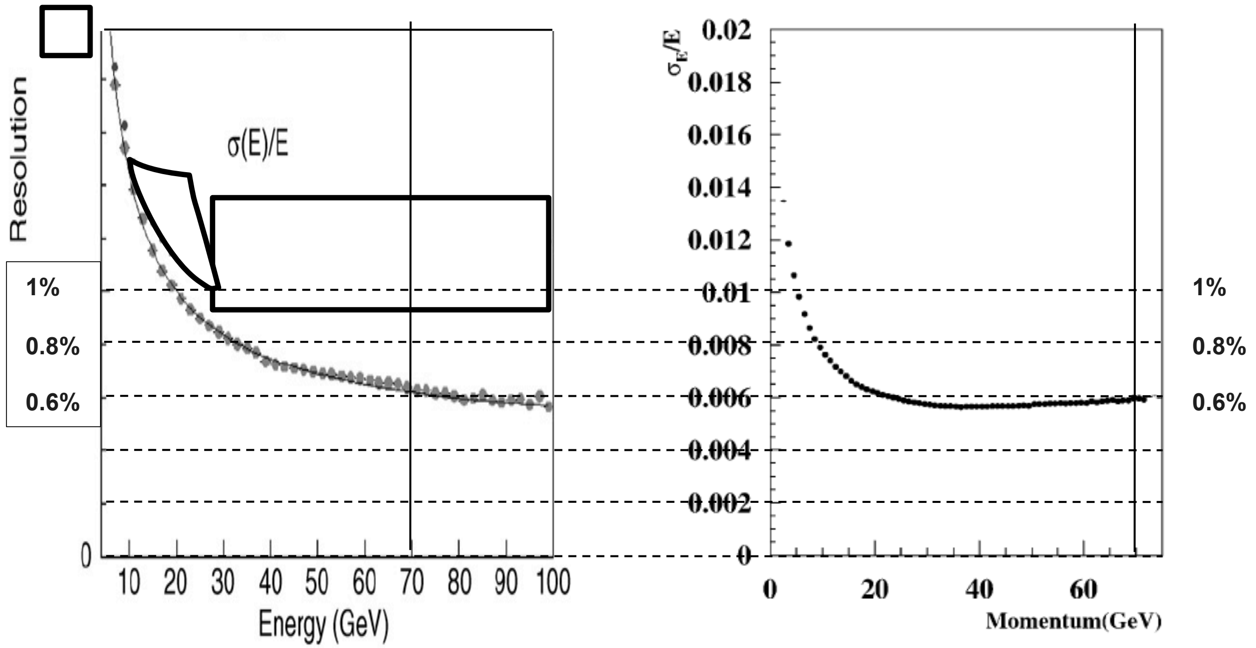

Sampling Calorimeters

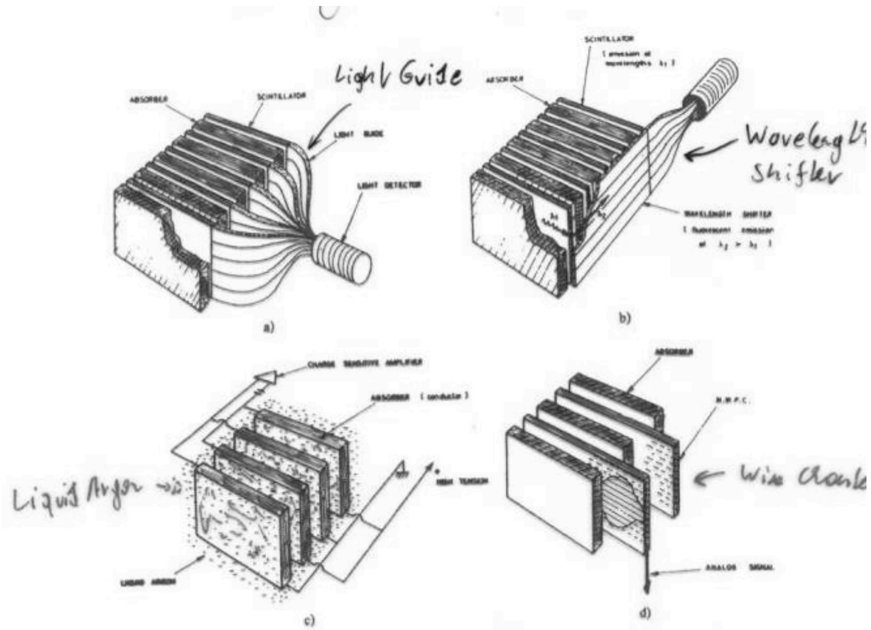

Alternation of "passive" absorber plates and "active" readout sections

Advantage:
- optimum choice of Absorber Material
- optimum choice of Signal Readout
- Compact and cheap Construction

"passive": Pb, Fe ....

"active": Scintillator (Signal -> Photons)
Noble Liquid, e.g. Ar (Signal -> e^-, I^+)
Wire Chambers (Signal -> e^-, I^+)

Energy resolution of sampling calorimeters is in general worse than that of homogeneous calorimeters, owing to the sampling fluctuations – the fluctuation of ratio of energy deposited in the active and passive material.

The resolution is typically in the range 5-20%/Sqrt[E(GeV)] for EM calorimeters. On the other hand they are relatively easy to segment longitudinally and laterally and therefore they usually offer better space resolution and particle identification than homogeneous calorimeters.

The active medium can be scintillators (organic), solid state detectors, gas detectors or liquids.

Sampling Fraction = Energy deposited in Active/Energy deposited in passive material.

Hadronic Calorimetry

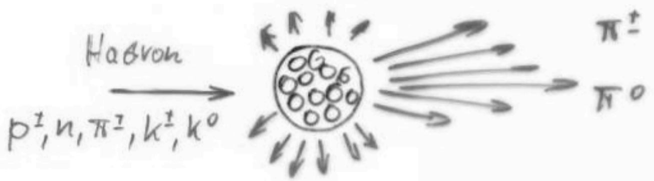

Strong Interaction

Approximate Energy Distribution

~50%	~20%	~30%
π^+, π^- ; $\pi^0 \to \gamma\gamma$	Nuclear Excitation	Slow Nucleons
π^+, π^- ; $\pi^+, \pi^-, \pi^0 \to \gamma\gamma$	5-30 MeV	
Hadron kaskade	p, n, γ	

$\pi^0 \to \gamma\gamma \to$ Electromagnetic Component

In Hadronic Cascades the Longitudinal Shower is given by the Absorption Length λ_a $\quad I \sim e^{-\frac{x}{\lambda_a}}$

In typical Detector Materials λ_a is much larger than X_0

$$\lambda \sim \frac{1}{\rho} \cdot 35\, A^{\frac{1}{3}}$$

	ρ	X_0	λ
Fe	7.87	1.76 cm	~17 cm
Pb	11.35	0.56 cm	~17 cm

Energy Resolution:

- A large Fraction of the Energy 'disappears' into
  - Binding Energy of emitted Nucleons
  - $\pi \to \mu + \nu$ which are not absorbed
- π^0's Decaying into $\gamma\gamma$ start an EM Cascade ($\tau \sim 10^{-16}$ s)

– Energy Resolution is worse than for EM Calorimeters

Hadron Calorimeters are Large because λ is large

Hadron Calorimeters are large and heavy because the hadronic interaction length λ, the 'strong interaction equivalent' to the EM radiation length X_0, is large (5-10 times larger than X_0)

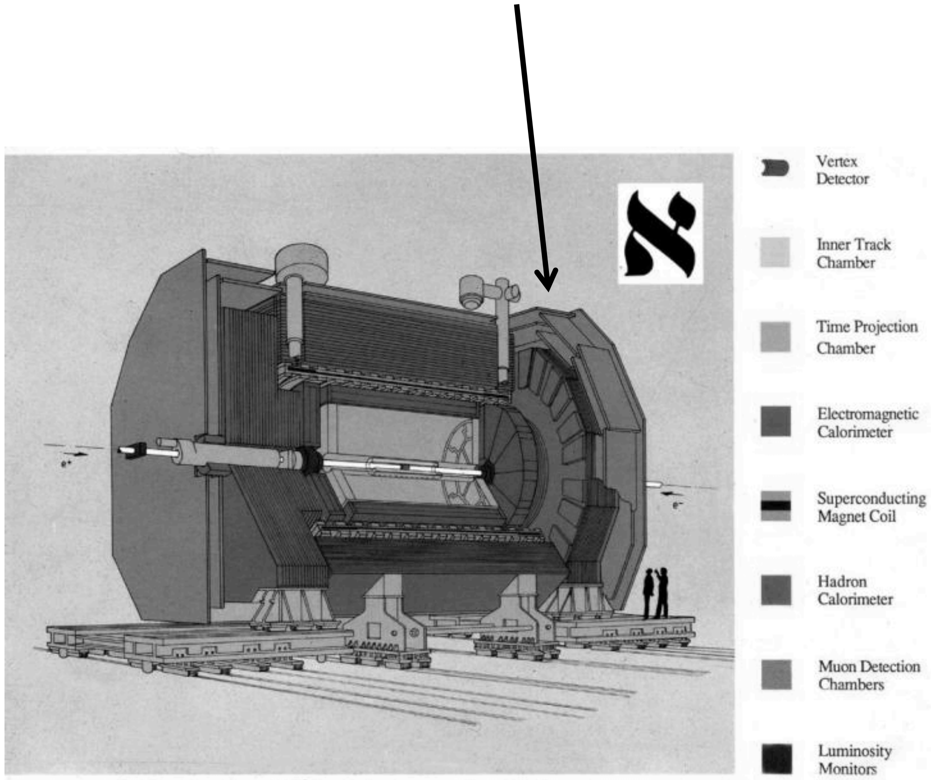

Fig. 1 - The ALEPH Detector

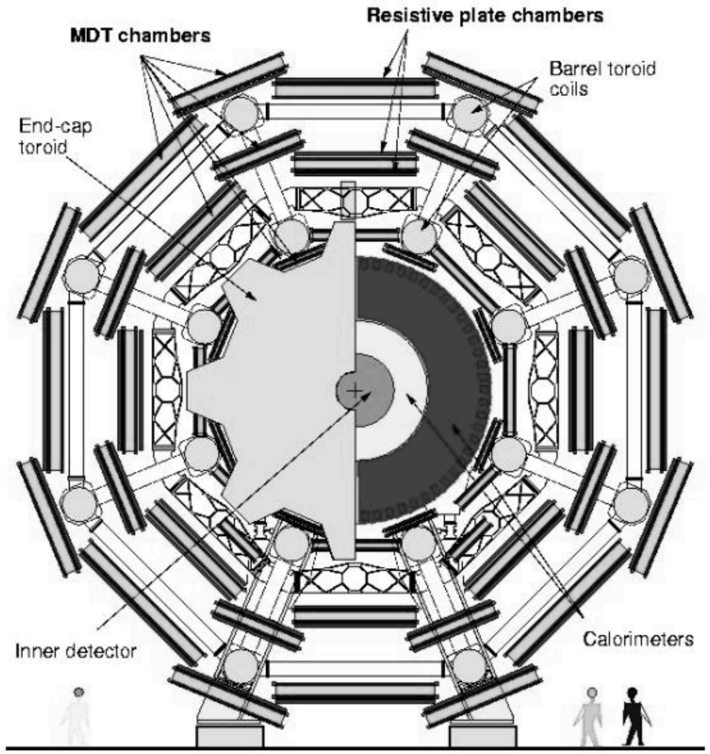

Because part of the energy is 'invisible' (nuclear excitation, slow nucleons), the resolution of hadron calorimeters is typically worse than in EM calorimeters 20-100%/Sqrt[E(GeV)] .

Hadron Calorimeters

By analogy with EM showers, the energy degradation of hadrons proceeds through an increasing number of (mostly) strong interactions with the calorimeter material.

However the complexity of the hadronic and nuclear processes produces a multitude of effects that determine the functioning and the performance of practical instruments, and make hadronic calorimeters more complicated instruments to optimize.

By analogy with EM showers, the energy degradation of hadrons proceeds through an increasing number of (mostly) strong interactions with the calorimeter material.

The hadronic interaction produces two classes of effects:

First, energetic secondary hadrons are produced with a mean free path of λ between interactions. Their momenta are typically a fair fraction of the primary hadron momentum i.e. at the GeV scale.

Second, in hadronic collisions with the material nuclei, a significant part of the primary energy is consumed in nuclear processes such as excitation, nucleon evaporation, spallation etc., resulting in particles with characteristic nuclear energies on the MeV scale.

C.W. Fabjan and F. Gianotti, Rev. Mod. Phys., Vol. 75, N0. 4, October 2003

Because part of the energy is therefore ‘invisible’, the resolution of hadron calorimeters is typically worse than in EM calorimeters 20-100%/Sqrt[E(GeV)] .

Hadron Calorimeters

The signals from an electron or photon entering a hadronic calorimeter is typically larger than the signal from a hadron cascade because the hadroic interactions produce a fair fraction of invisible effects (excitations, neutrons …).

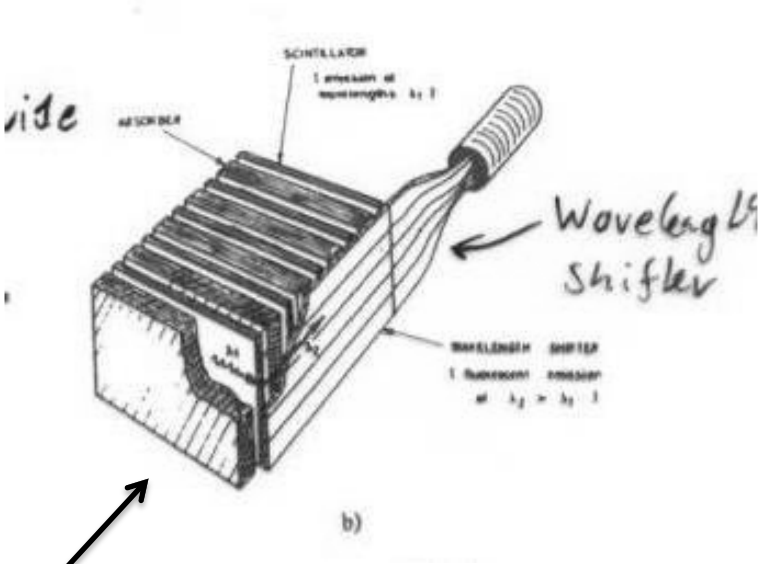

Pion 10GeV

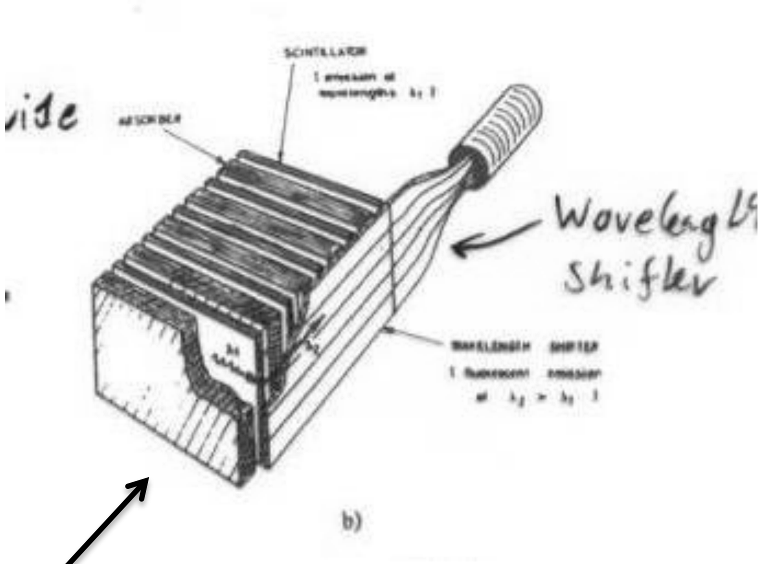

Electron 10GeV

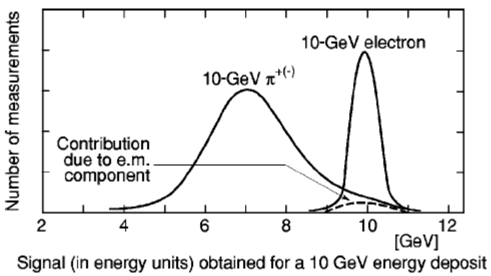

Hadron Calorimeters

Because a fair fraction of shower particles consists of π_0 which instantly decay into two photons, part of the hadronic cascade becomes an EM cascade – ‘and never comes back’.

Because the EM cascade had a larger response than the Hardon cascade, the event/event fluctuation of produced π_0 particles causes a strong degradation of the resolution.

Is it possible to build a calorimeter that has the same response (signal) for a 10GeV electron and 10GeV hadron ? → compensating calorimeters.

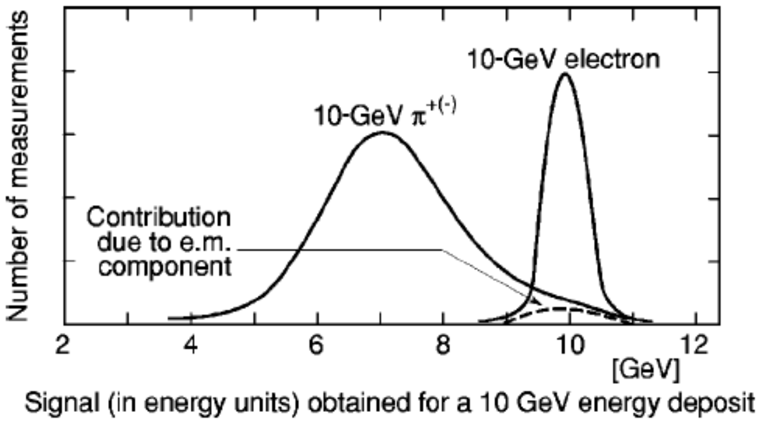

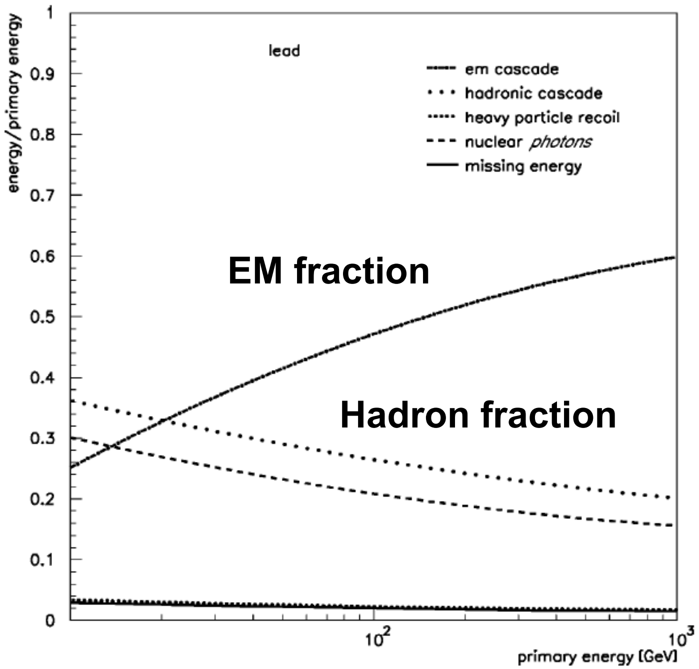

FIG. 21. Characteristic components of proton-initiated cascades in lead. With increasing primary energy the π^0 component increases (Ferrari, 2001).

Compensating Hadron Calorimeters

In a homogeneous calorimeter it is clearly not possible to have the same response for electrons and hadrons.

For sampling calorimeters the sampling frequency and thickness of active and possibe layers can be tunes such that the signal for electrons and hadrons is indeed equal !

Using Uranium or Lead with scintillators, hadron calorimters with excellen energy resolution and linearity have been built.

Energy resolution

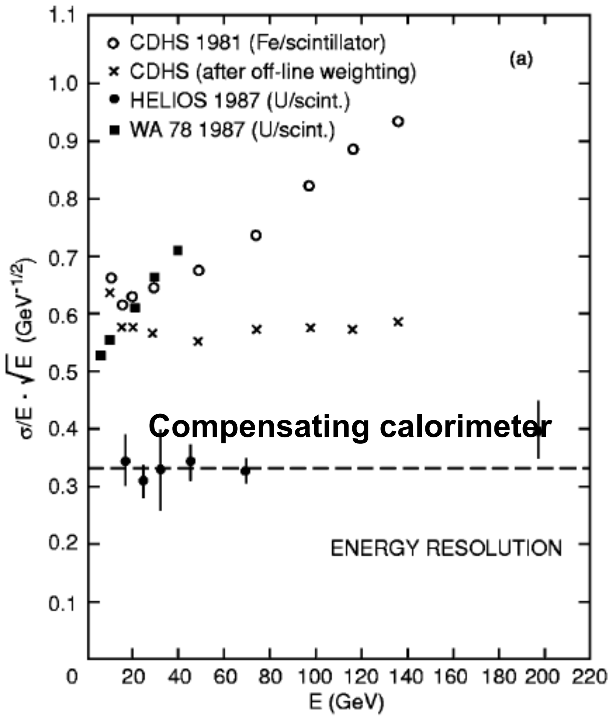

Linearity

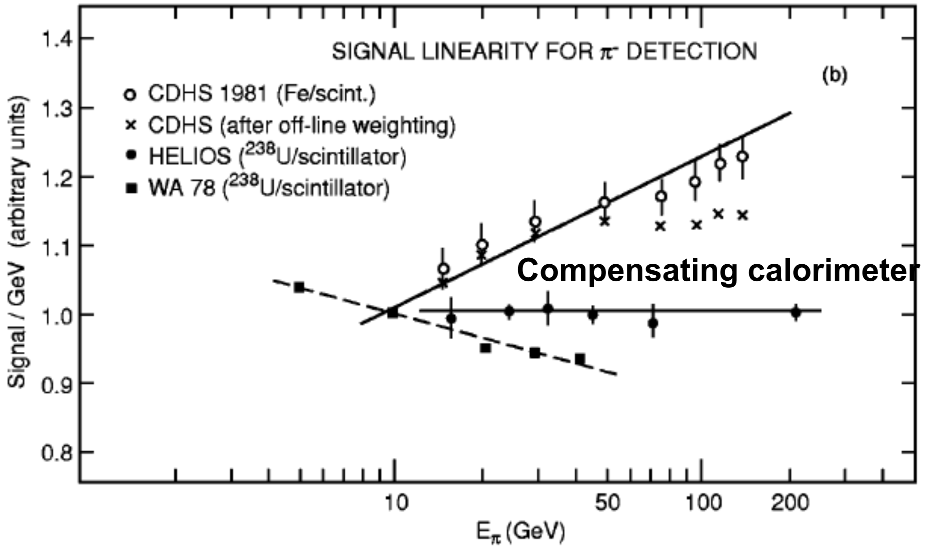

Compensating Hadron Calorimeters

Resolution and linearity of a hadron calorimeter is best if e/h=1. For all other values e/h<>1 the resolution in linearity is worse.

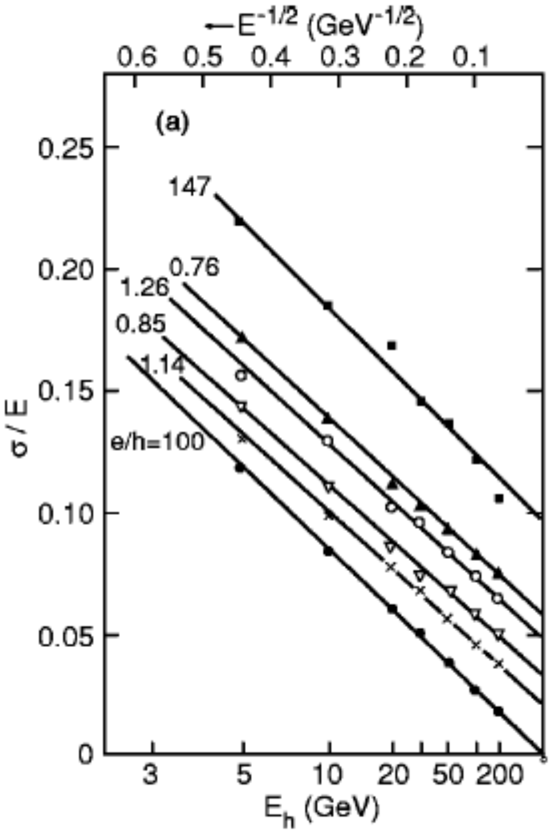

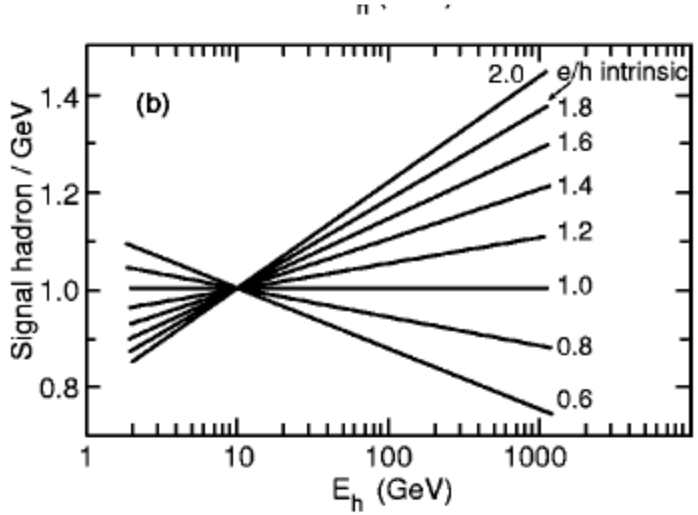

FIG. 24. Monte Carlo simulation of the effects of $e/\pi \neq 1$ on energy resolution (a) and response linearity (b) of hadron calorimeters with various values for e/h (intrinsic), where h (intrinsic) denotes the response to the purely hadronic component of the shower (Wigmans, 1988).

Calorimetry

Calorimeters are attractive in our field for various reasons:

In contrast with magnet spectrometers, in which the momentum resolution deteriorates linearly with the particle momentum, on most cases the calorimeter energy resolution improves as 1/Sqrt(E), where E is the energy of the incident particle. Therefore calorimeters are very well suited for high-energy physics experiments.

In contrast to magnet spectrometers, calorimeters are sensitive to all types of particles, charged and neutral. They can even provide indirect detection of neutrinos and their energy through a measurement of the event missing energy.

Calorimeters are commonly used for trigger purposes since they can provide fast signals that are easy to process and interpret.

They are space and therefore cost effective. Because the shower length increases only logarithmically with energy, the detector thickness needs to increase only logarithmically with the energy of the particles. In contrast for a fixed momentum resolution, the bending power BL^2 of a magnetic spectrometer must increase linearly with the particle momentum.

C.W. Fabjan and F. Gianotti, Rev. Mod. Phys., Vol. 75, N0. 4, October 2003

Particle Identification

How do you distinguish Kaons, Pions, Protons ?

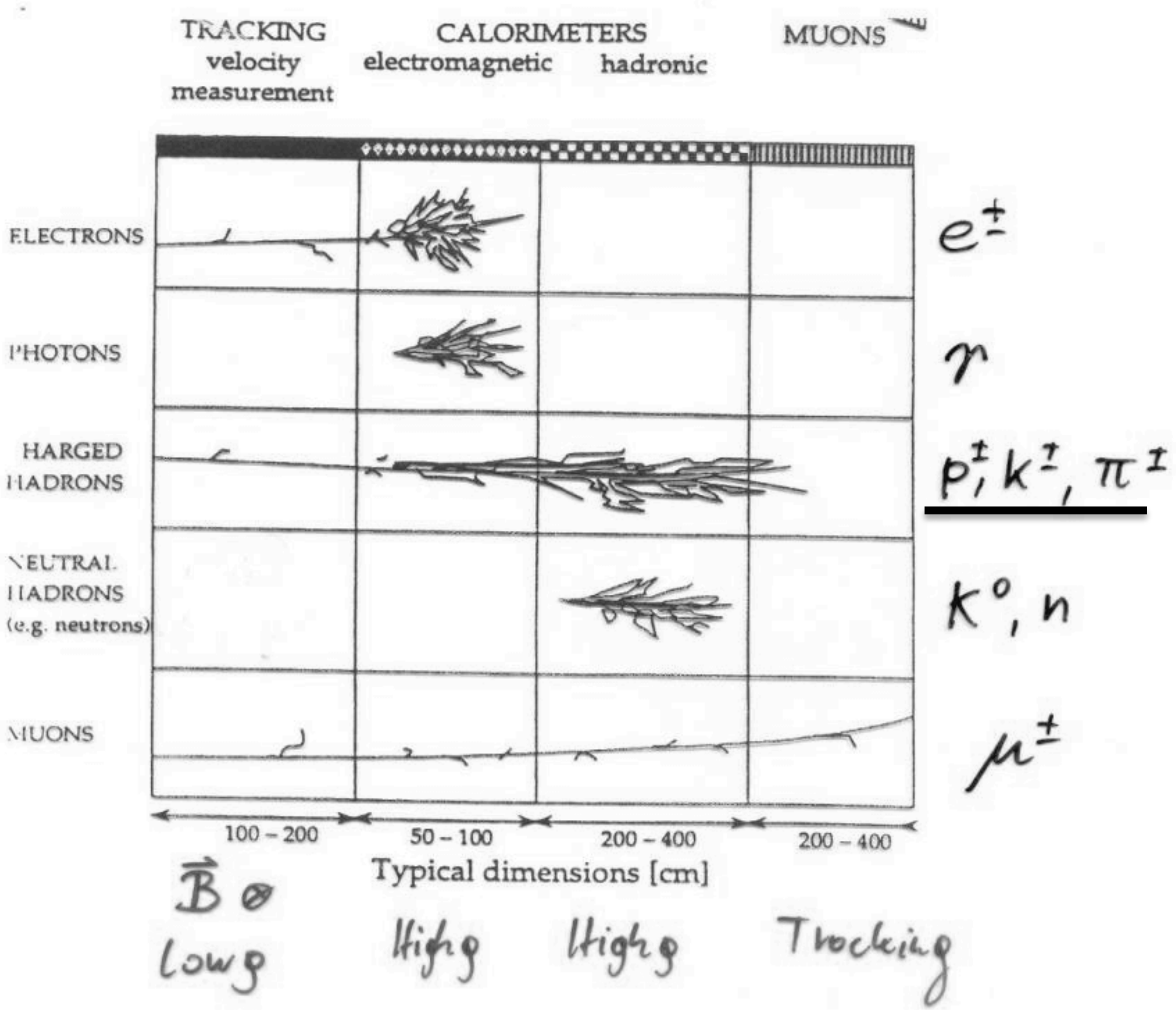

dE/dx

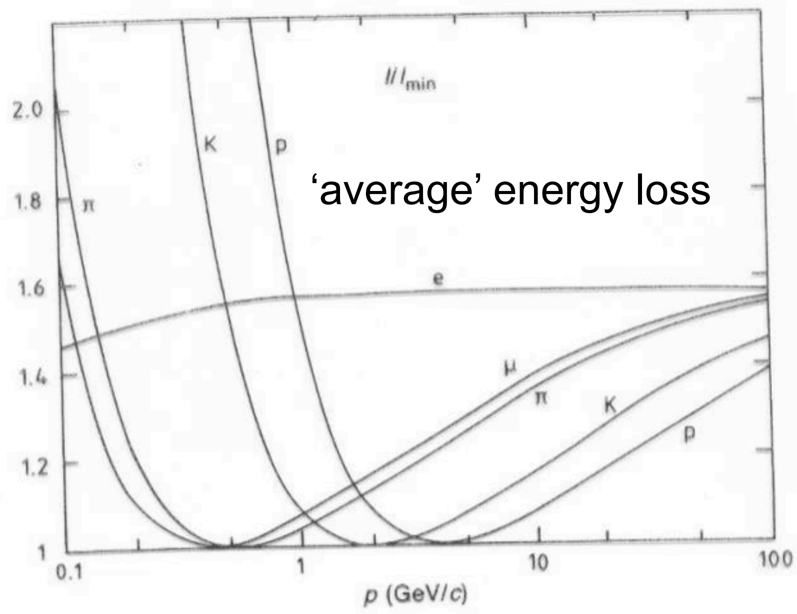

Measured energy loss

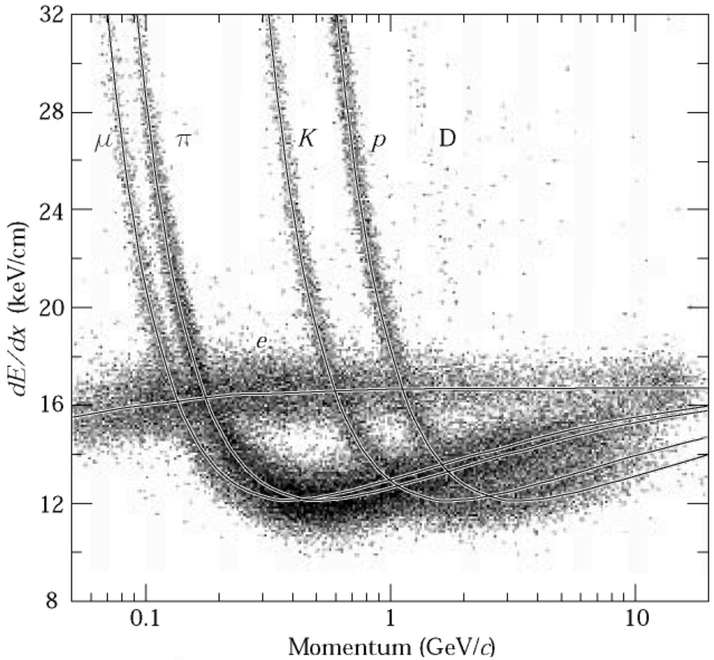

STAR TPC

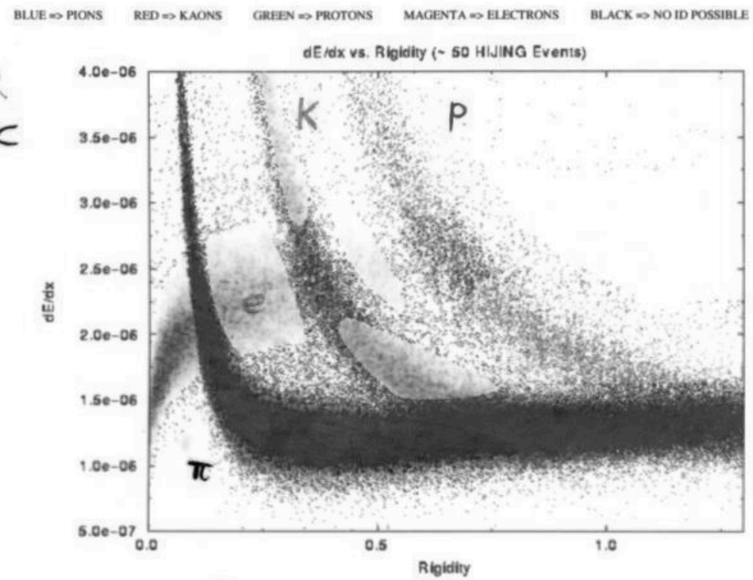

In certain momentum ranges, particles can be identified by measuring the energy loss.

Time of Flight (TOF)

E.g: $D = 2\,m$, $\sigma_t = 100\,ps$ $(10^{-10}\,s)$

3σ Significance $\rightarrow$ $T = t_2 - t_1 > 300\,ps$

$p = mv\gamma \rightarrow v = \dfrac{c}{\sqrt{1+\frac{m^2c^2}{p^2}}}$, $T = \dfrac{D}{v}$

$$T = \frac{D}{c}\sqrt{1+\frac{m^2c^2}{p^2}}$$

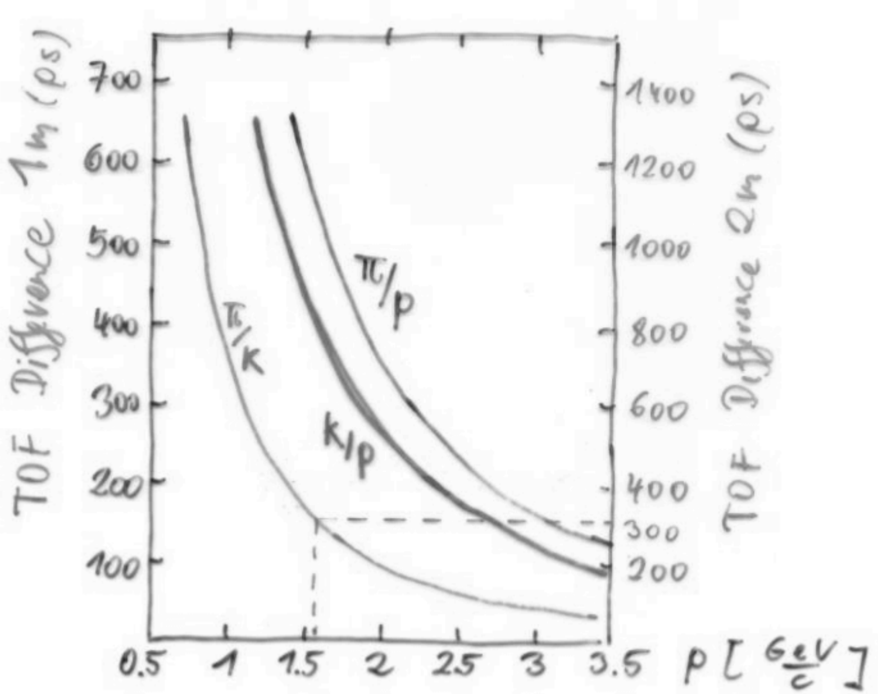

NA49 combined particle ID: TOF + dE/dx (TPC)

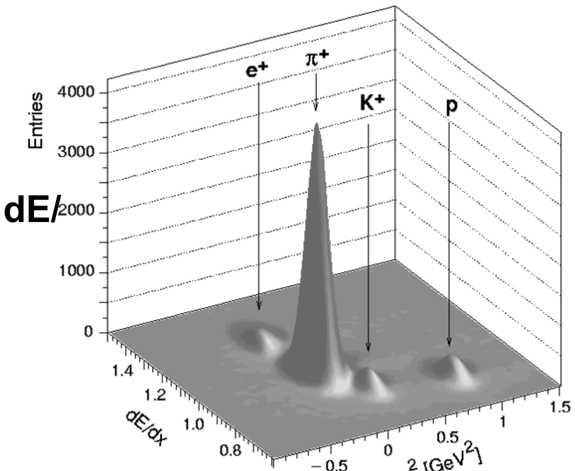

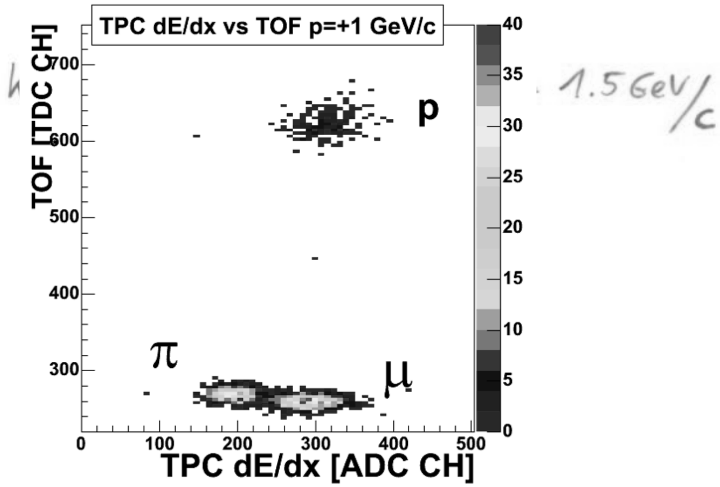

ALICE TOF: Velocity distribution for different particle types

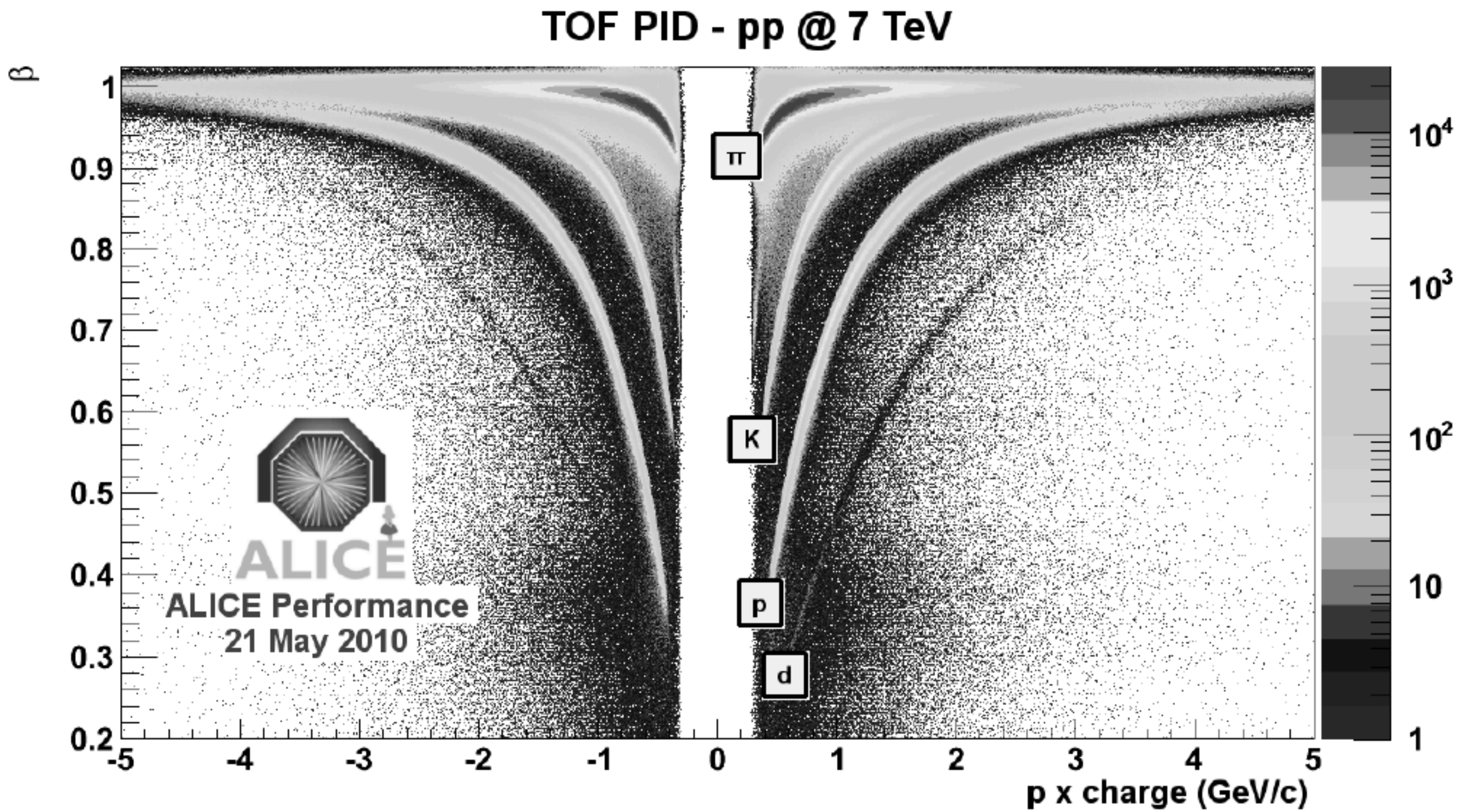

Combining different PID techniques in ALICE

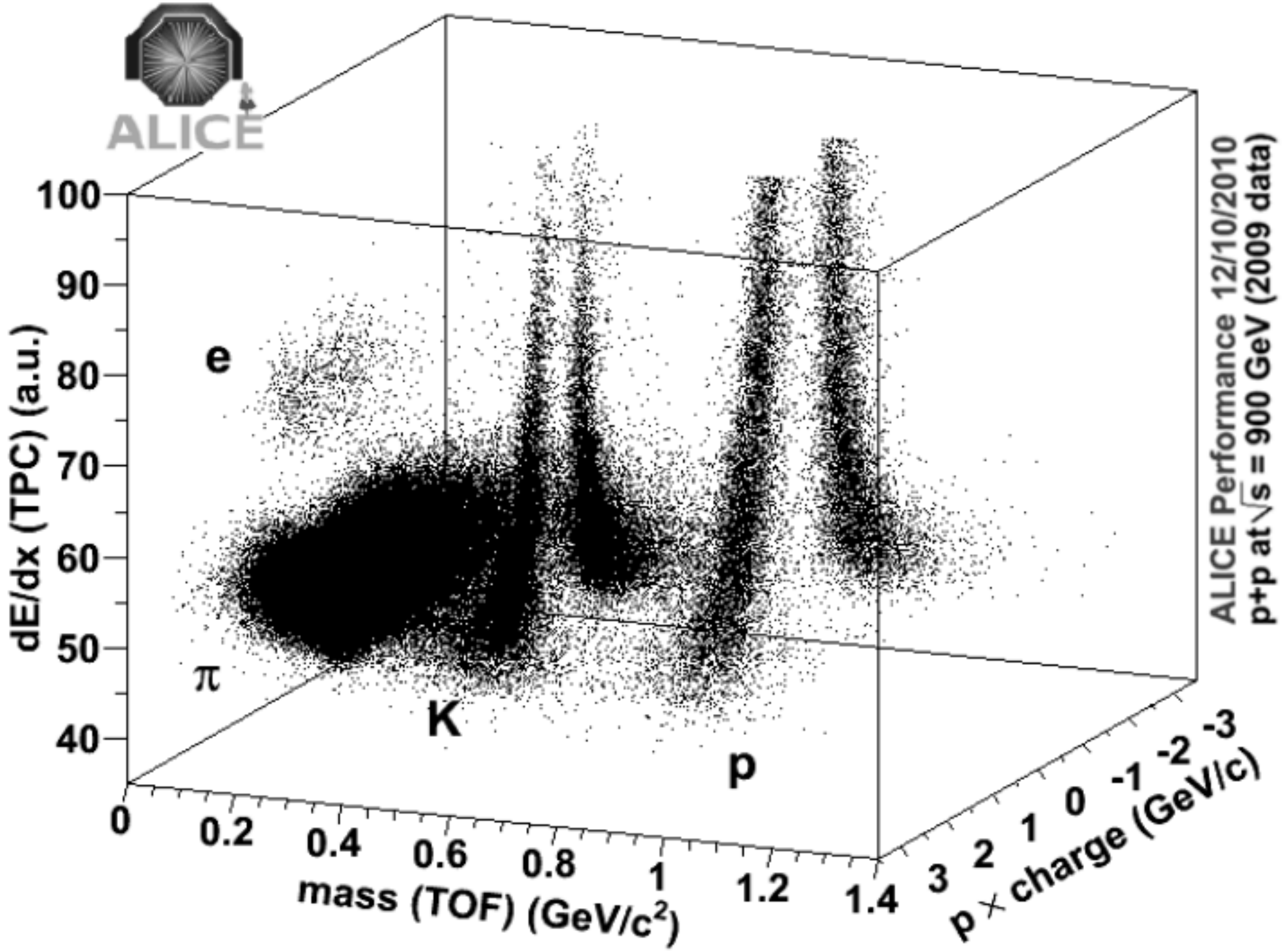

Ring Imaging Cherenkov Detector

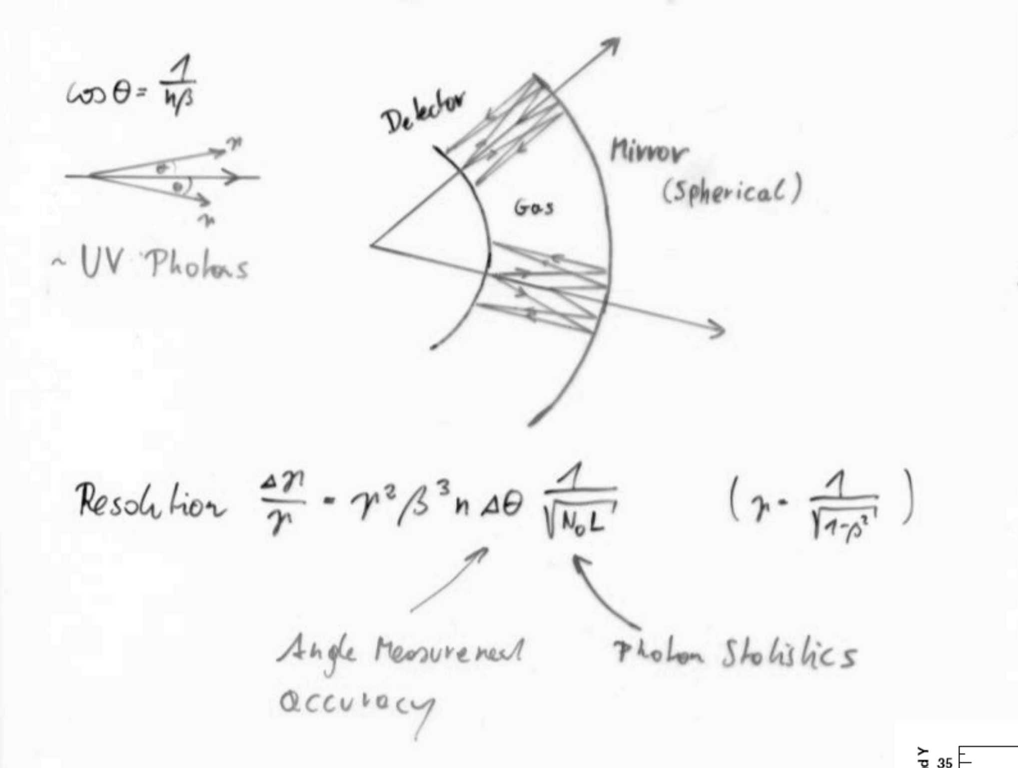

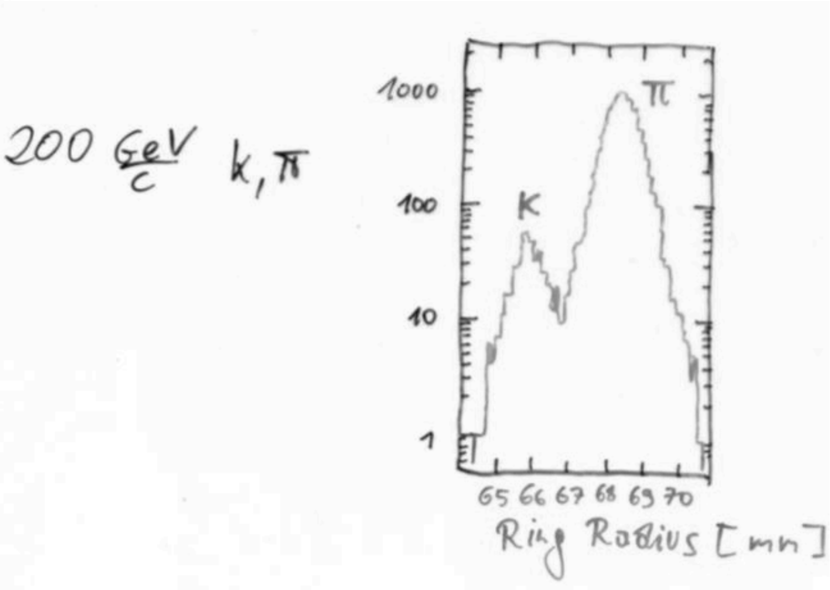

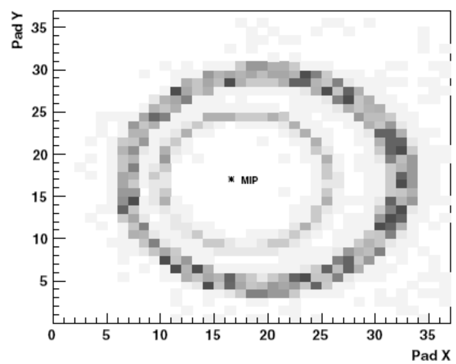

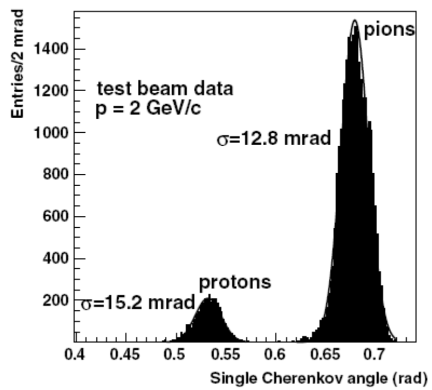

Particle ID summary

Example: If we want to distinguish Kaons and Pions of a given Momentum, what technology can we use and how long must the detector be ?

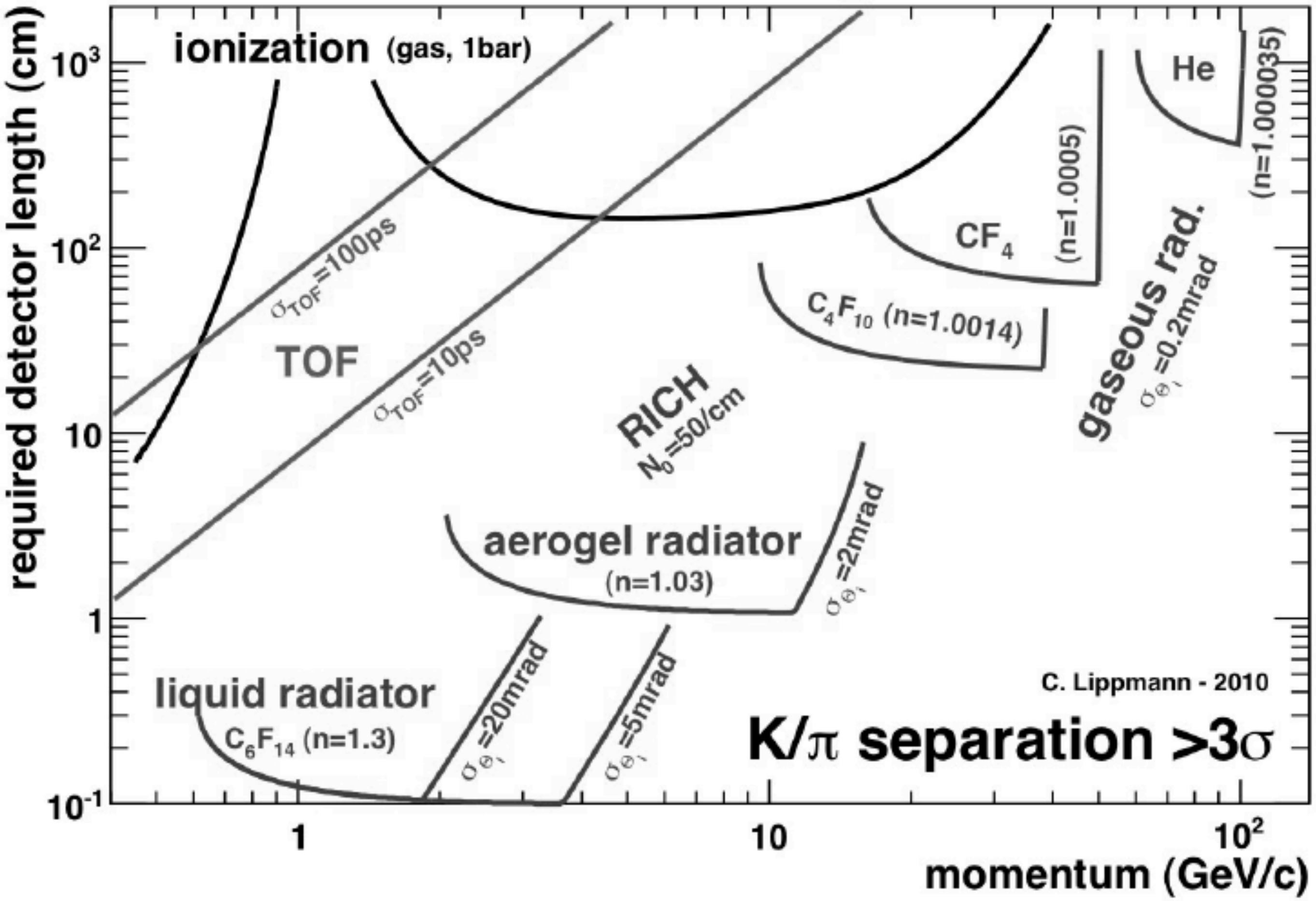

Nature was kind enough to provide a possibility for all momentum ranges

Signals, Electronics, Trigger, DAQ

Cloud Chambers 1910-1950ies

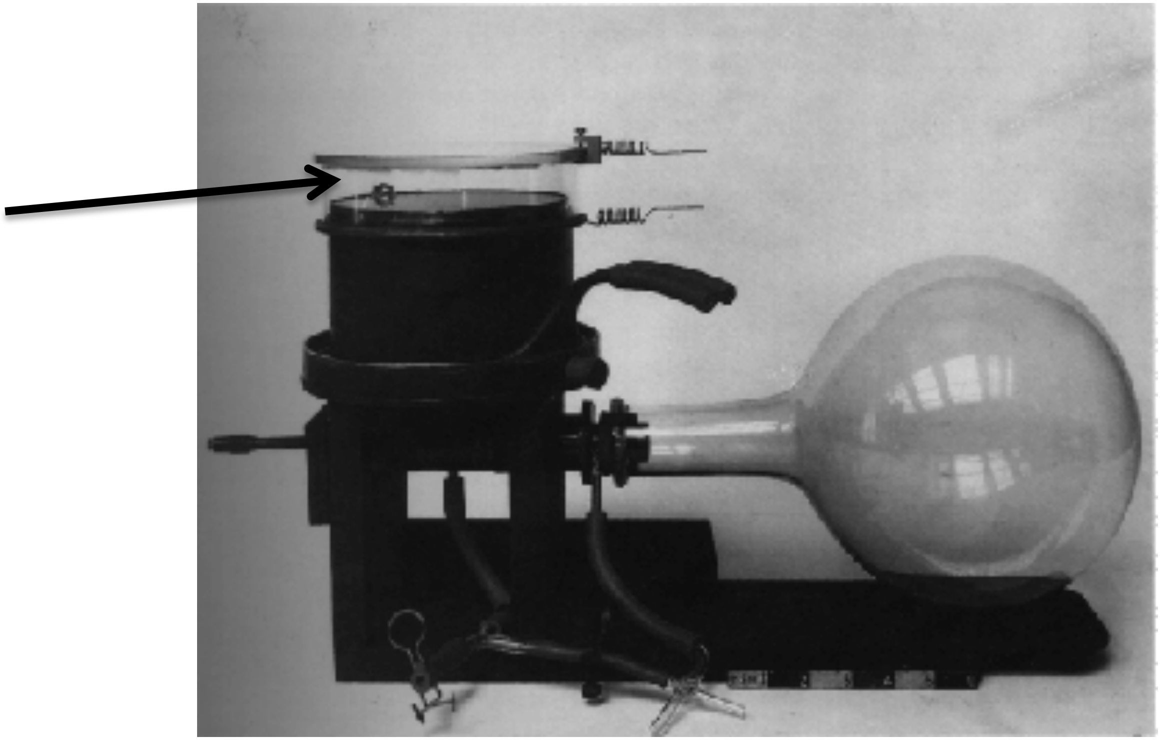

Wilson Cloud Chamber 1911

The ions produced by a charged particle are leading to condensation in supersaturated water vapor. One finds small water droplets along the track that can be photographed.

Cloud Chamber 1910-1950ies

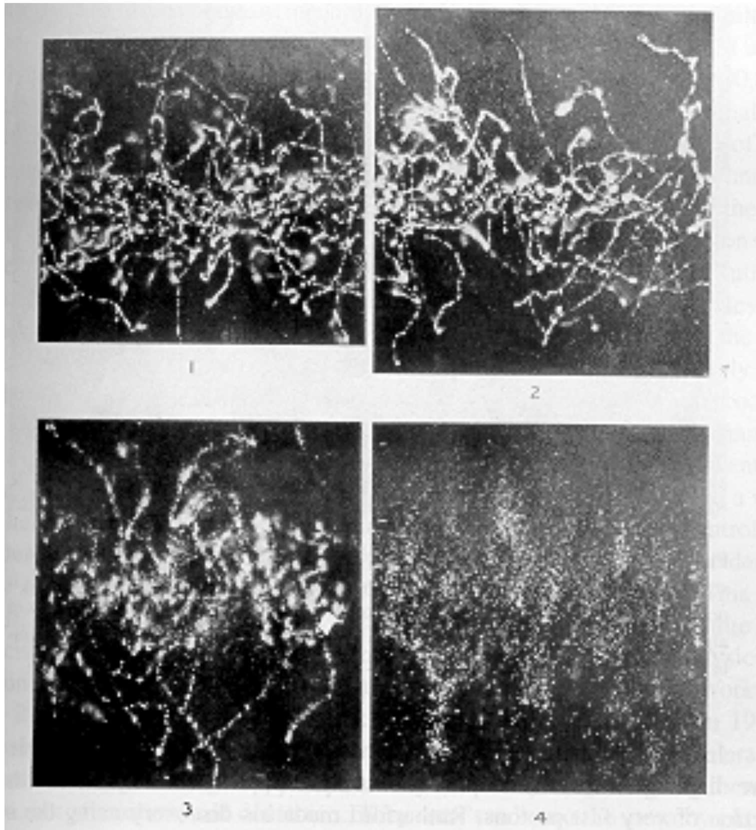

X-rays, Wilson 1912

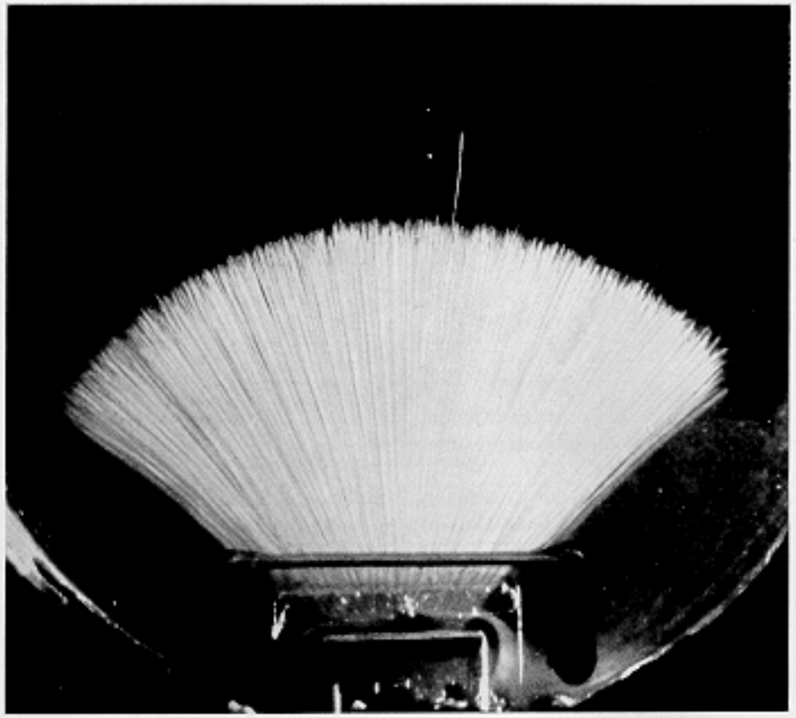

Fig. 13. K. Philipp, Naturwiss. 14, 1203 (1926).

Alphas, Philipp 1926

Cloud Chamber 1910-1950ies

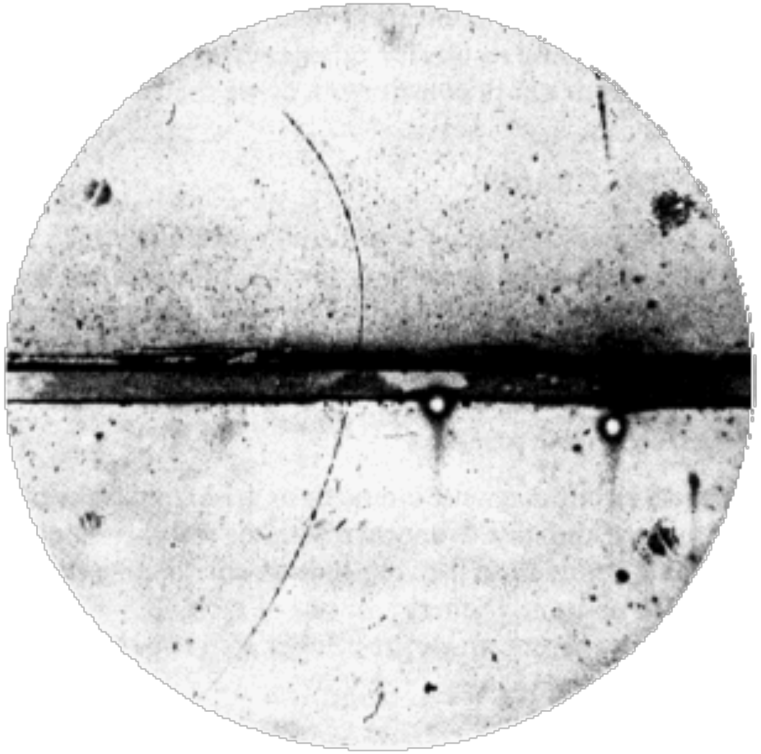

Positron discovery,
Carl Andersen 1933

Magnetic field 15000 Gauss,
chamber diameter 15cm. A 63 MeV positron passes through a 6mm lead plate, leaving the plate with energy 23MeV.

The ionization of the particle, and its behaviour in passing through the foil are the same as those of an electron.

Cloud Chamber 1910-1950ies

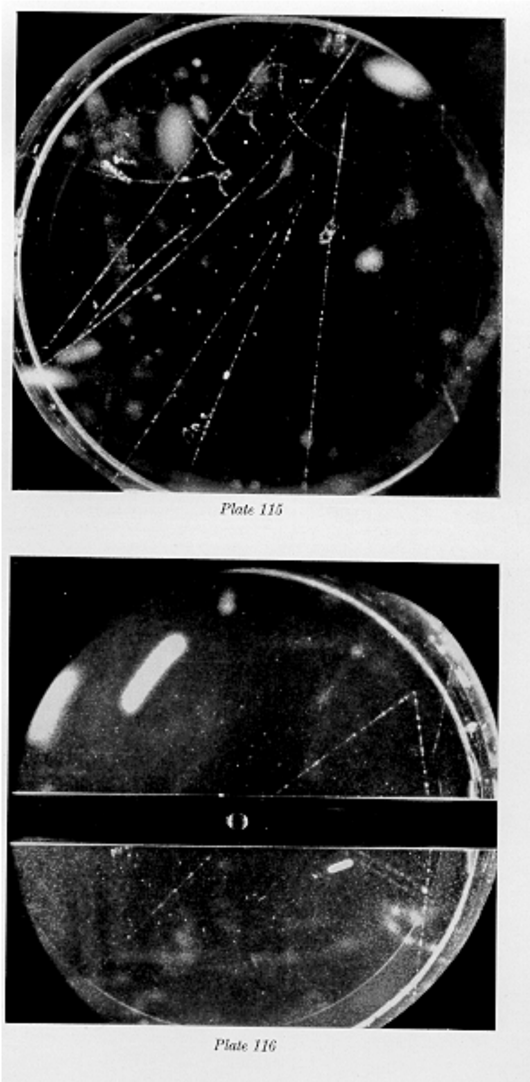

Rochester and Wilson

First observation of the "V0" particles in cosmic rays during the 1940ies. (now known as Kaon and Lambda)

' … The V0 particle originates in a nuclear Interaction outside the chamber and decays after traversing about one third of the chamber.
The momenta of the secondary particles are 1.6+-0.3 BeV/c and the angle between them is 12 degrees … '

Nuclear Emulsion 1930ies to Present

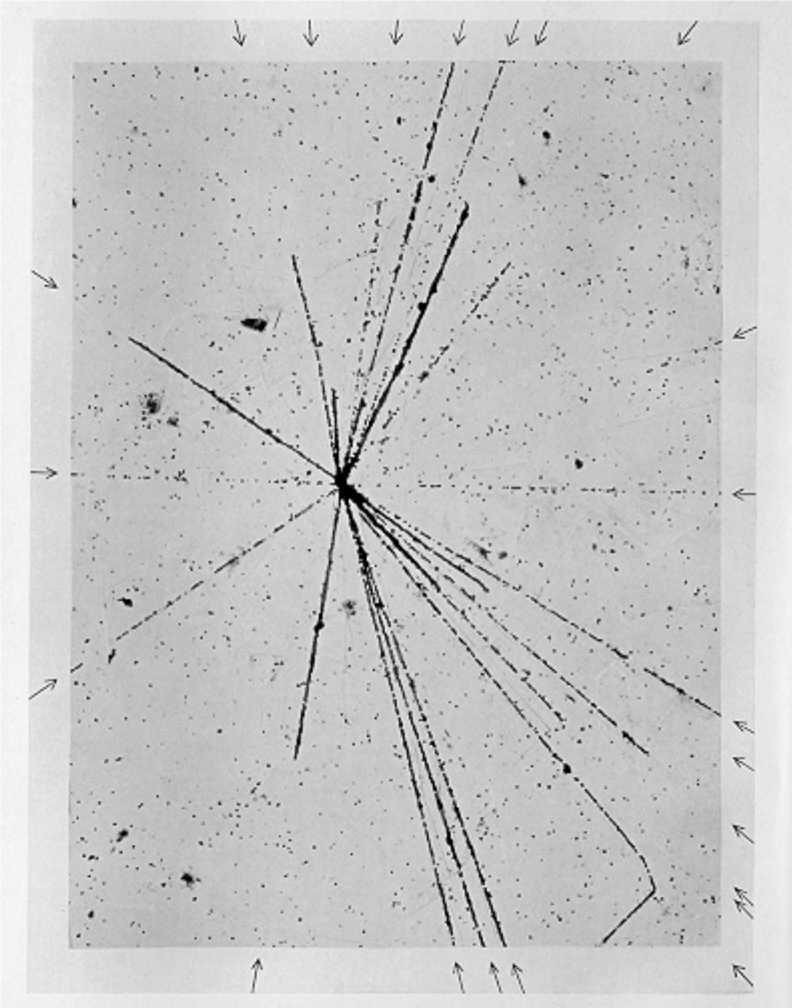

'EXPLOSIVE' DISINTEGRATION OF A NUCLEUS

Film played an important role in the discovery of radioactivity but was first seen as a means of studying radioactivity rather than photographing individual particles.

Emulsions were exposed to cosmic rays at high altitude for a long time (months) and then analyzed under the microscope. In 1937, nuclear disintegrations from cosmic rays were observed in emulsions.

The high density of film compared to the cloud chamber 'gas' made it easier to see energy loss and disintegrations.

Nuclear Emulsion

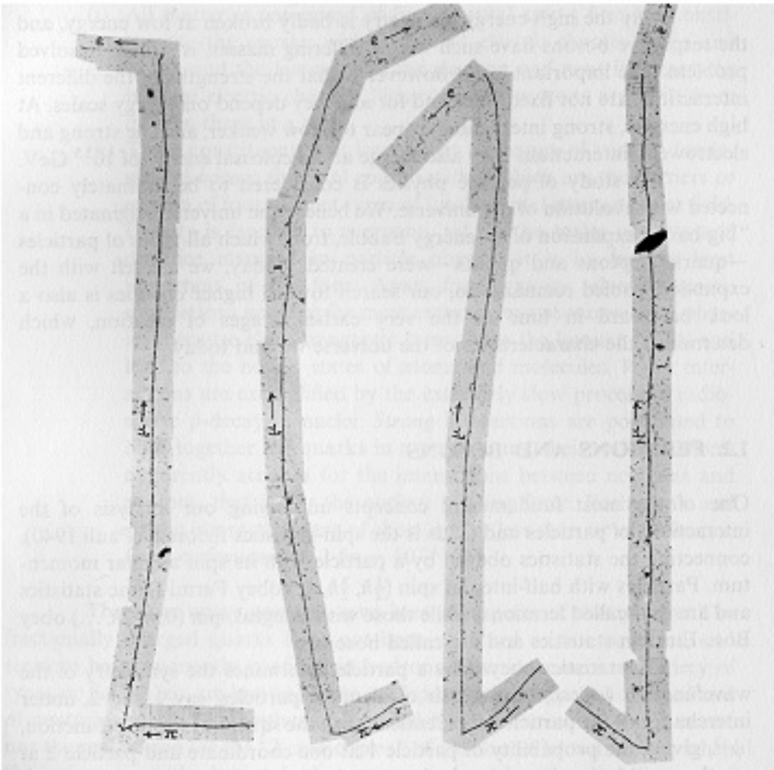

Discovery of muon and pion

Discovery of the Pion:

The muon was discovered in the 1930ies and was first believed to be Yukawa’s meson that mediates the strong force.

The long range of the muon was however causing contradictions with this hypothesis.

In 1947, Powell et. al. discovered the Pion in Nuclear emulsions exposed to cosmic rays, and they showed that it decays to a muon and an unseen partner.

The constant range of the decay muon indicated a two body decay of the pion.

Chamber 1950ies to early 1980ies

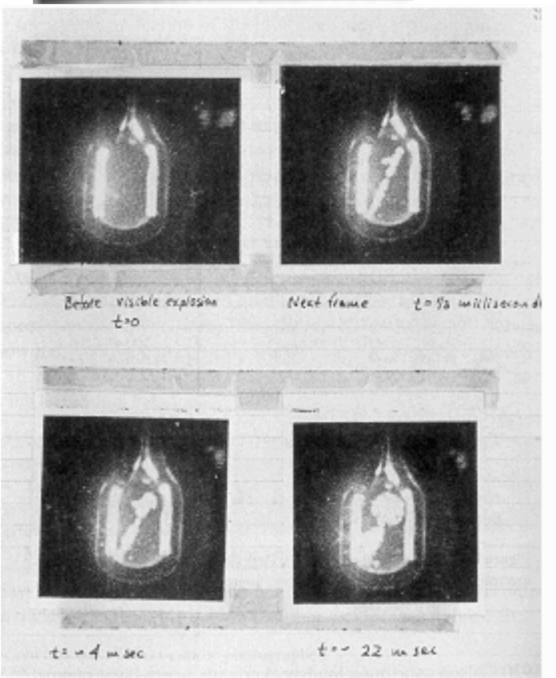

Figure 5.5 Bubble chamber movies (1952). Glaser first filmed distinct track:

In the early 1950ies Donald Glaser tried to build on the cloud chamber analogy:

Instead of supersaturating a gas with a vapor one would superheat a liquid. A particle depositing energy along it's path would then make the liquid boil and form bubbles along the track.

In 1952 Glaser photographed first Bubble chamber tracks. Luis Alvarez was one of the main proponents of the bubble chamber.

The size of the chambers grew quickly

1954:	**2.5"(6.4cm)**
1954:	**4" (10cm)**
1956:	**10" (25cm)**
1959:	**72" (183cm)**
1963:	**80" (203cm)**
1973:	**370cm**

Bubble Chamber

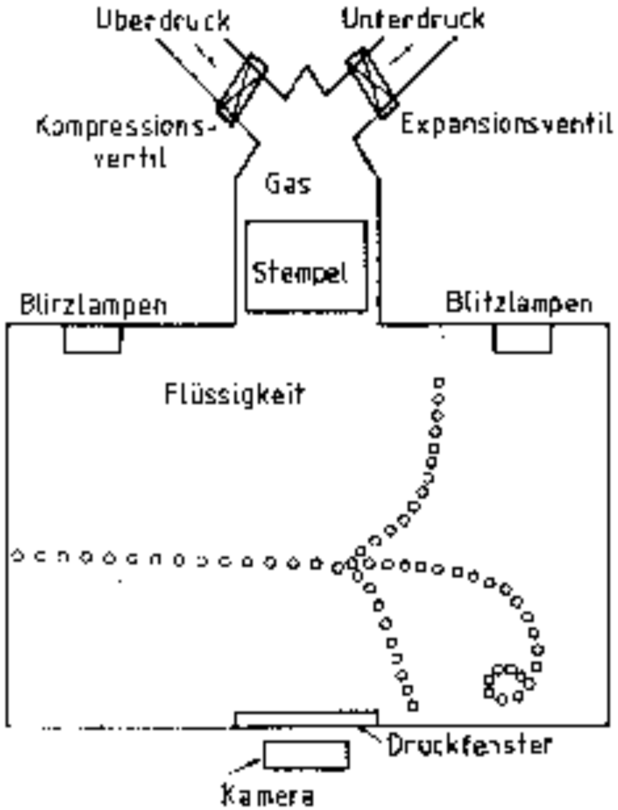

'old bubbles'

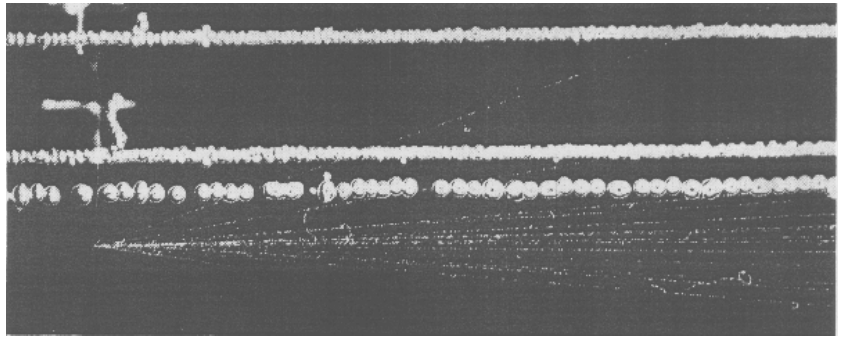

'new bubbles'

The Bubble Chamber can not be triggered, i.e. the bubble chamber had to be already in the superheated state when the particle was entering. Because in the 50ies particle physics moved to accelerators it was possible to synchronize the chamber compression with the arrival of the beam.

For data analysis one had to look through millions of pictures.

Bubble Chamber

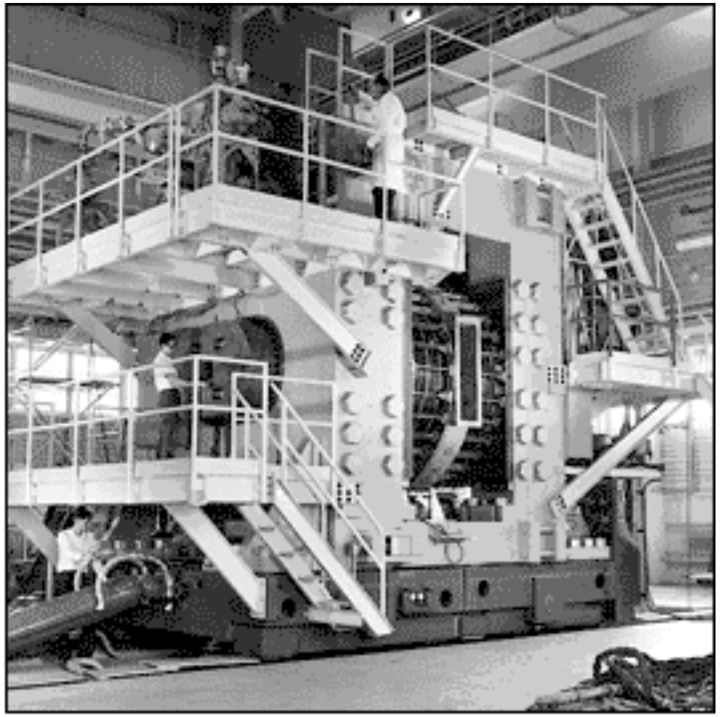

The 80-inch Bubble Chamber

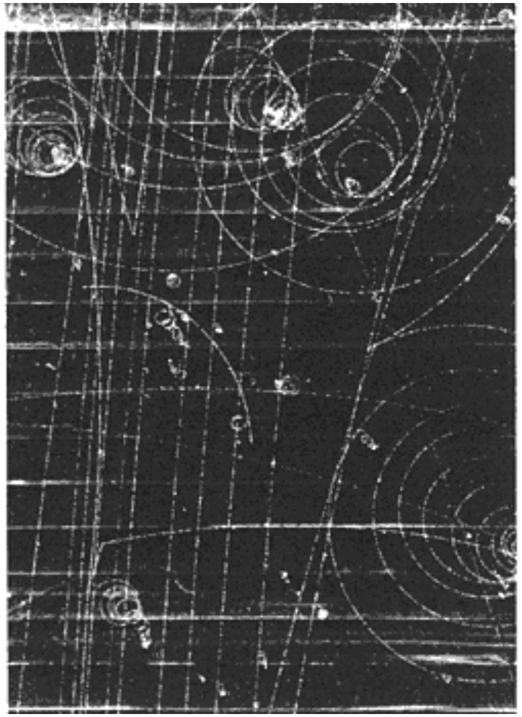

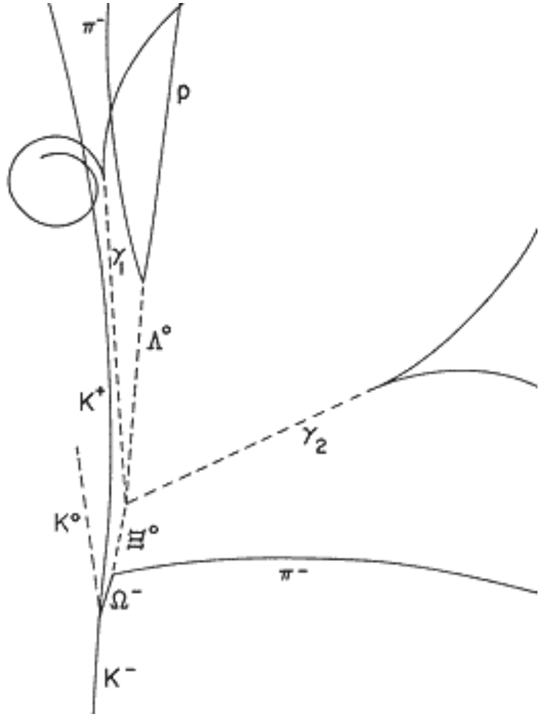

BNL, First Pictures 1963, 0.03s cycle

Discovery of the Ω^- in 1964

Bubble Chamber

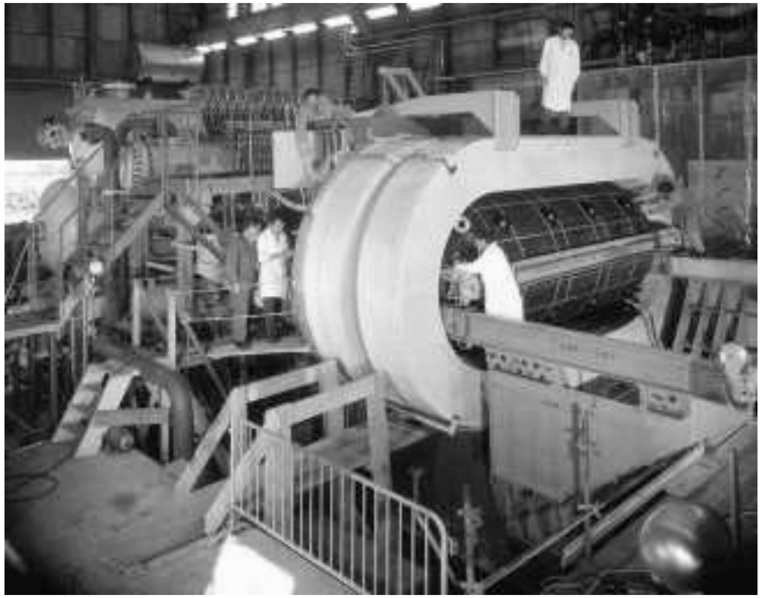

Can be seen outside the Microcosm Exhibition

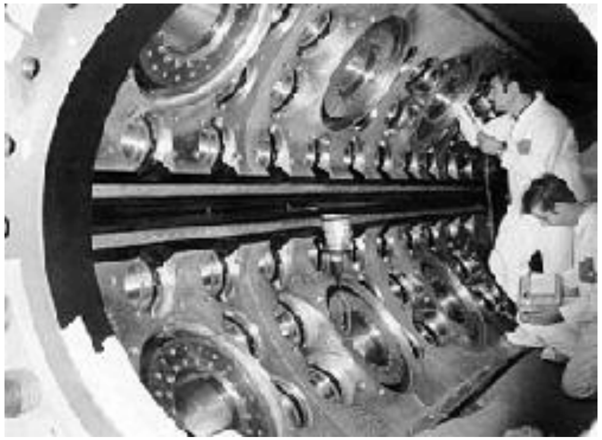

Gargamelle, a very large heavy-liquid (freon) chamber constructed at Ecole Polytechnique in Paris, came to CERN in 1970.
It was 2 m in diameter, 4 m long and filled with Freon at 20 atm.

With a conventional magnet producing a field of almost 2 T, Gargamelle in 1973 was the tool that permitted the discovery of neutral currents.

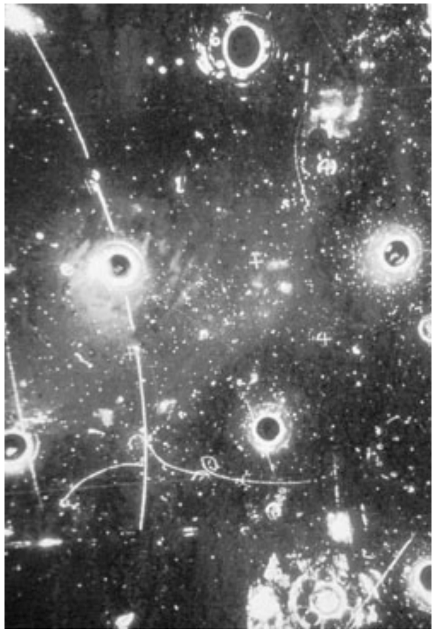

Bubble Chamber

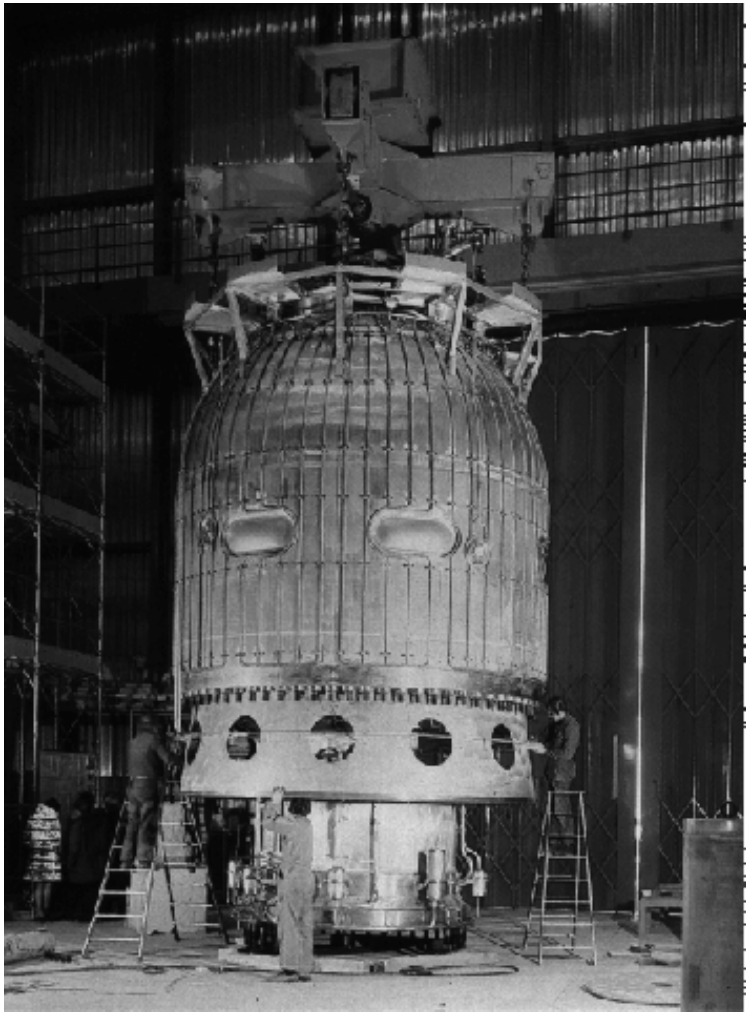

Can be seen outside the Microcosm Exhibition

3.7 meter hydrogen bubble chamber at CERN, equipped with the largest superconducting magnet in the world.

During its working life from 1973 to 1984, the "Big European Bubble Chamber" (BEBC) took over 6 million photographs.

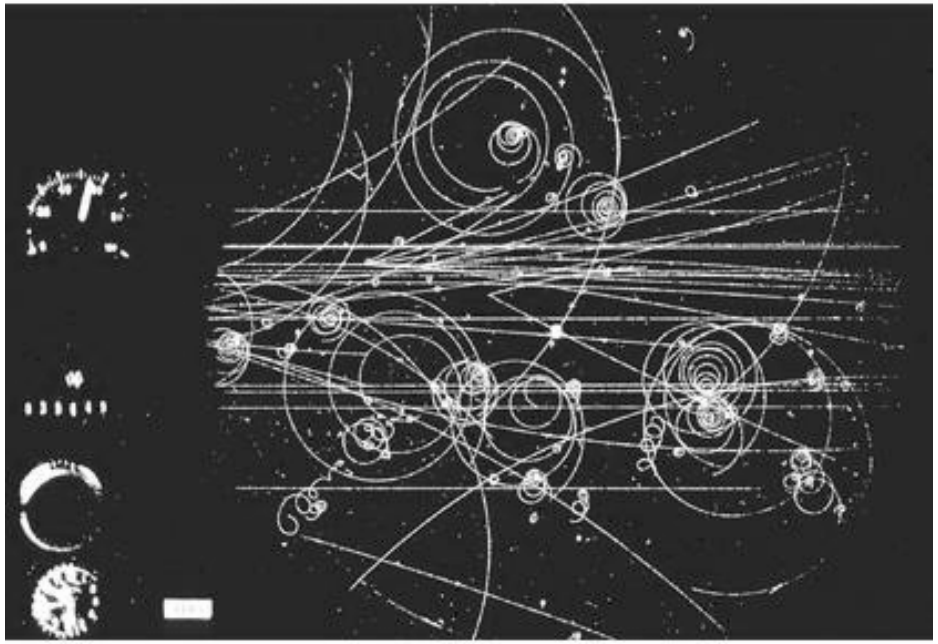

Bubble Chambers

The excellent position (5μm) resolution and the fact that target and detecting volume are the same (H chambers) makes the Bubble chamber almost unbeatable for reconstruction of complex decay modes.

The drawback of the bubble chamber is the low rate capability (a few tens/ second). E.g. LHC 10^9 collisions/s.

The fact that it cannot be triggered selectively means that every interaction must be photographed.

Analyzing the millions of images by ‘operators’ was a quite laborious task.

That’s why electronics detectors took over in the 70ties.

Detector + Electronics 1925

'Über das Wesen des Compton Effekts'
W. Bothe, H. Geiger, April 1925

Bohr, Kramers, Slater Theorie:

"Energy is only conserved statistically"
→ testing Compton effect

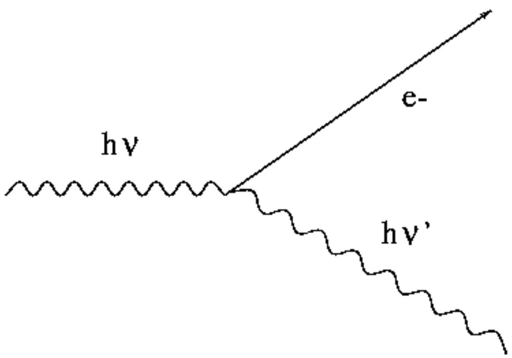

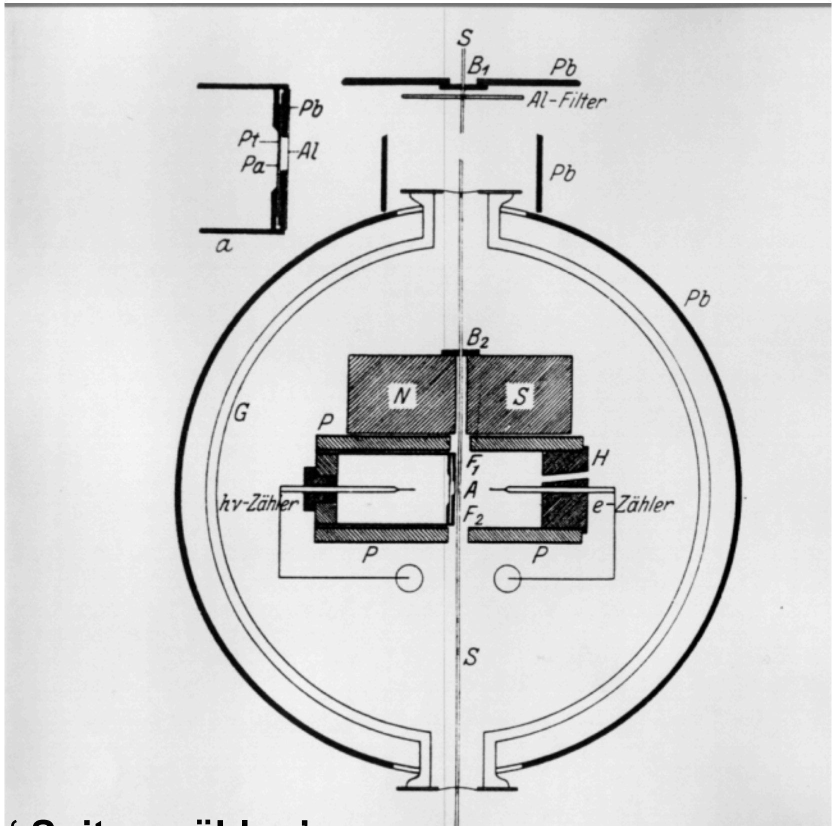

' Spitzenzähler '

Fig. 2.

Detector + Electronics 1925

'Über das Wesen des Compton Effekts', W. Bothe, H. Geiger, April 1925

- **''Electronics'':**
  - **Cylinders 'P' are on HV.**
  - **The needles of the counters are insulated and connected to electrometers.**

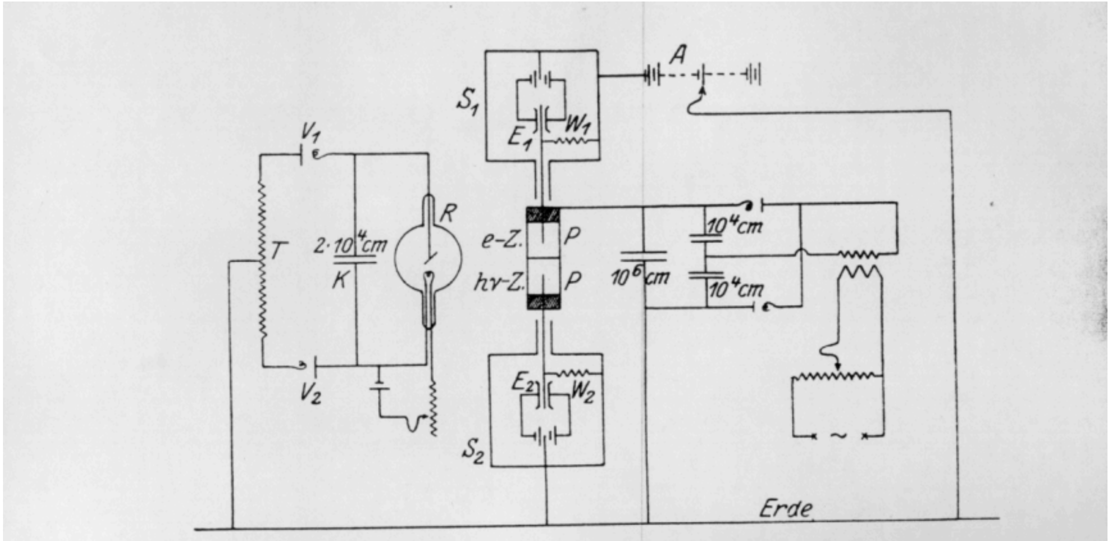

- **Coincidence Photographs:**
  - **A light source is projecting both electrometers on a moving film role.**
  - **Discharges in the counters move the electrometers , which are recorded on the film.**
  - **The coincidences are observed by looking through many meters of film.**

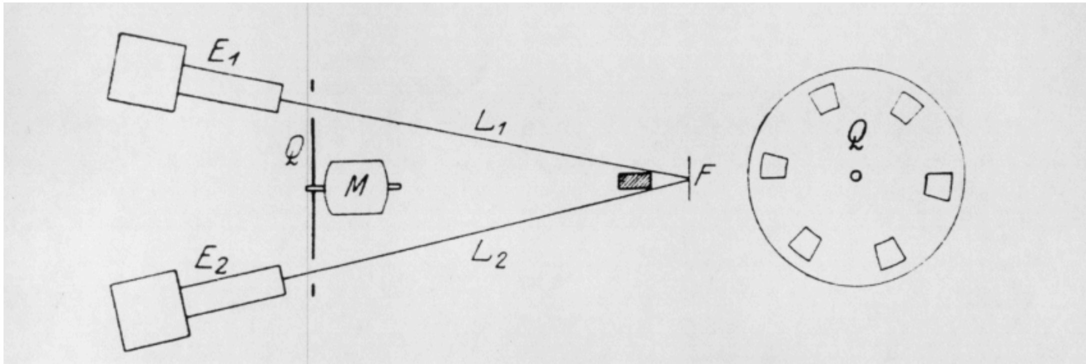

Fig. 4. Photographische Registrierung.

Detector + Electronics 1929

In 1928 the long known Geiger counter (Geiger and Rutherford 1906) was properly understood by Walther Müller and it became the most important instrument for cosmic ray physics for a long time to come.

→ Geiger Müller Counter

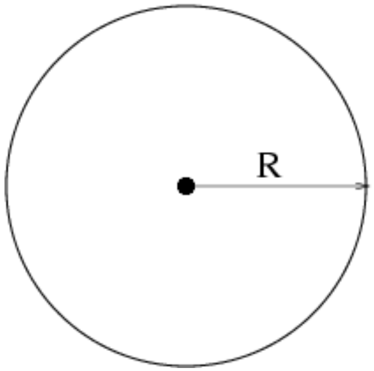

‘Zur Vereinfachung von Koinzidenzzählungen’
(‘On the simplification of coincidence counting’)
W. Bothe, November 1929

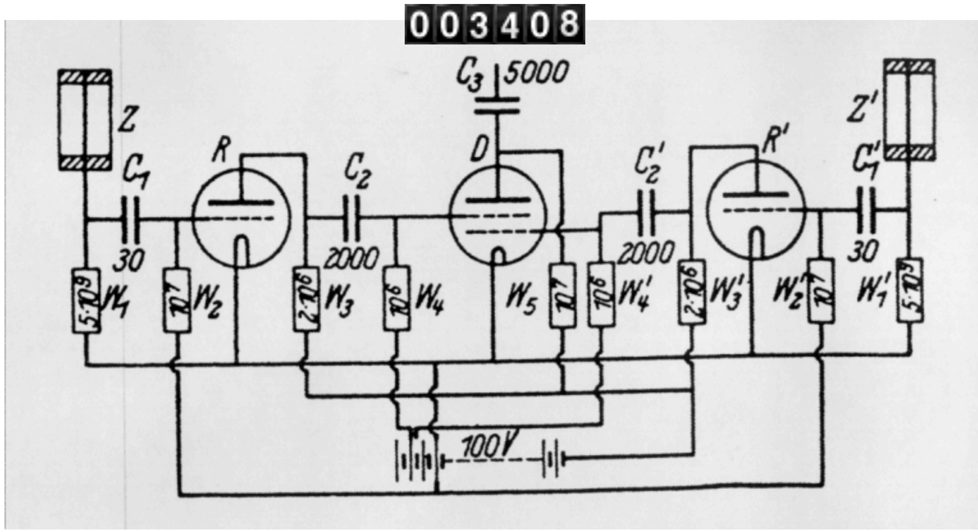

First electronics for coincidence counting.

→ coincidence = a signal in both detectors during a certain time window

1930 - 1934

Cosmic ray telescope 1934

Rossi 1930: Coincidence circuit for n tubes

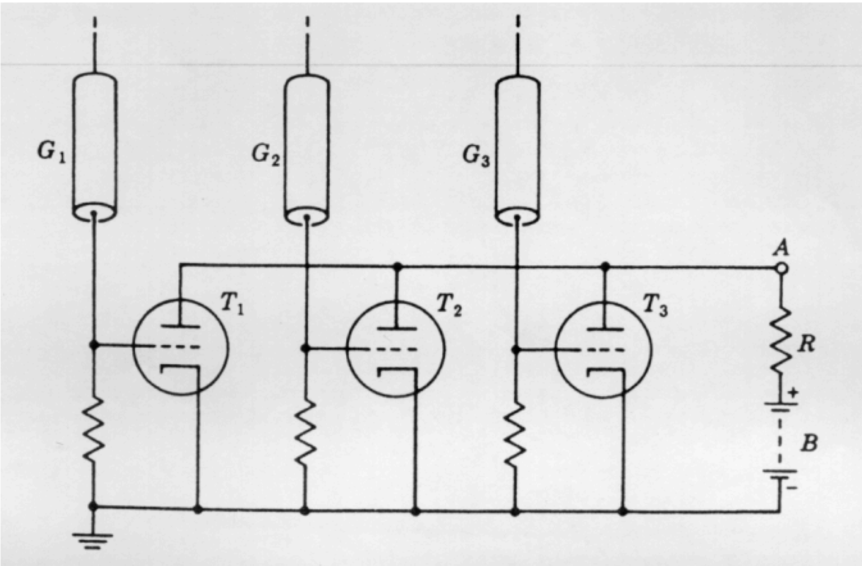

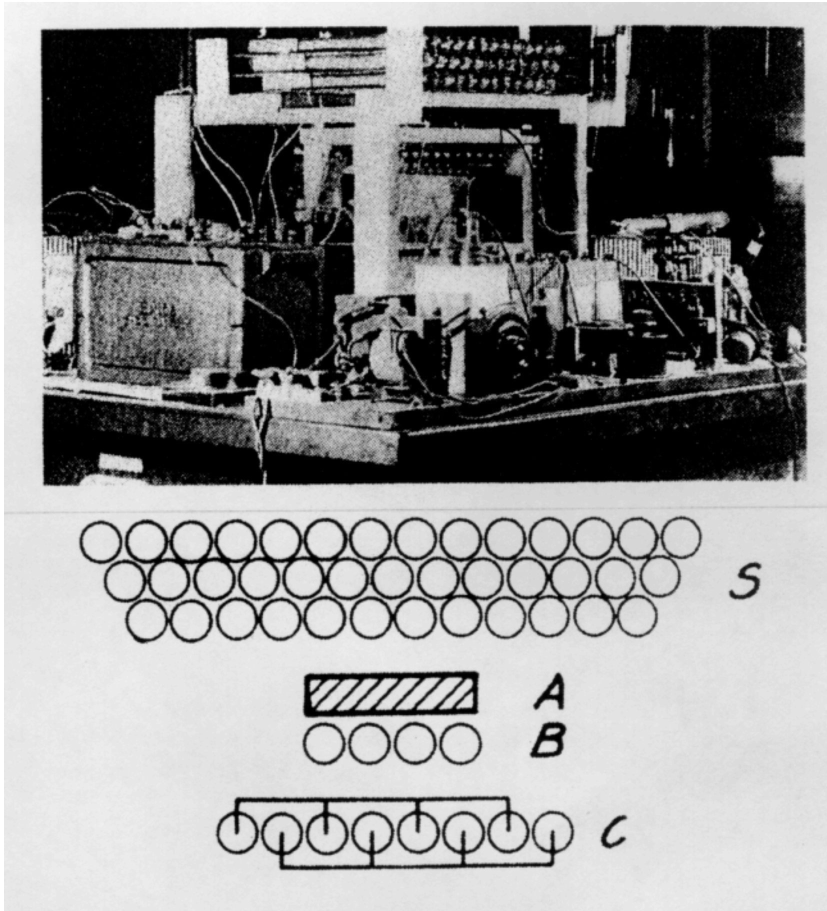

Geiger Counters

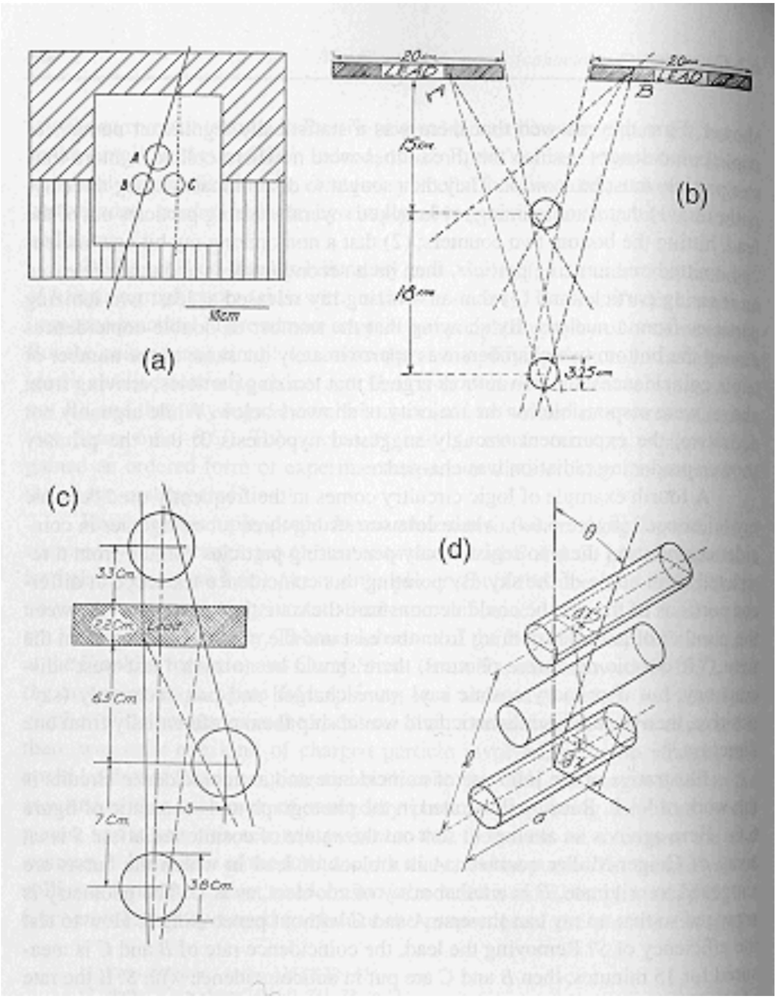

By performing coincidences of Geiger Müller tubes e.g. the angular distribution of cosmic ray particles could be measured.

Scintillators, Cerenkov light, Photomultipliers

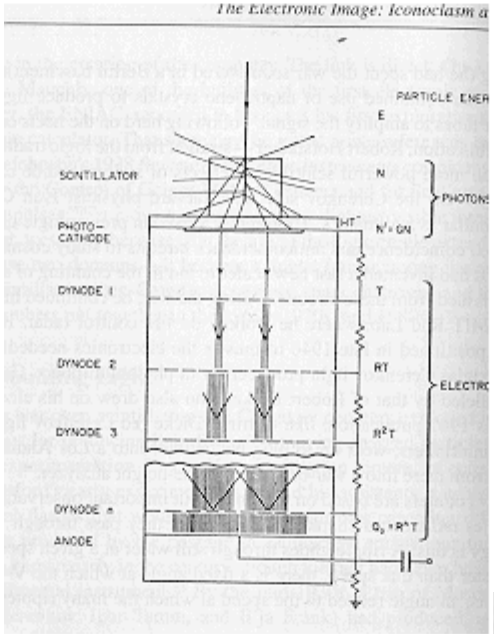

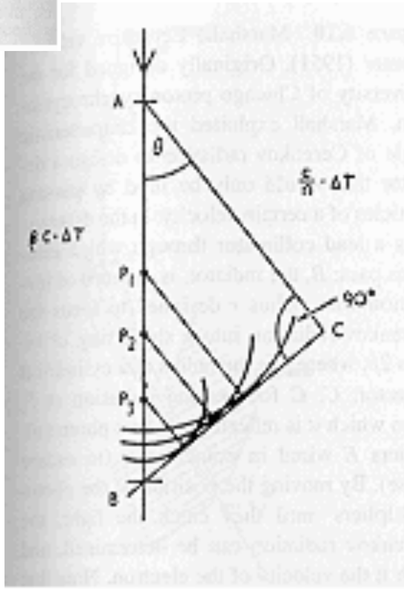

In the late 1940ies, scintillation counters and Cerenkov counters exploded into use.

Scintillation of materials on passage of particles was long known.

By mid 1930 the bluish glow that accompanied the passage of radioactive particles through liquids was analyzed and largely explained (Cerenkov Radiation).

Mainly the electronics revolution begun during the war initiated this development.

High-gain photomultiplier tubes, amplifiers, scalers, pulse-height analyzers.

Anti Neutrino Discovery 1959

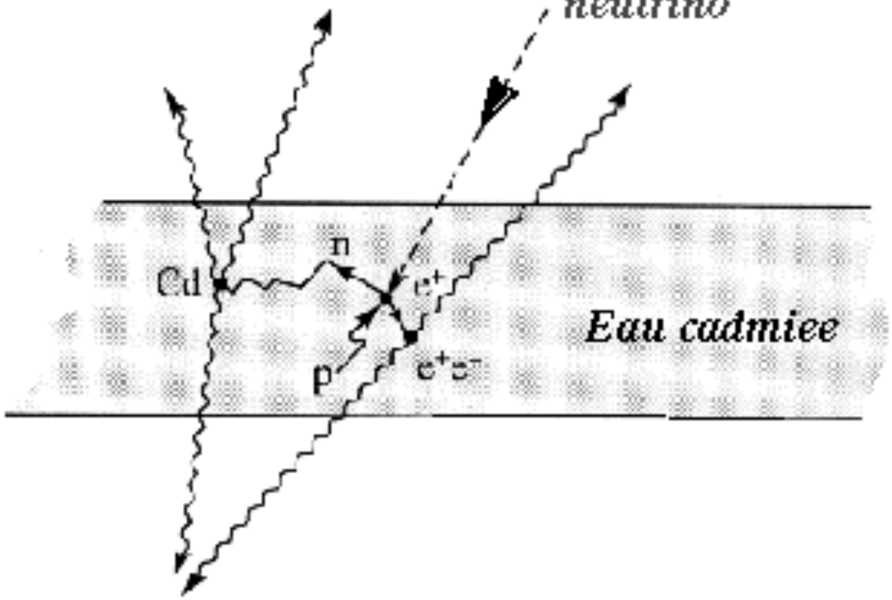

$\bar{\nu} + p \rightarrow n + e^+$

Reines and Cowan experiment principle consisted in using a target made of around 400 liters of a mixture of water and cadmium chloride.

The anti-neutrino coming from the nuclear reactor interacts with a proton of the target matter, giving a positron and a neutron.

The positron annihilates with an electron of the surrounding material, giving two simultaneous photons and the neutron slows down until it is eventually captured by a cadmium nucleus, implying the emission of photons some 15 microseconds after those of the positron annihilation.

Signal:
Coincidence of two photons in opposite direction and a photon cascade after about 15 microseconds.

Cloud Chamber 1931, triggered 'readout'

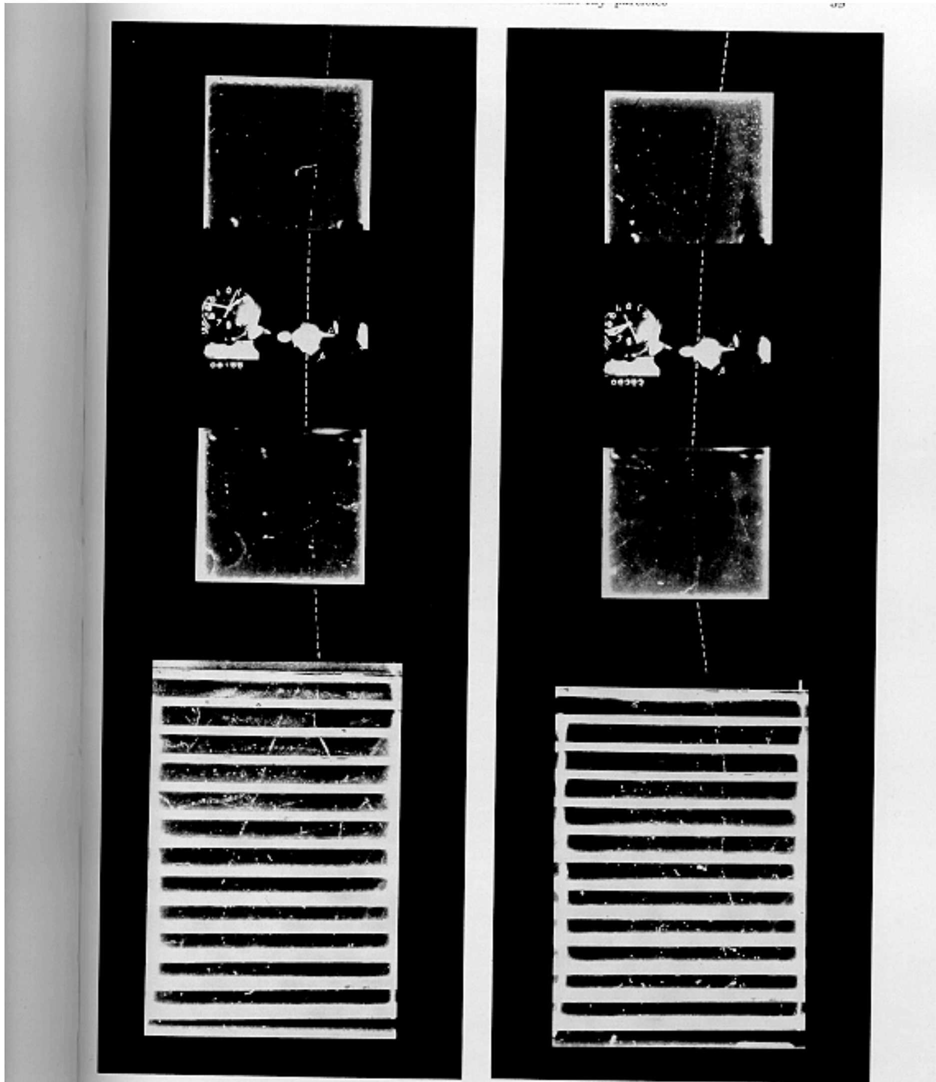

Plate 68 Plate 69

1931 Blackett and Occhialini began work on a counter controlled cloud chamber for cosmic ray physics to observe selected rare events.

The coincidence of two Geiger Müller tubes above and below the Cloud Chamber triggers the expansion of the volume and the subsequent Illumination for photography.

→ First triggered experiments !

Spark Counters triggered 'readout'

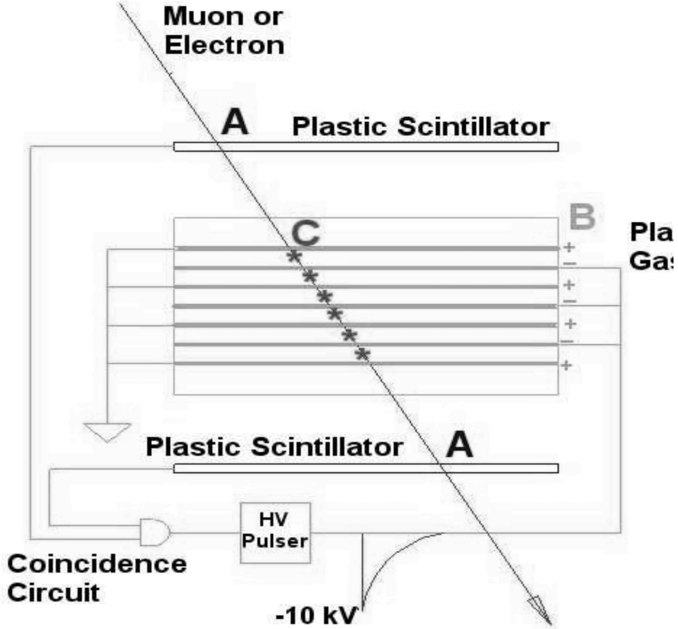

The Spark Chamber was developed in the early 60ies.

Schwartz, Steinberger and Lederman used it in discovery of the muon neutrino

A charged particle traverses the detector and leaves an ionization trail.

The scintillators trigger an HV pulse between the metal plates and sparks form in the place where the ionization took place.

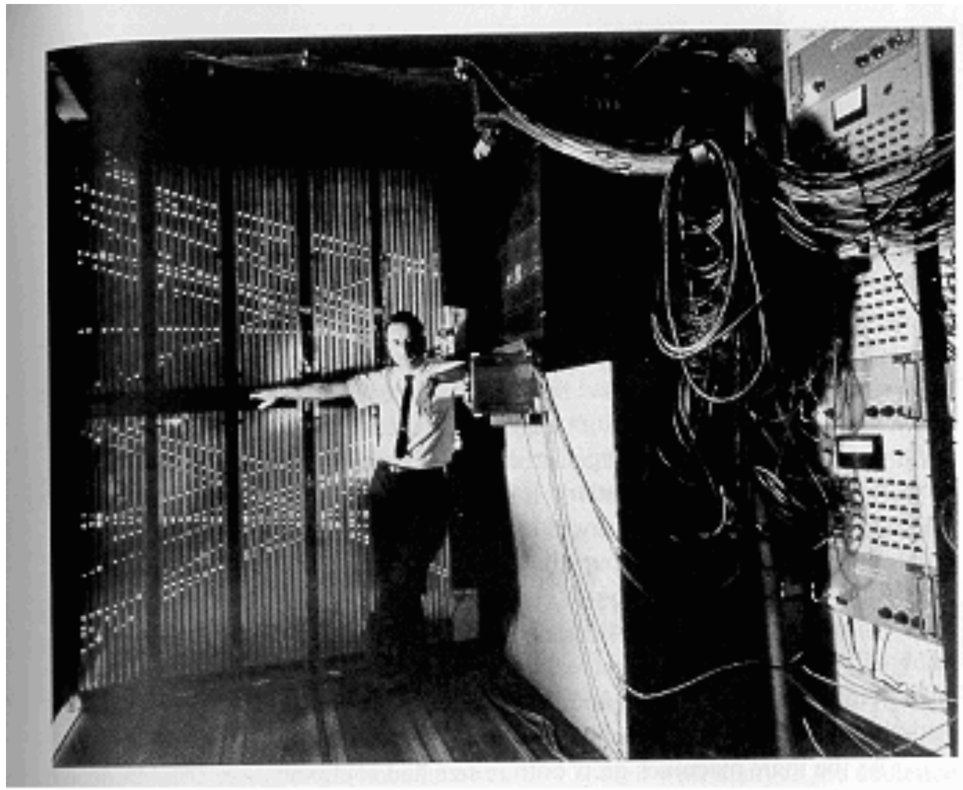

W, Z-Discovery 1983/84

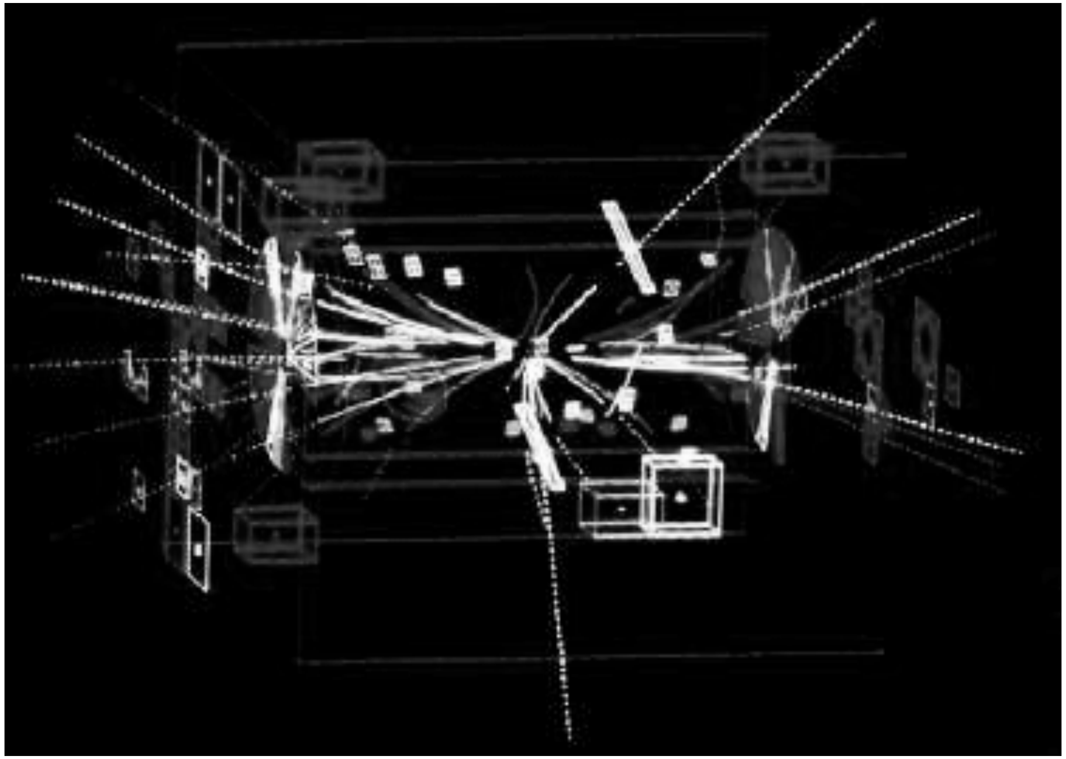

With the availability of cheap electronics devices for readout, the imaging and logic detectors turned into ‘electronics imaging’ detectors.

Z decaying into two high energy electrons. Iconic example of the new generation of ‘electronic imaging’ detectors.

UA1 used a very large wire chamber. Can now be seen in the CERN Microcosm Exhibition.

Moore’s Law

Electronics, Volume 38, Number 8, April 19, 1965

Cramming more components onto integrated circuits

With unit cost falling as the number of components per circuit rises, by 1975 economics may dictate squeezing as many as 65,000 components on a single silicon chip

By Gordon E. Moore

Moore’s Law

Wikipedia:

Moore's law describes a long-term trend in the history of computing hardware. The number of transistors that can be placed inexpensively on an integrated circuit doubles approximately every two years. This trend has continued for more than half a century and is expected to continue until 2015 or 2020 or later.

The capabilities of many digital electronic devices are strongly linked to Moore's law: processing speed, memory capacity, sensors and even the number and size of pixels in digital cameras.
All of these are improving at (roughly) exponential rates as well.

This exponential improvement has dramatically enhanced the impact of digital electronics in nearly every segment of the world economy → and clearly in Particle Physics.

Moore’s Law

Number of CPU Transistors

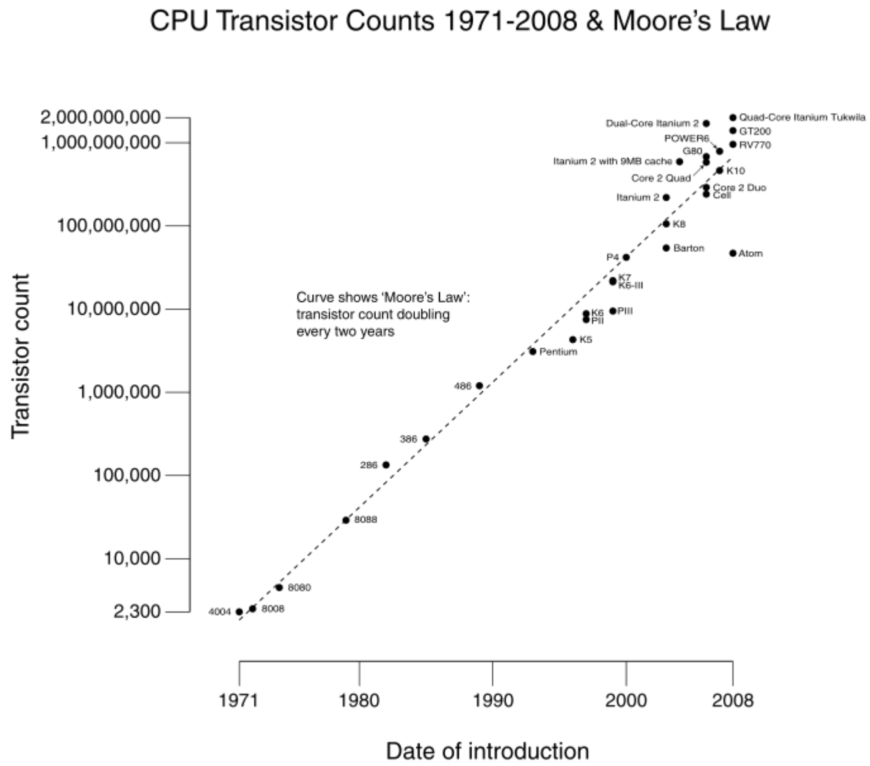

Calculations per second per 1000$

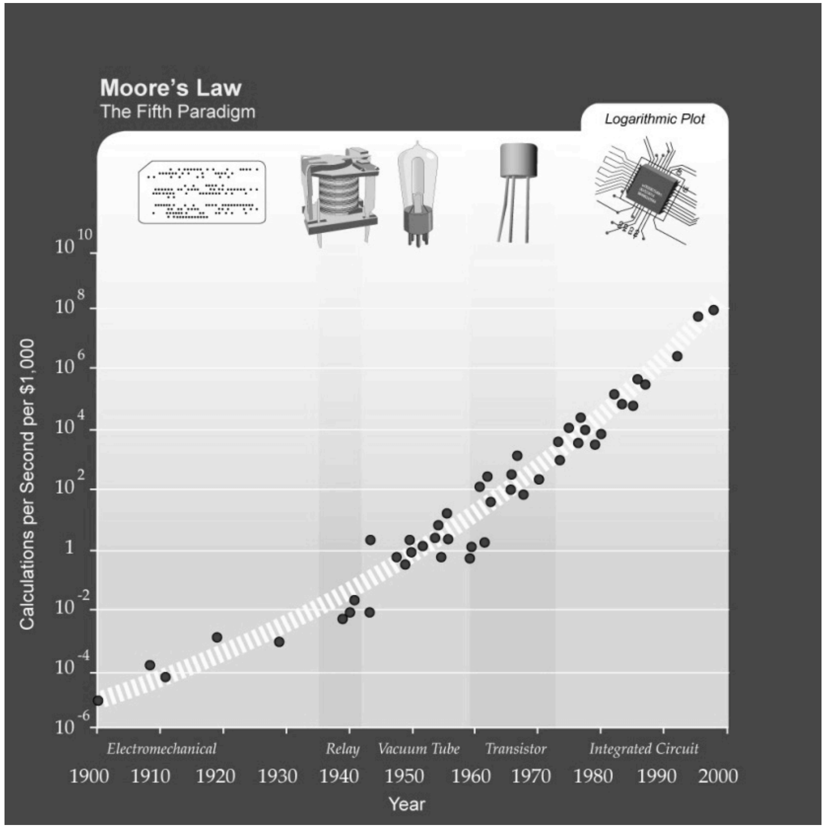

Moore’s Law

Transistor Sizes:

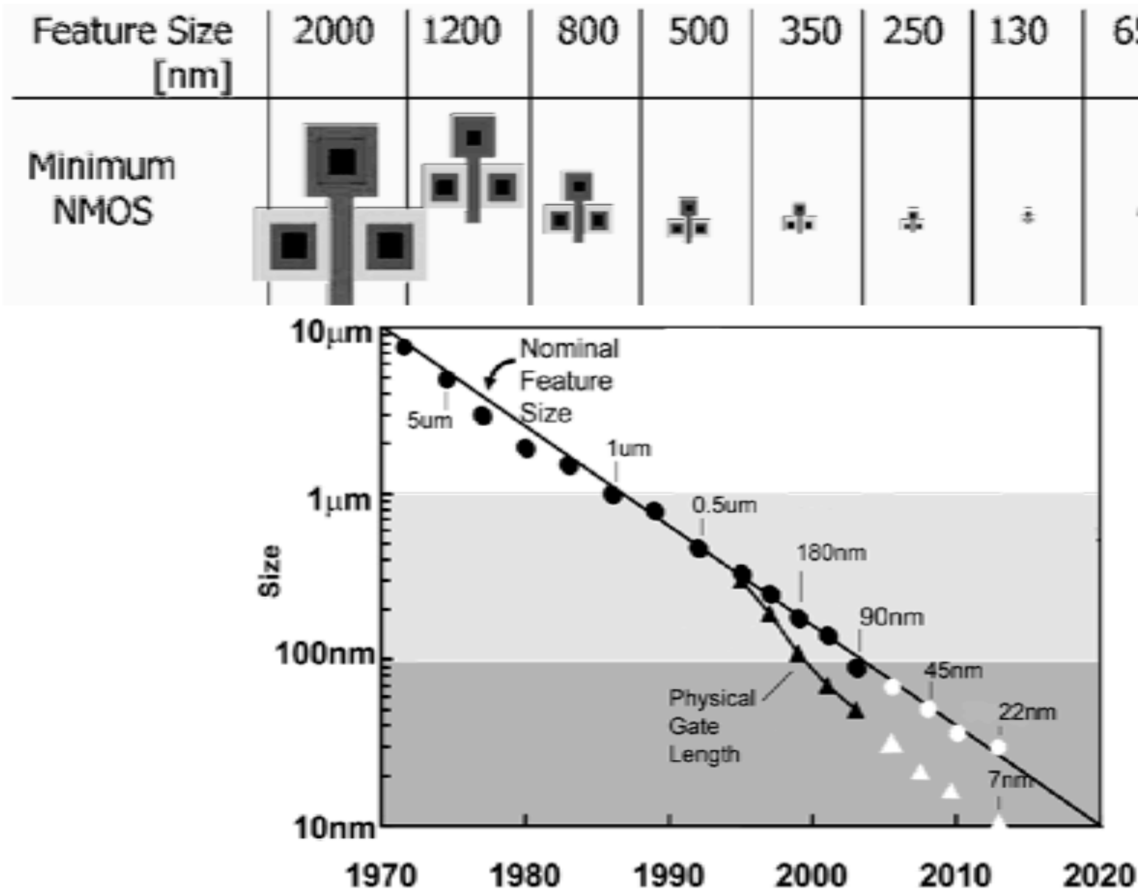

The Challenge at LHC

- **Interactions/s:**
  Lum = 10^{34} $cm^{-2}s^{-1}$=$10^7 mb^{-1}$Hz
  σ(pp) = 70 mb
  Interaction Rate, R = $7x10^8$ Hz

- **Events/beam crossing:**
  Δt = 25 ns = $2.5x10^{-8}$ s
  Interactions/crossing=17.5

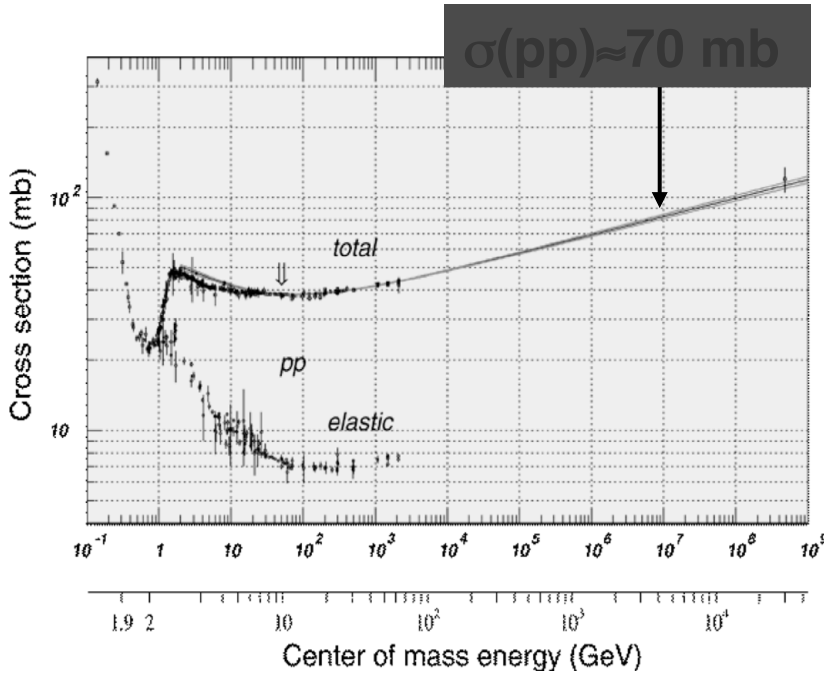

Selectivity: the Physics

- **Cross sections of physics processes vary over many orders of magnitude**
  - **Inelastic: 10^9 Hz**
  - **W→ $\ell\,\nu$: 10^2 Hz**
  - **t t production: 10 Hz**
  - **Higgs (100 GeV/c^2): 0.1 Hz**
  - **Higgs (600 GeV/c^2): 10^{-2} Hz**
- **QCD background**
  - **Jet E_T ~250 GeV: rate = 1 kHz**
  - **Jet fluctuations → electron bkg**
  - **Decays of K, π, b → muon bkg**
- **Selection needed: 1:10^{10-11}**
  - **Before branching fractions...**

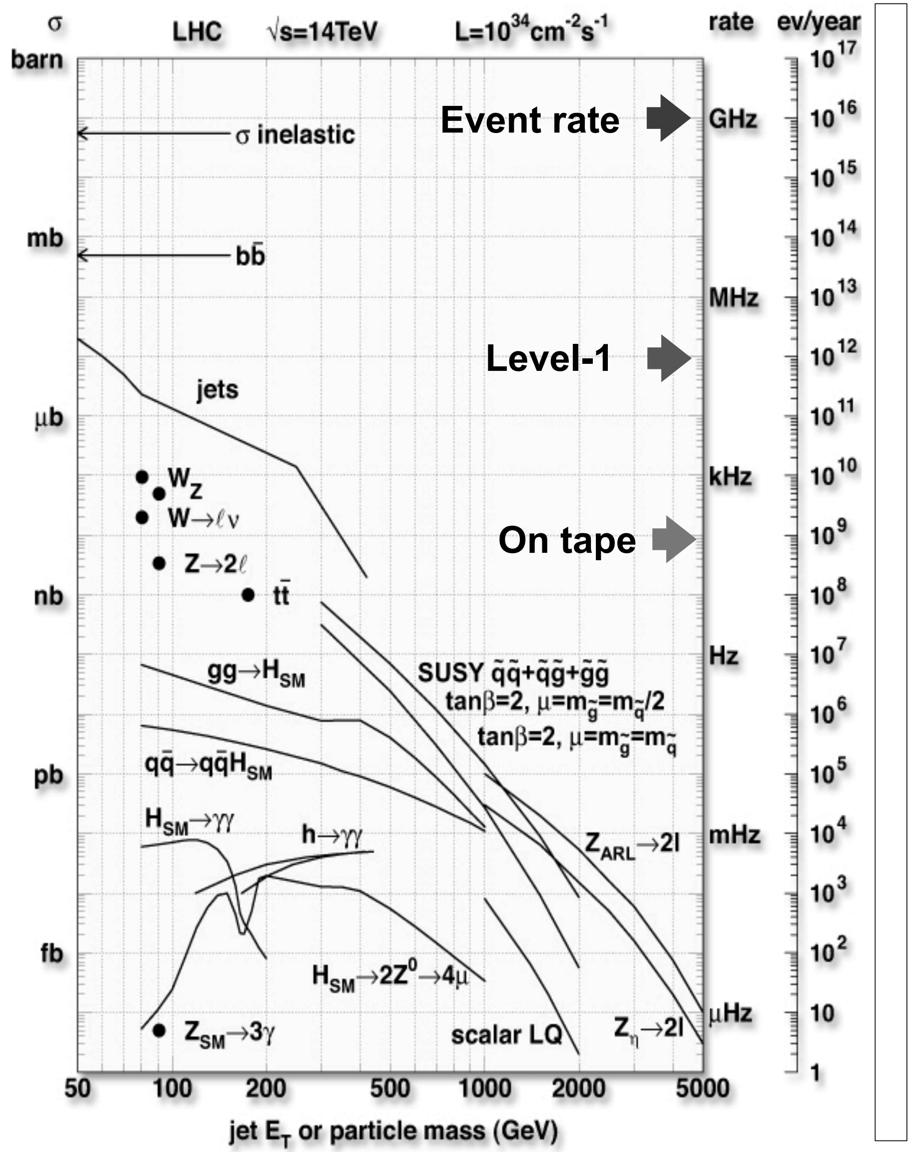

P. Sphicas – 2006 CERN summer student lectures

Time of Flight

LHC collision every 25ns, c=30cm/ns; in 25ns, s=7.5m

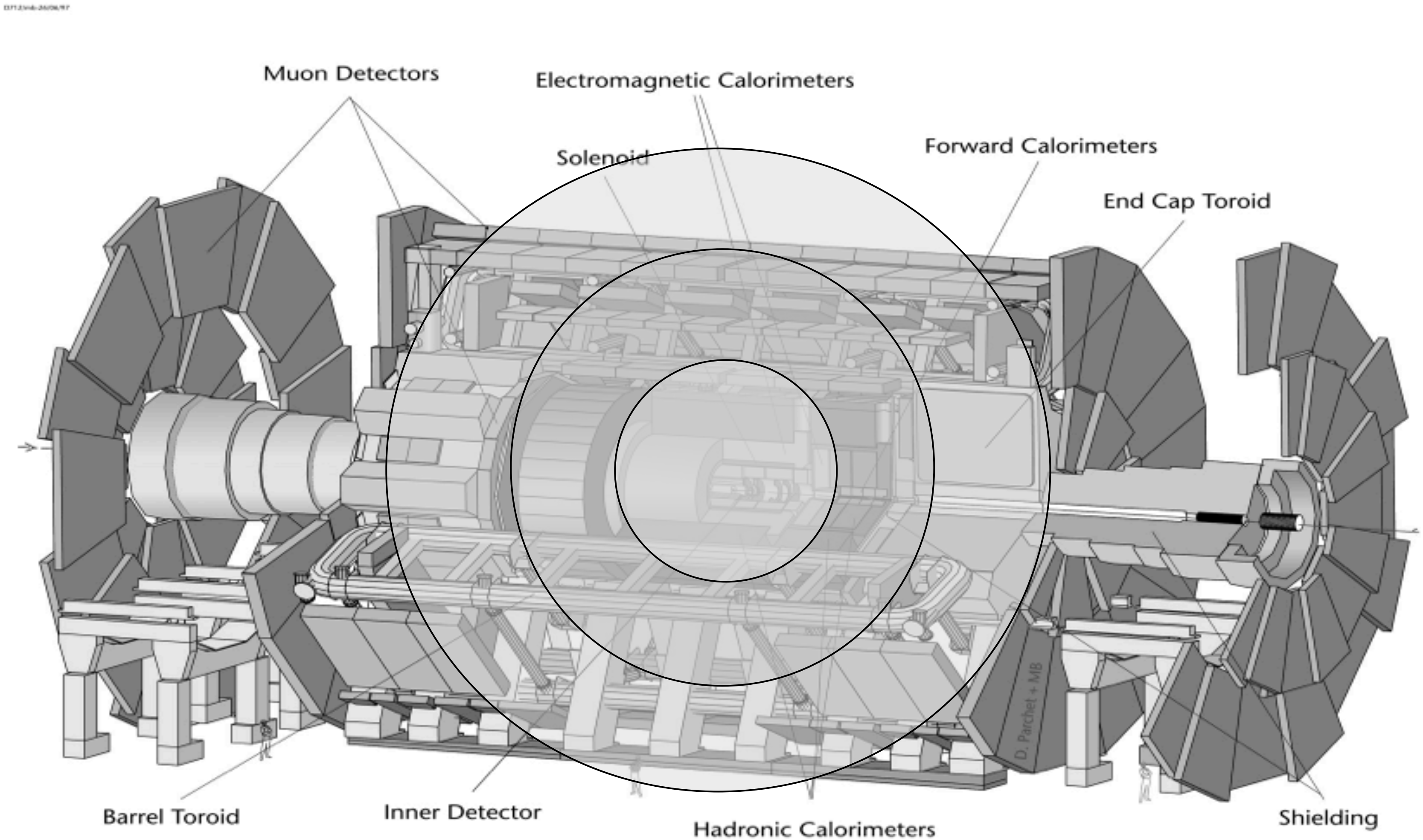

Triggering

Task:

Inspect detector information and provide a first decision on whether to keep the event or throw it out.

Detector data not (all) promptly available → Selection function is highly complex and is evaluated by successive approximations, the so called Trigger Levels.

Task at LHC →
Reduce the 40MHz interaction rate to 100Hz data rate on tape.

Measuring Temperature

A temperature sensor is connected to an Analog to Digital Converter (ADC) which is read out out by a PC.

The PC triggers the readout periodically.

e.g. Periodic Trigger

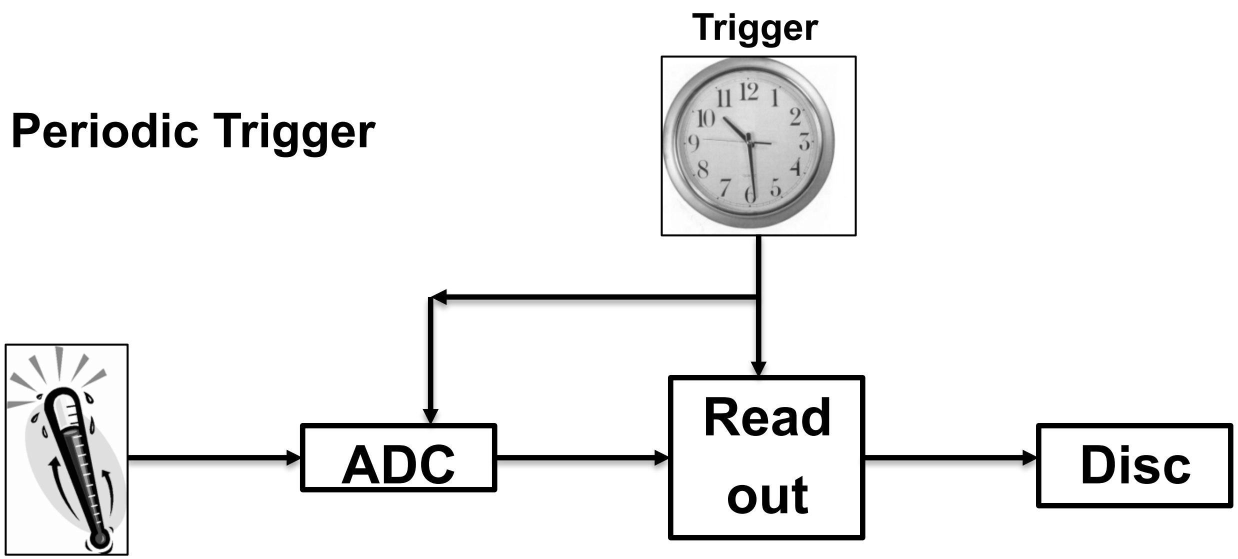

Measuring the β Spectrum

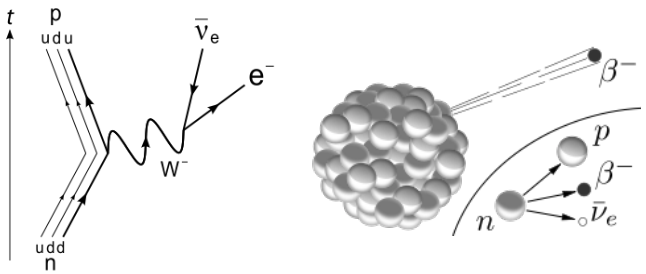

$$n \rightarrow p + e^- + \bar{\nu}_e$$

Trigger Latency

→ the time it takes the trigger to send the decision signal whether to read out or not

→ = the time the information has to be stored before being read out – e.g. delay

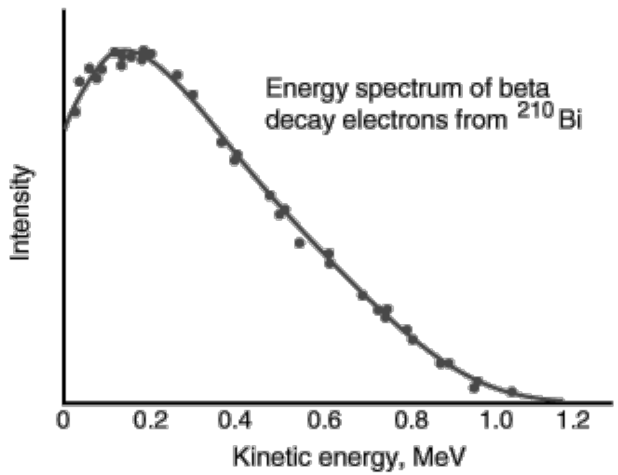

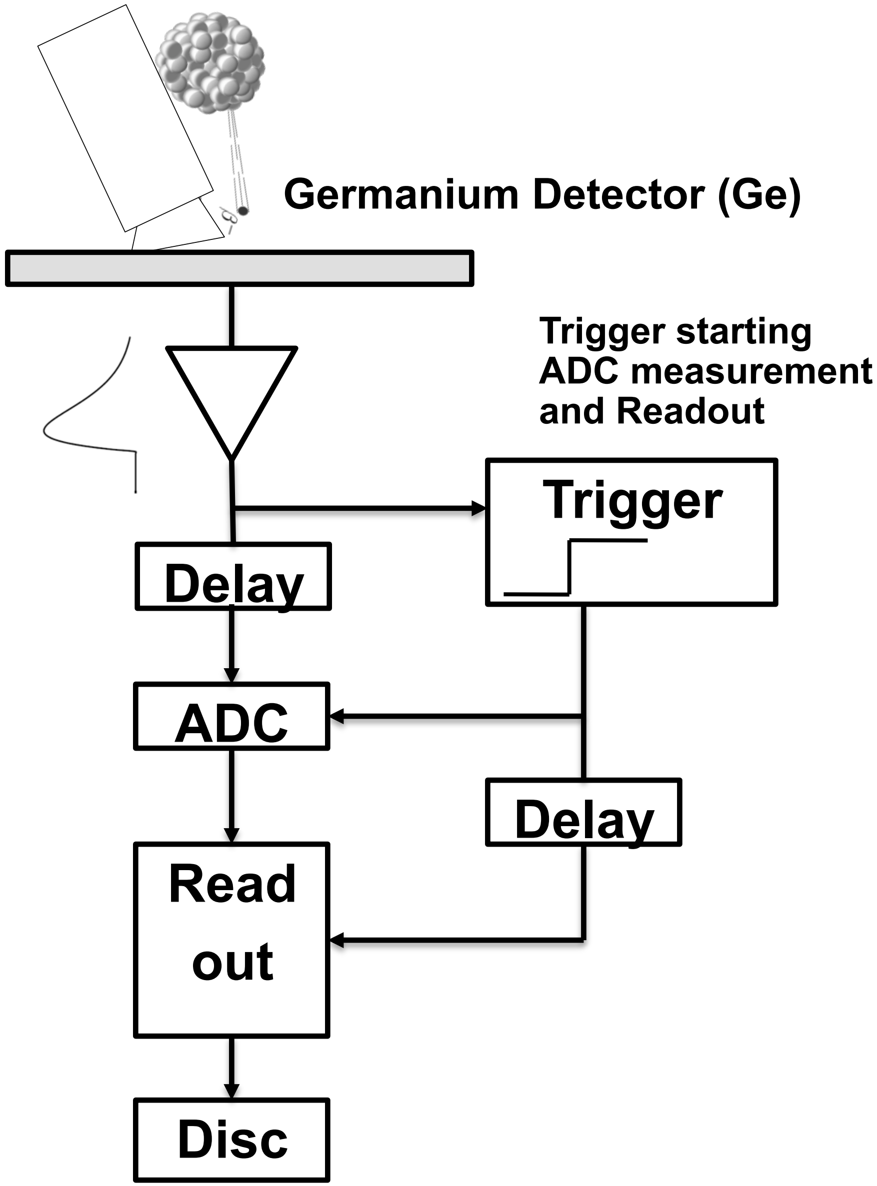

Measuring the β Spectrum

Not only β electrons will enter the detector but also cosmic rays will pass through the detector → background.

Placing a box of scintillators around the detector one can detect the cosmic rays that will traverse the detector, so by requiring the absence of a signal in the scintillator box together with the signal in the Ge detector one can eliminate the cosmic ray background from the measurement.

→ Veto

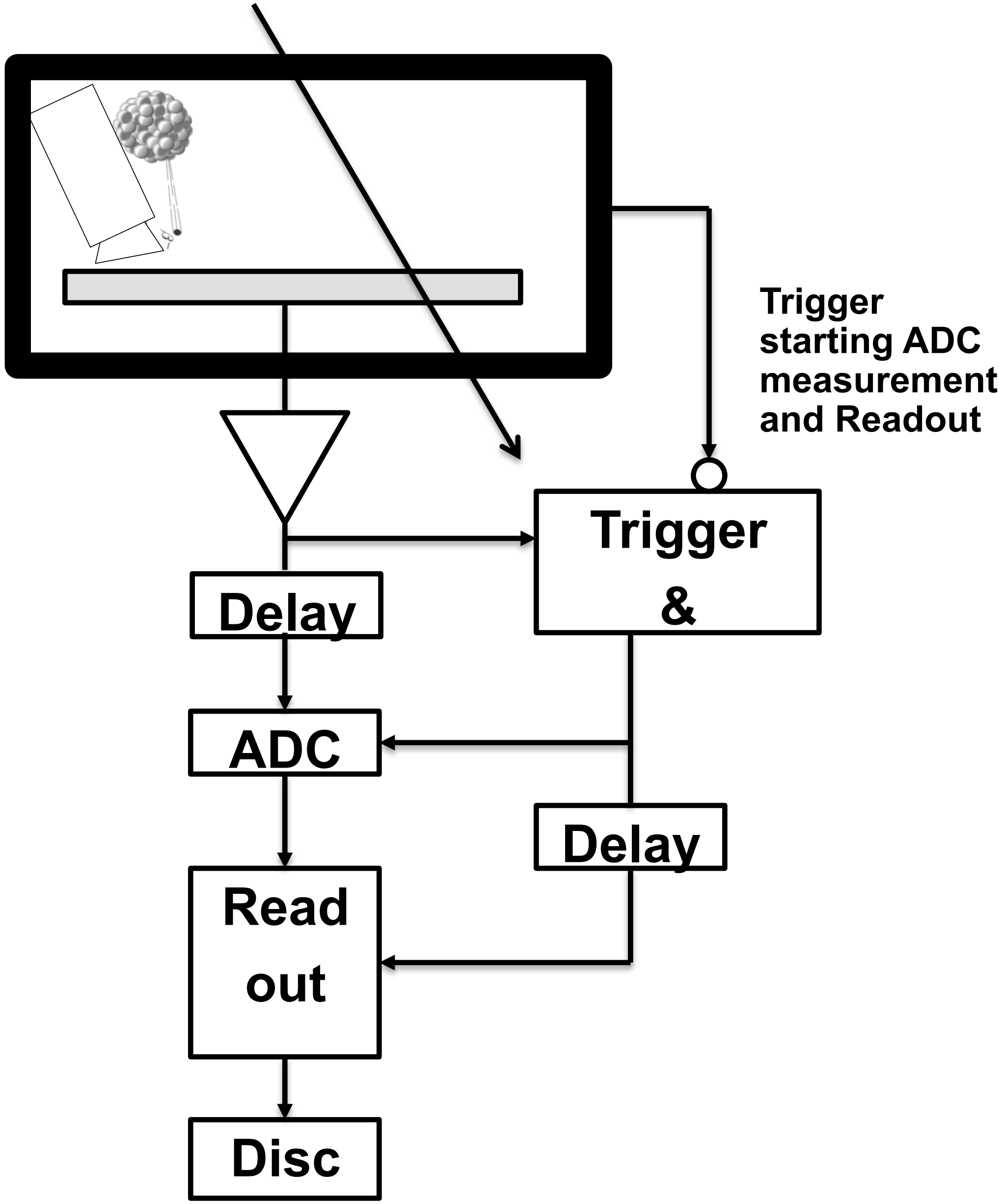

Measuring the Muon Lifetime

$$\mu^- \rightarrow e^- + \bar{\nu}_e + \nu_\mu, \quad \mu^+ \rightarrow e^+ + \nu_e + \bar{\nu}_\mu$$

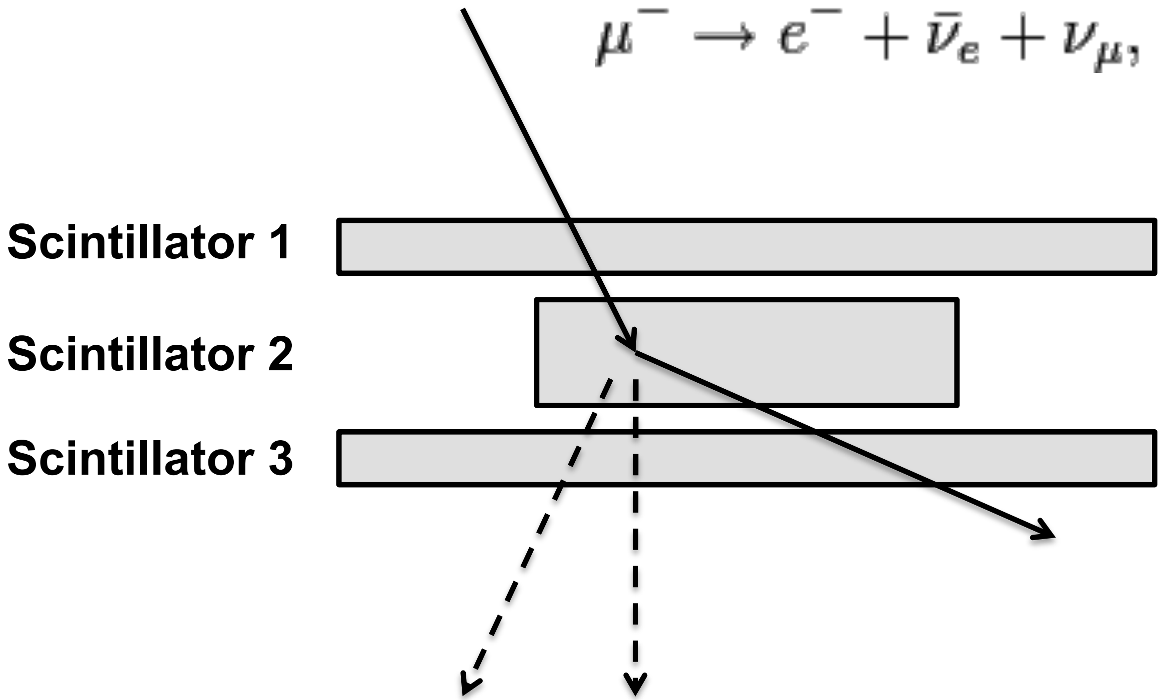

A Cosmic muon enters the setup and gets stuck in S2.

After some time it decays and the electron leaves through.

We start a clock with a coincidence of S1 AND S2 and NOT S3 (in a small time window of e.g. 100ns).

We stop the clock with a coincidence of S2 AND S3 and NOT S1 (in a small time window of e.g. 100ns).

The histogram of the measured times is an exponential distribution with an average corresponding to the muon lifetime.

Measuring the Muon Lifetime

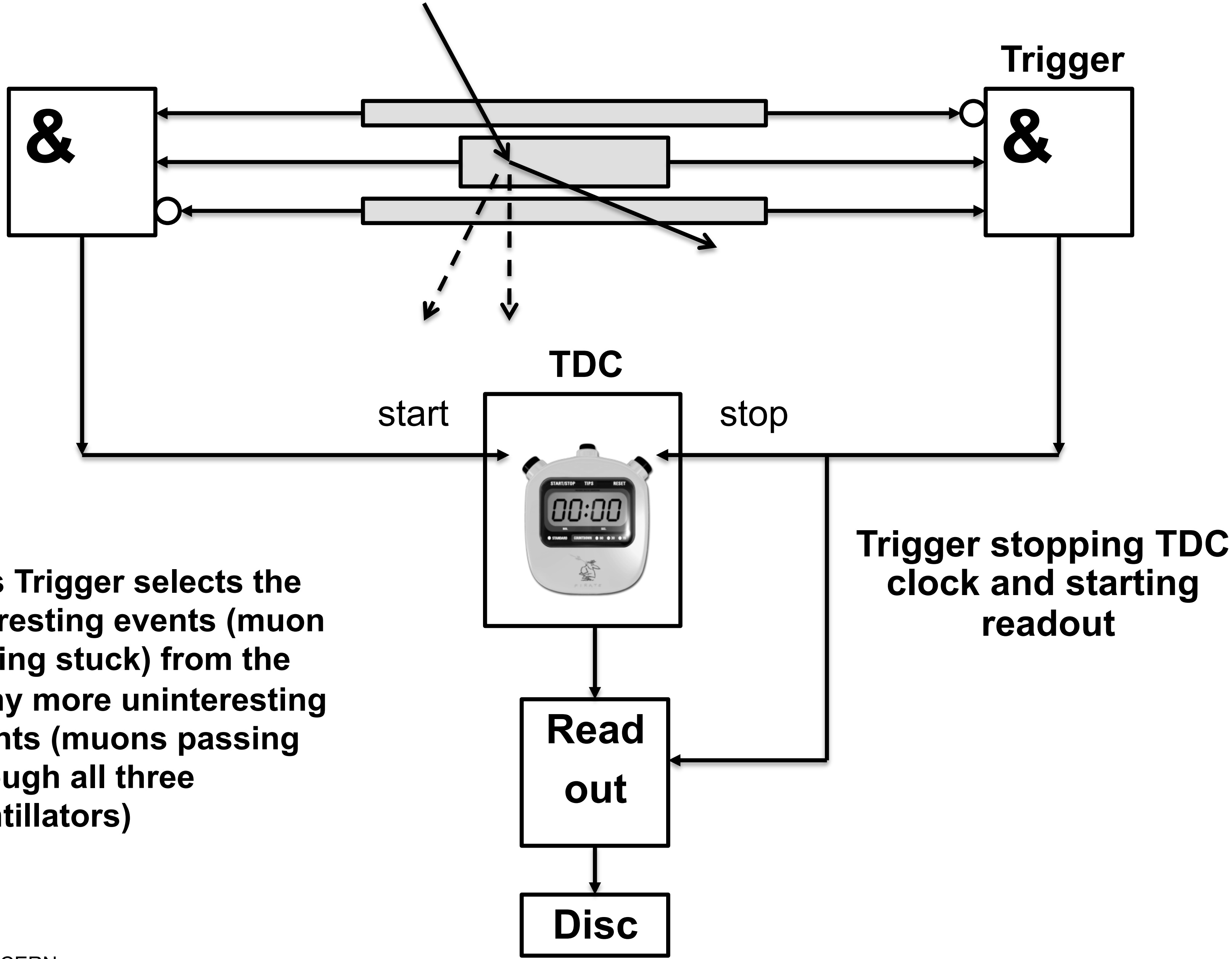

This Trigger selects the interesting events (muon getting stuck) from the many more uninteresting events (muons passing through all three scintillators)

Basic DAQ: periodic trigger

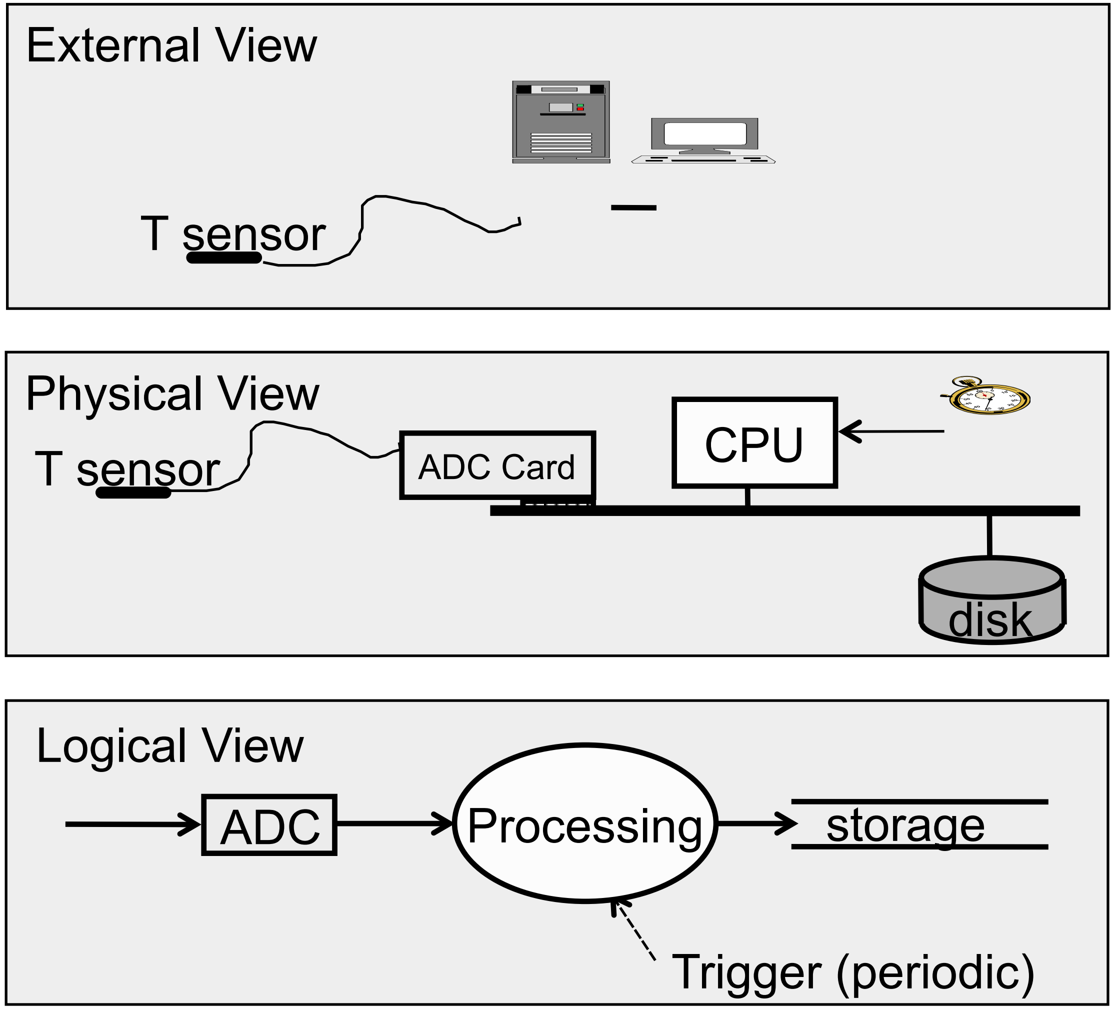

➔ Measure temperature at a fixed frequency

➔ The system is clearly limited by the time to process an "event"

➔ Example τ =1ms to

- ADC conversion +CPU processing +Storage

➔ Sustain ~1/1ms=1kHz ***periodic trigger*** rate

Basic DAQ: real trigger

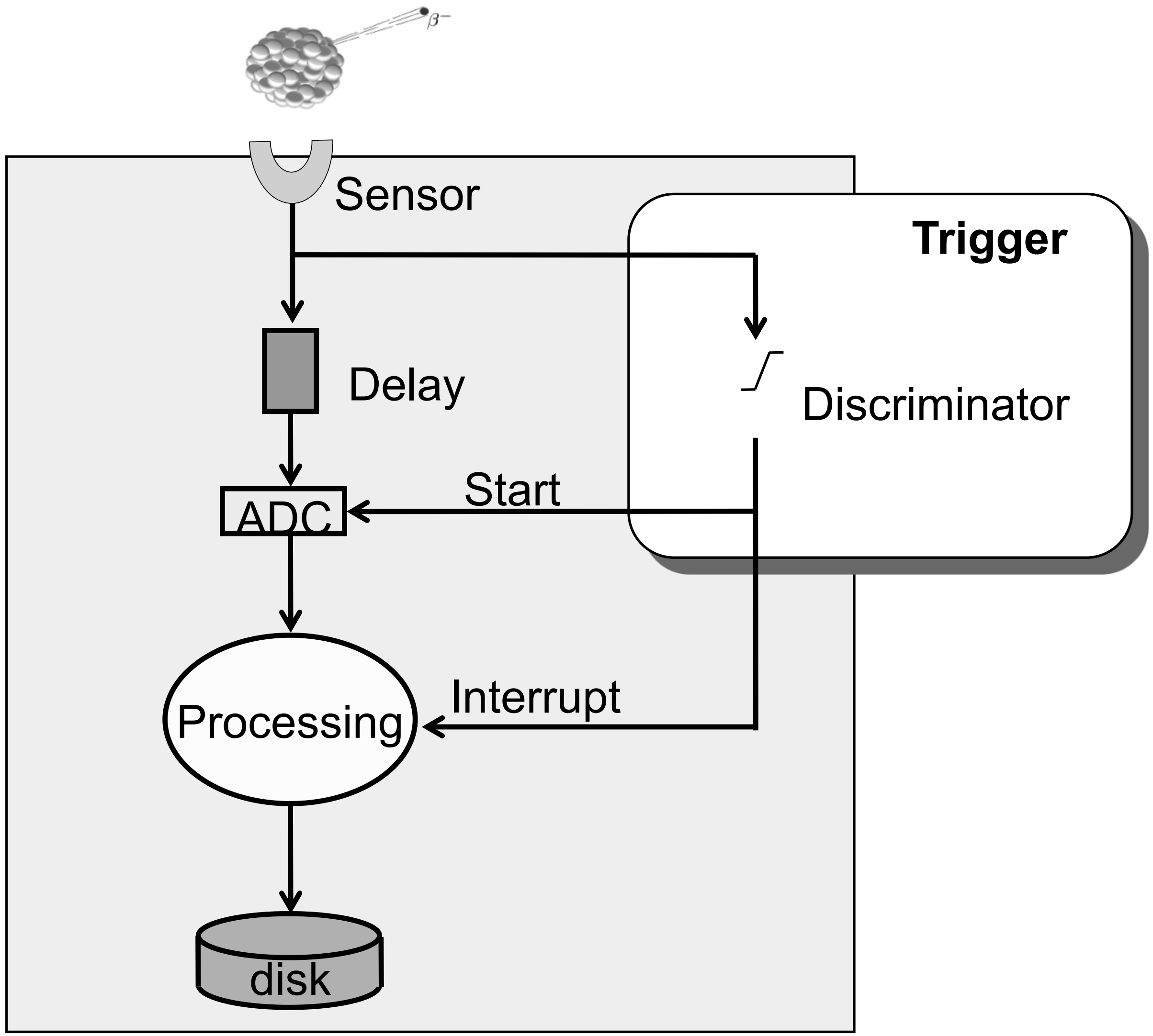

- ➔ Measure β decay properties
- ➔ Events are asynchronous and unpredictable
  - Need a **physics** trigger
- ➔ Delay compensates for the trigger latency

Basic DAQ: real trigger

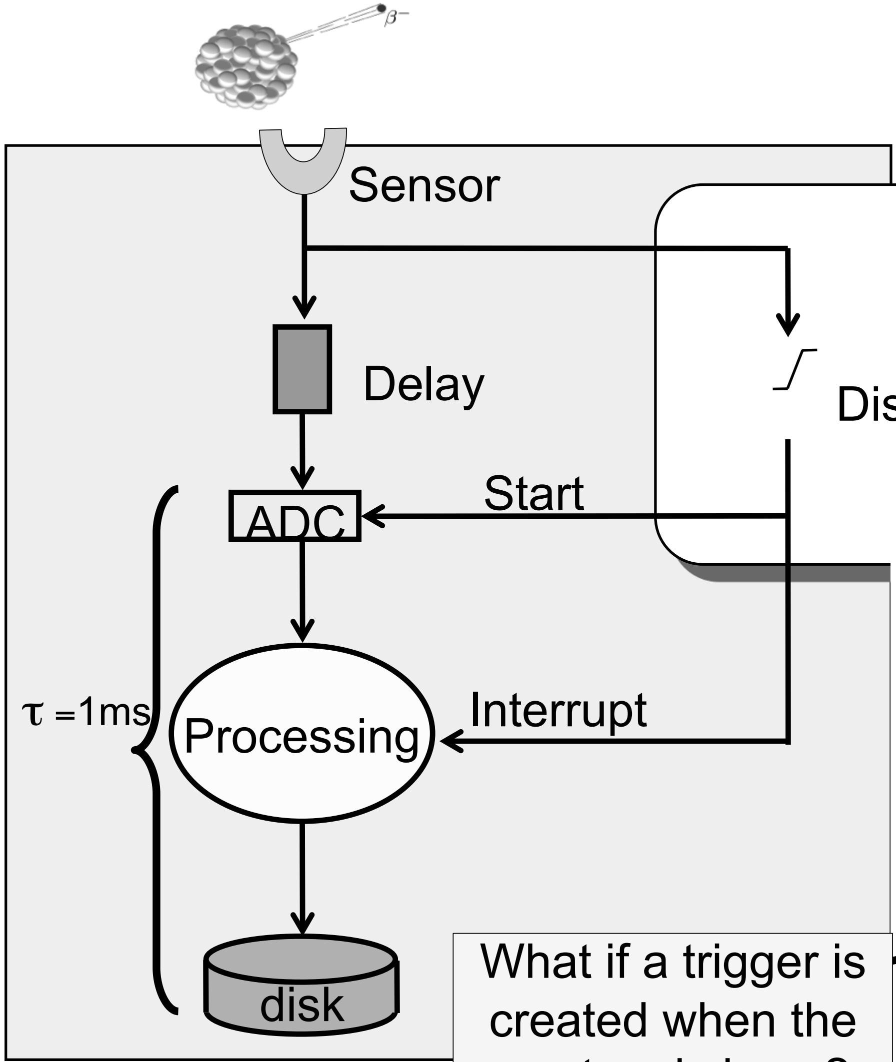

- ➔ Measure β decay properties
  - Need a **physics** trigger
- ➔ <u>Stochastic</u> process

Probability of time (in ms) between events for average decay rate of f=1kHz → τ =1ms

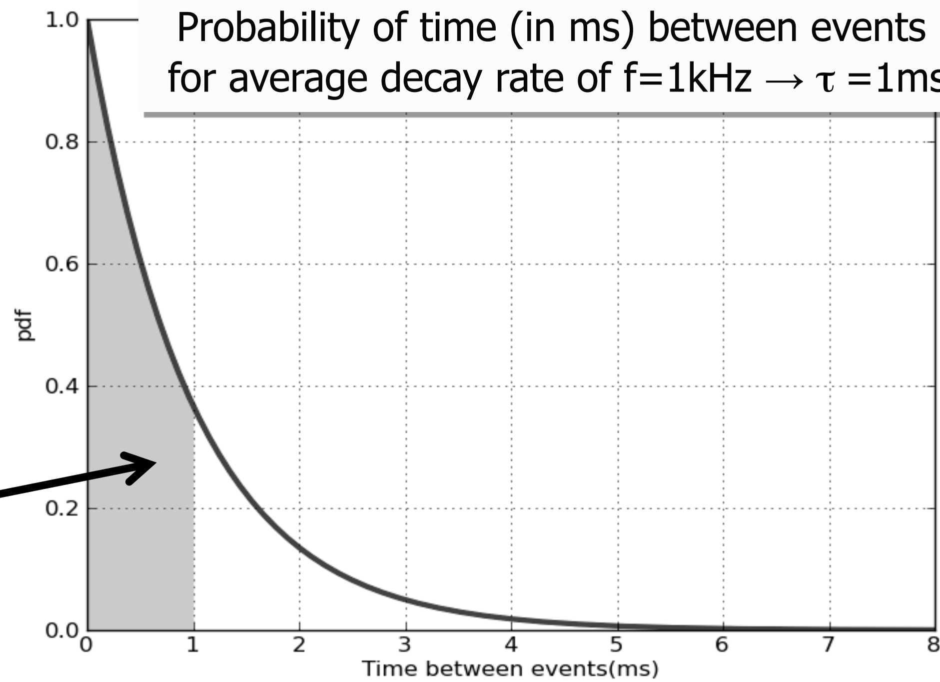

What if a trigger is created when the system is busy?

Basic DAQ: real trigger & busy logic

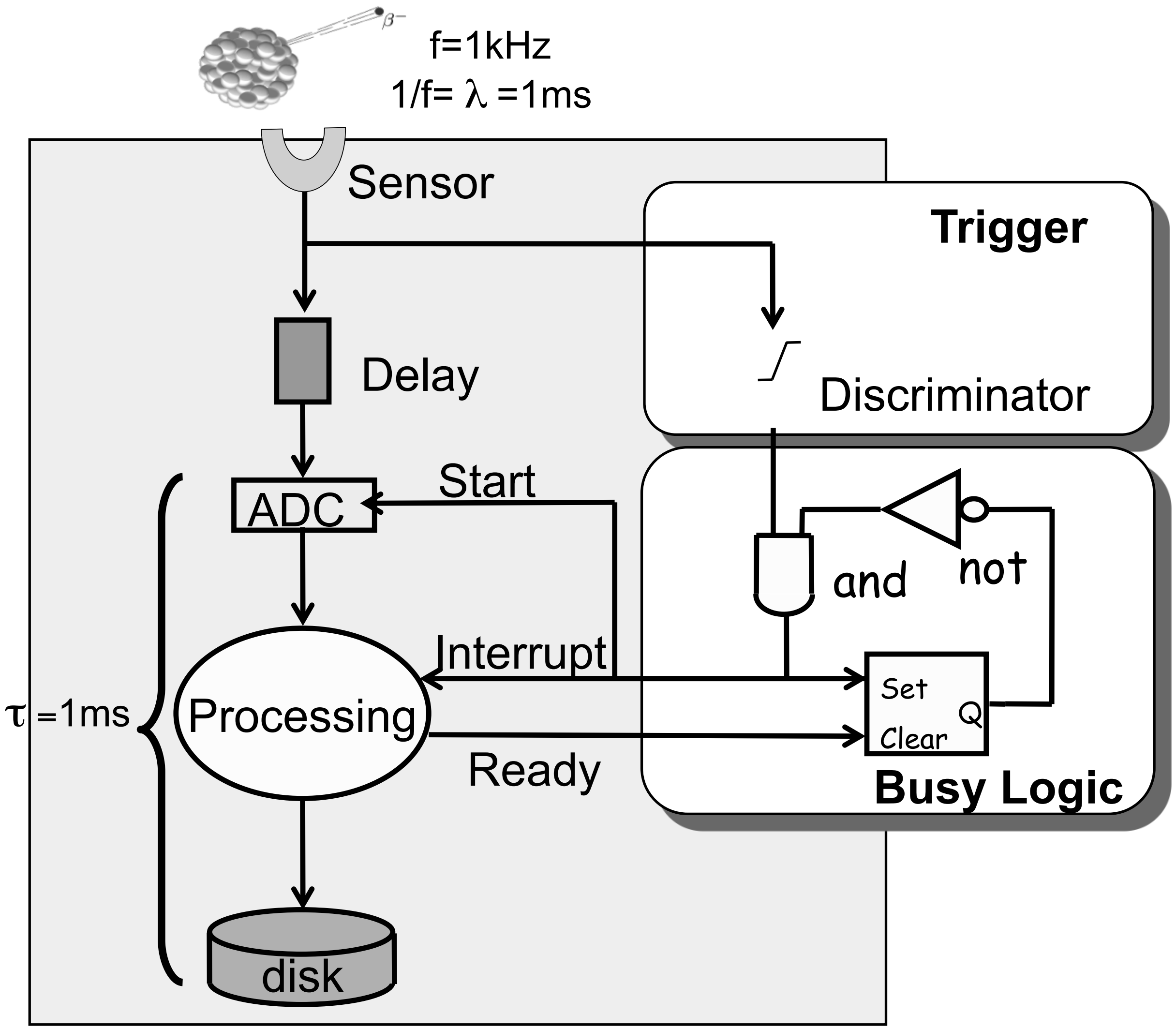

- ➔ Busy logic avoids triggers while processing
- ➔ Which (average) DAQ rate can we achieve now?
  - Reminder: τ=1ms was sufficient to run at 1kHz <u>with a clock trigger</u>

DAQ Deadtime & Efficiency (1)

Define ν as average DAQ frequency

$\nu\tau \rightarrow$ DAQ system is busy - $(1 - \nu\tau) \rightarrow$ DAQ system is free

$$f(1 - \nu\tau) = \nu \rightarrow \nu = \frac{f}{1 + f\tau} < f$$

$$\epsilon = \frac{N_{saved}}{N_{tot}} = \frac{1}{1 + f\tau} < 100\%$$

➔ Define DAQ deadtime (d) as the ratio between the time the system is busy and the total time. In our example d=0.1%/Hz

➔ Due to the fluctuations introduced by the stochastic process the efficiency will always be less 100%

- In our specific example, d=0.1%/Hz, f=1kHz → ν=500Hz, ε=50%

DAQ Deadtime & Efficiency (2)

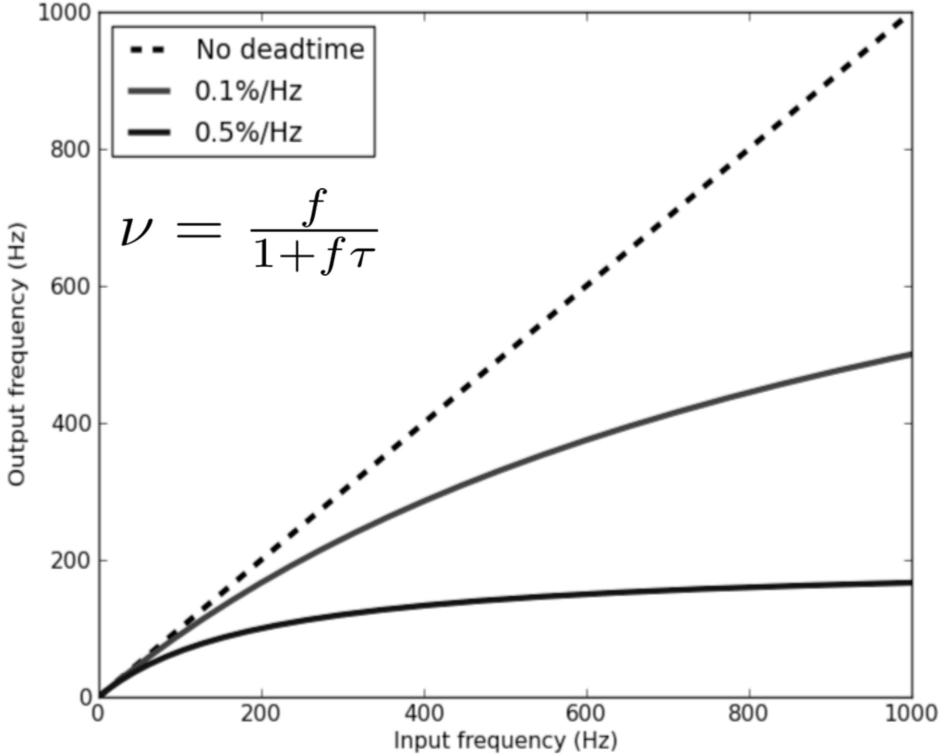

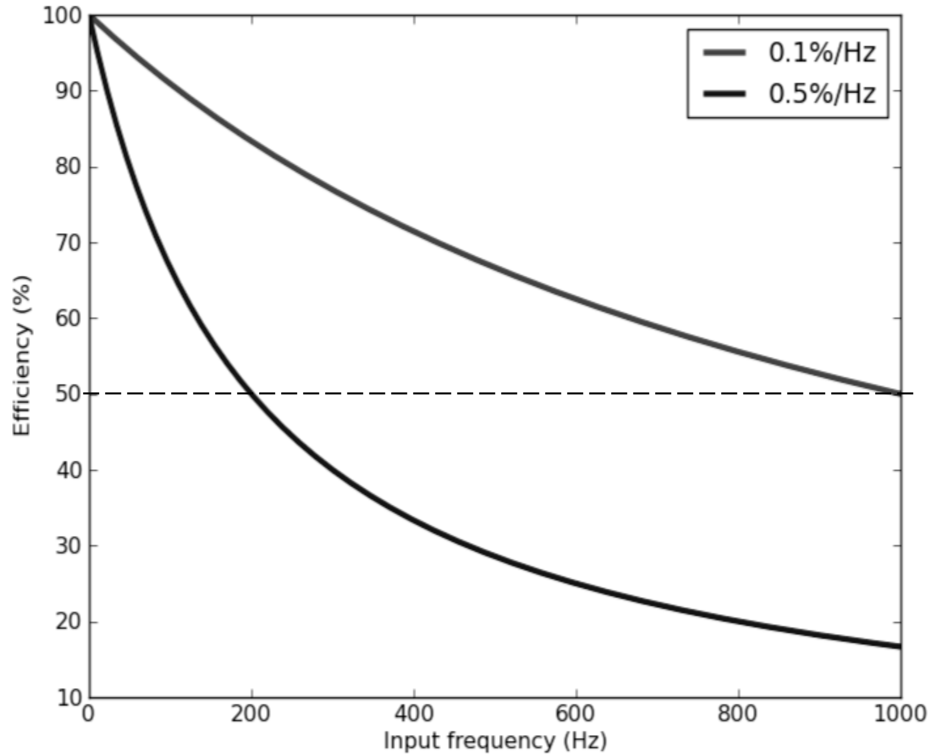

➔ If we want to obtain ν~f (ϵ~100%) → fτ<<1 → τ<<λ

- f=1kHz, ϵ=99% → τ<0.1ms → 1/τ>10kHz

➔ In order to cope with the input signal fluctuations, we have to over-design our DAQ system by a factor 10. <u>This is very inconvenient!</u> Can we mitigate this effect?

Basic DAQ: De-randomization

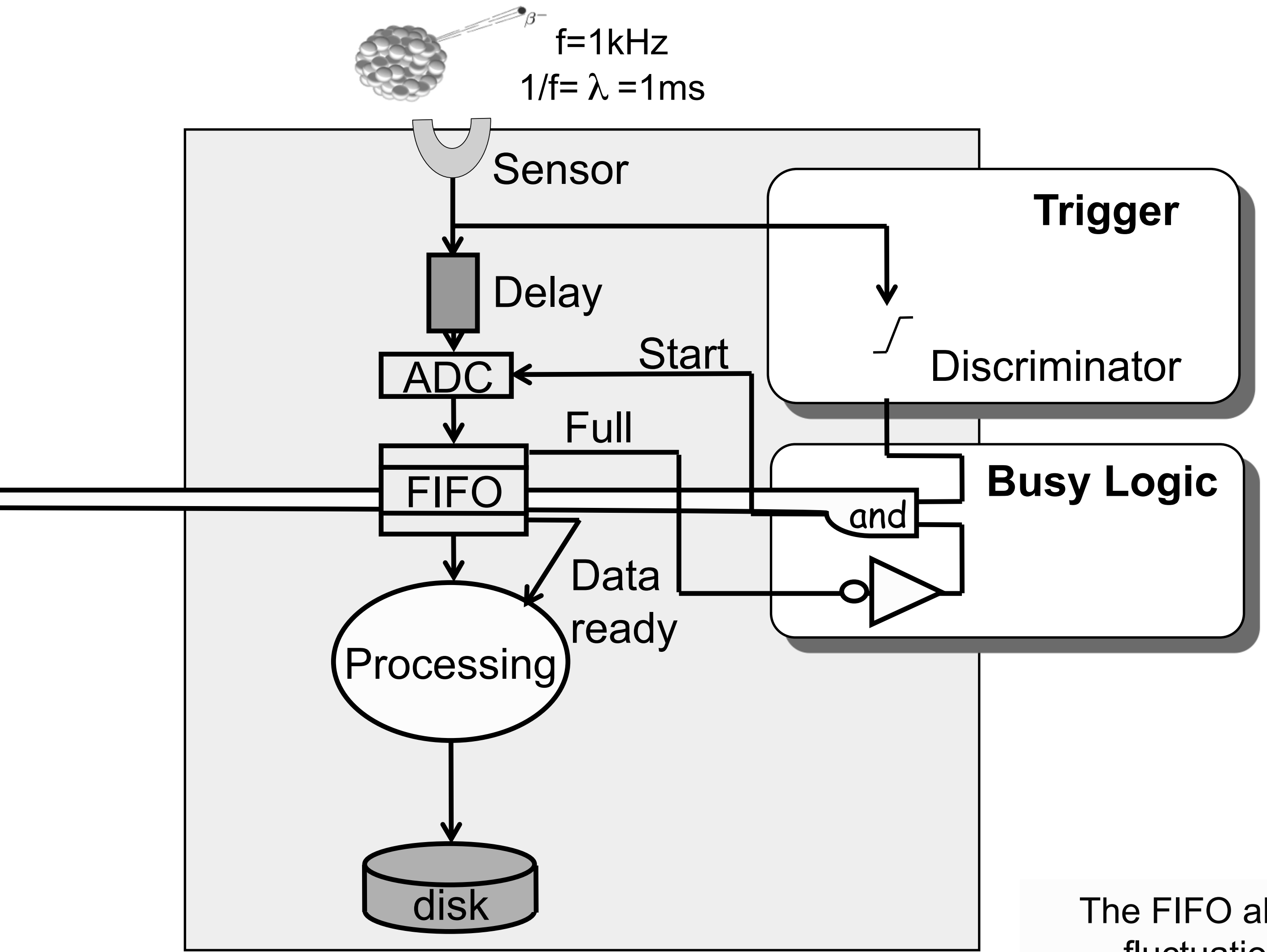

➔ First-In First-Out

- Buffer area organized as a queue
- Depth: number of cells
- Implemented in HW and SW

➔ FIFO introduces an additional latency on the data path

The FIFO absorbs and smooths the input fluctuation, providing a ~steady (De-randomized) output rate

De-randomization: queuing theory

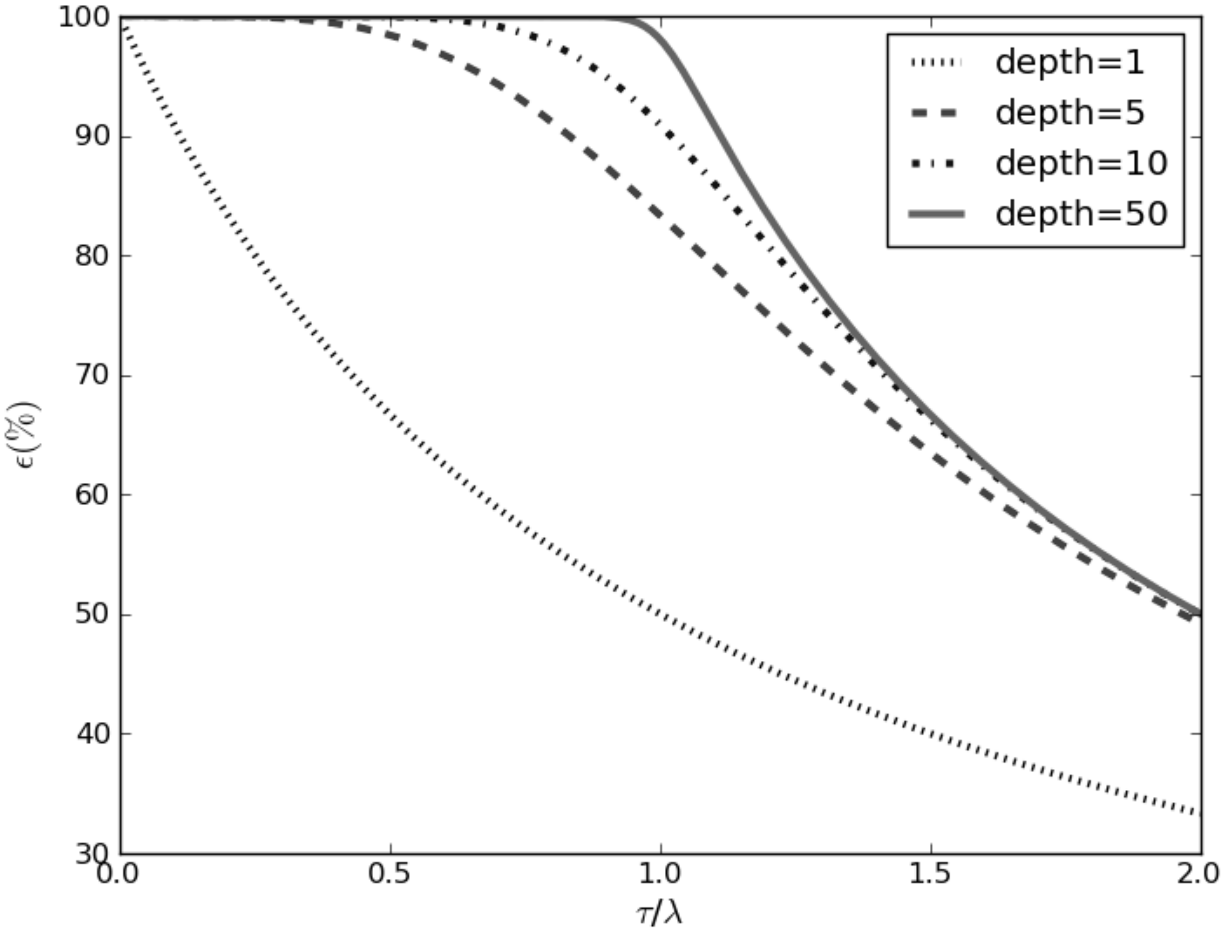

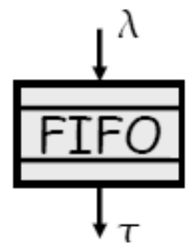

➔ We can now attain a FIFO efficiency ~100% with $\tau \sim \lambda$

- Moderate buffer size

Analytic calculation possible for very simple systems only. Otherwise simulations must be used.

De-randomization: summary

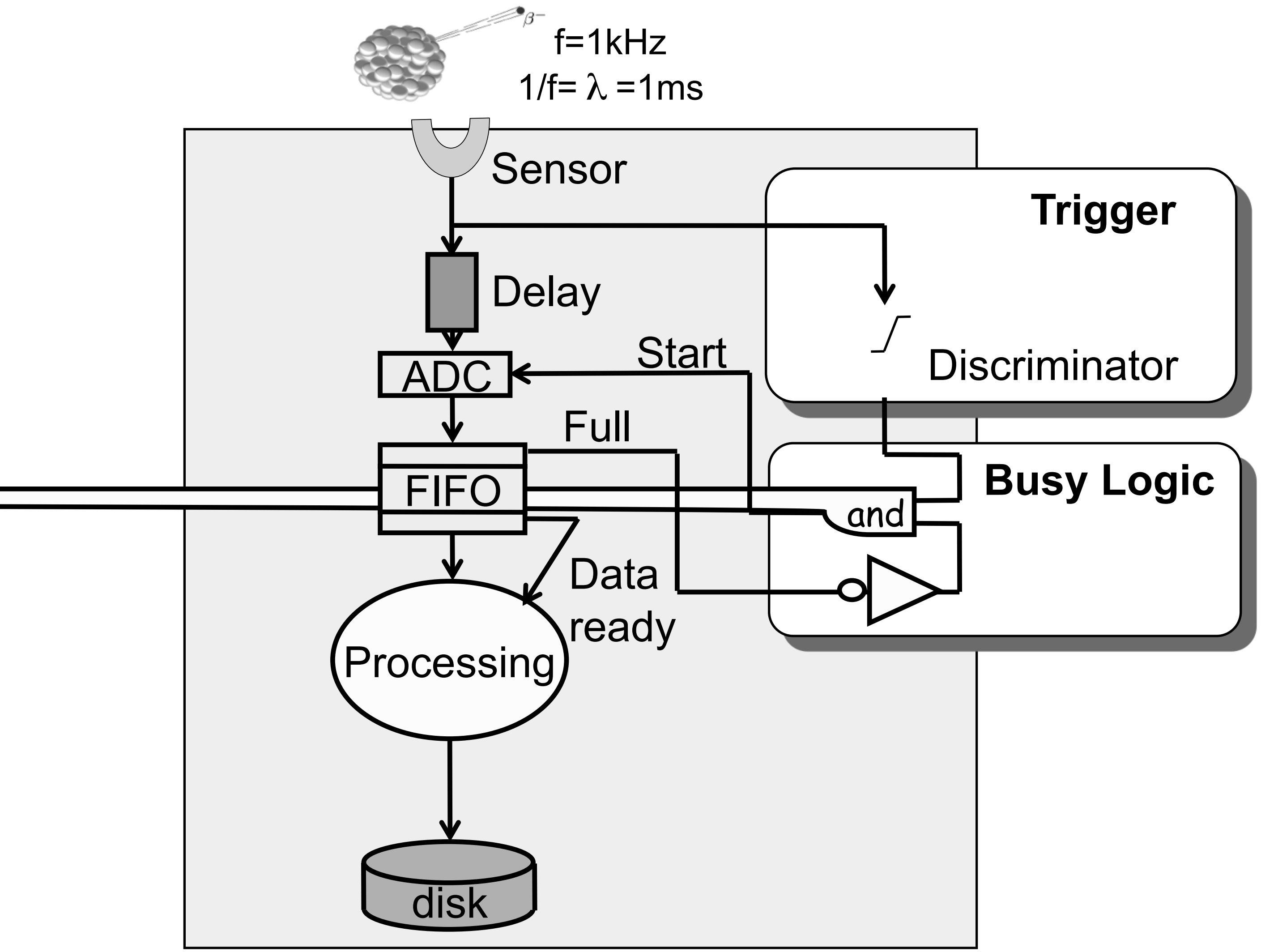

➔ Almost 100% efficiency and minimal deadtime are achieved if

- ADC is able to operate at rate >>f
- Data processing and storing operates at ~f

➔ The FIFO decouples the low latency front-end from the data processing

- Minimize the amount of "unnecessary" fast components

➔ Could the delay be replaced with a "FIFO"?

- Analog pipelines → Heavily used in LHC DAQs

De-randomization: summary

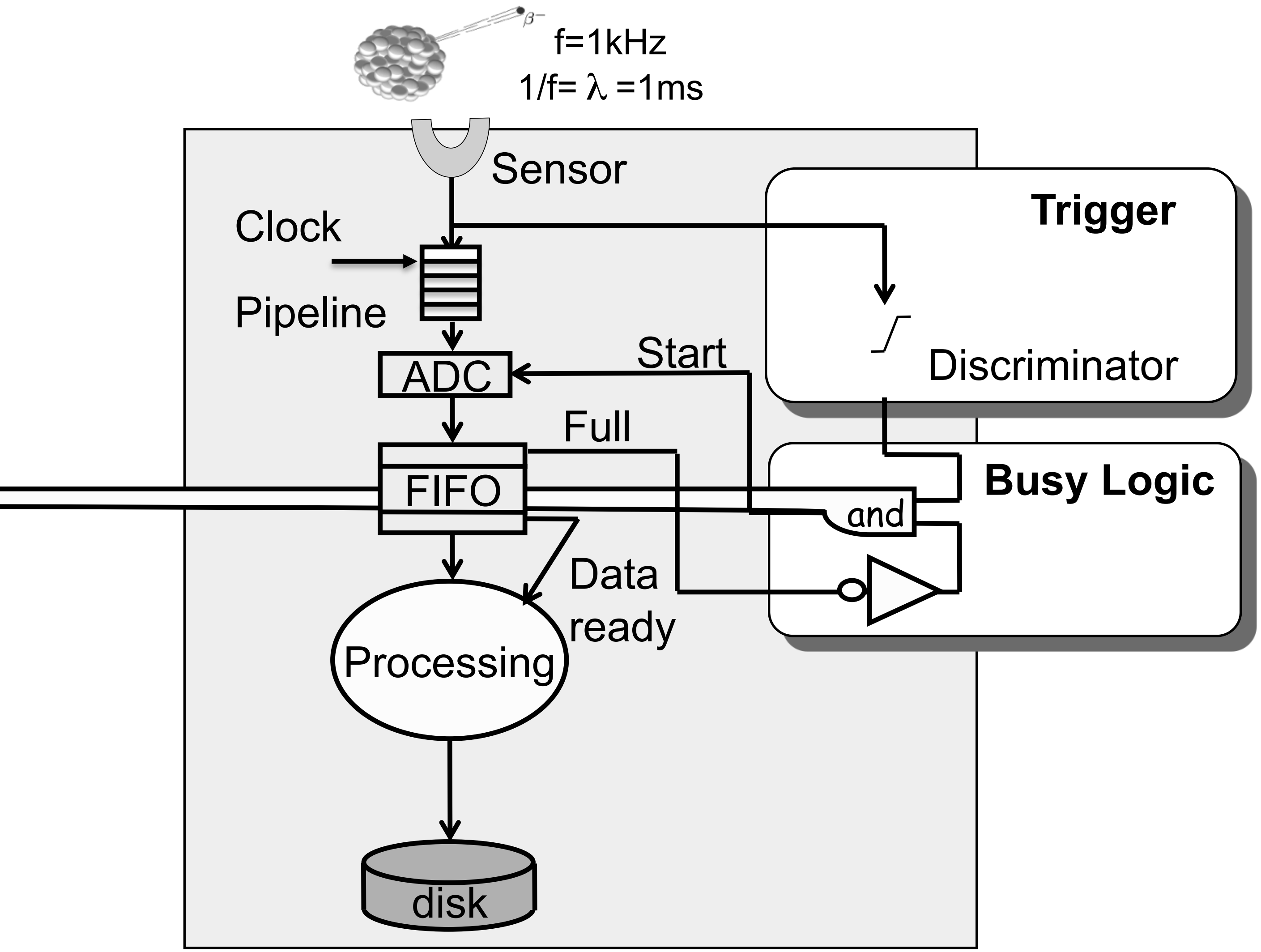

- **Analog pipelines → Heavily used in LHC DAQs**

Basic DAQ: collider mode

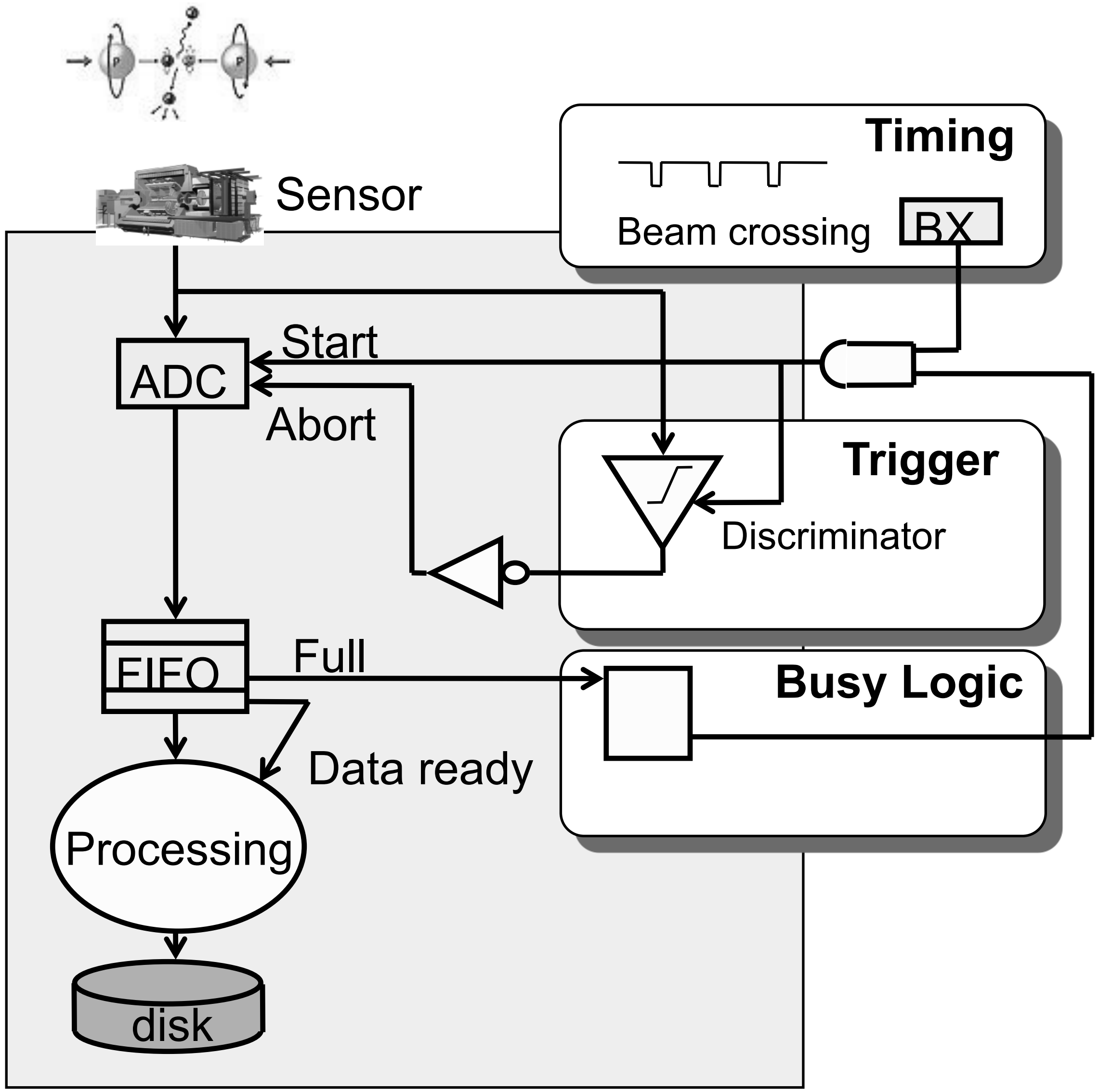

- ➔ Particle collisions are synchronous
- ➔ Trigger rejects uninteresting events
- ➔ Even if collisions are synchronous, the triggers (i.e. good events) are unpredictable
- ➔ De-randomization is still needed

Readout and Data Acquisition

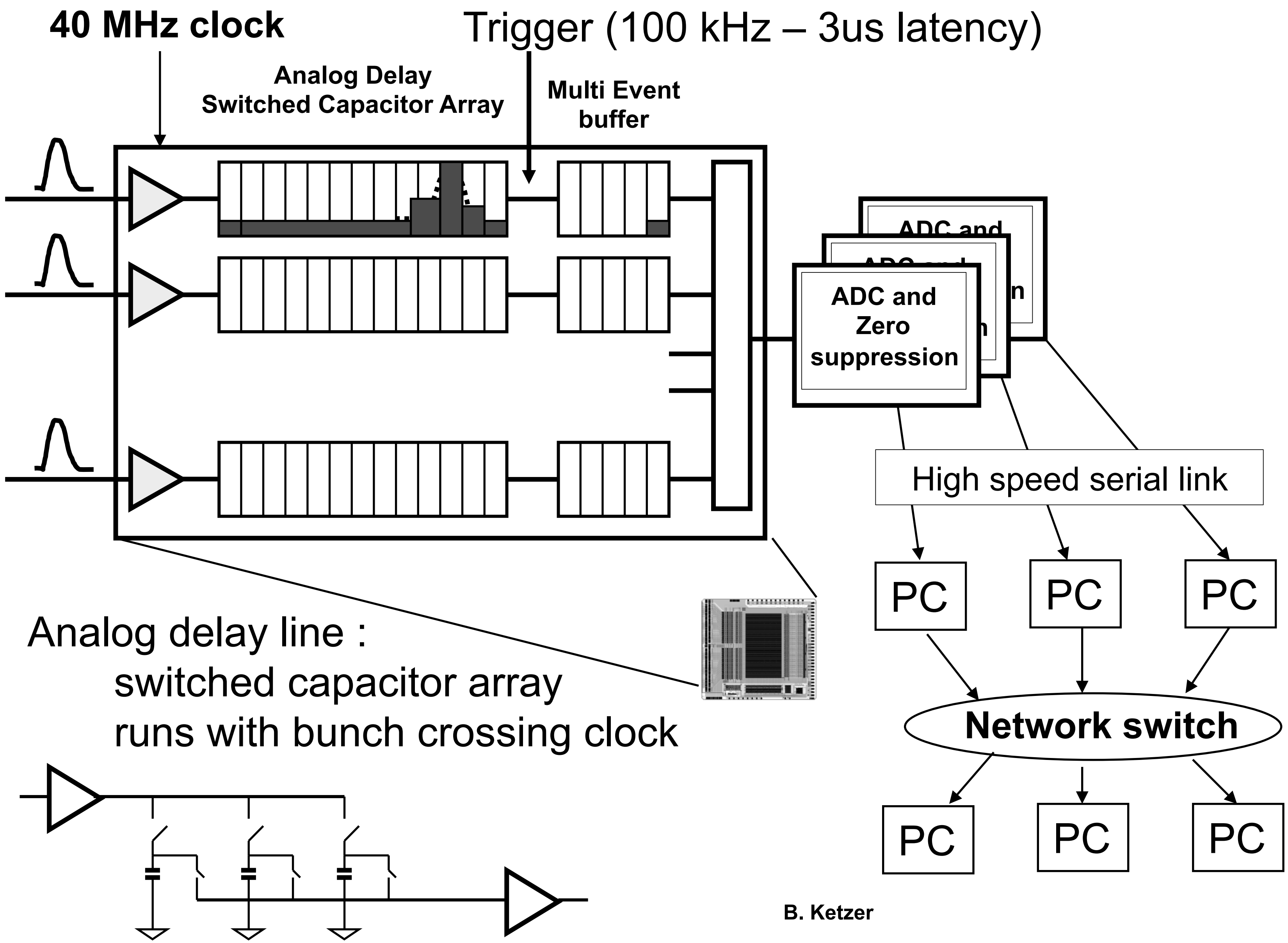

B. Ketzer

Readout and Data Acquisition

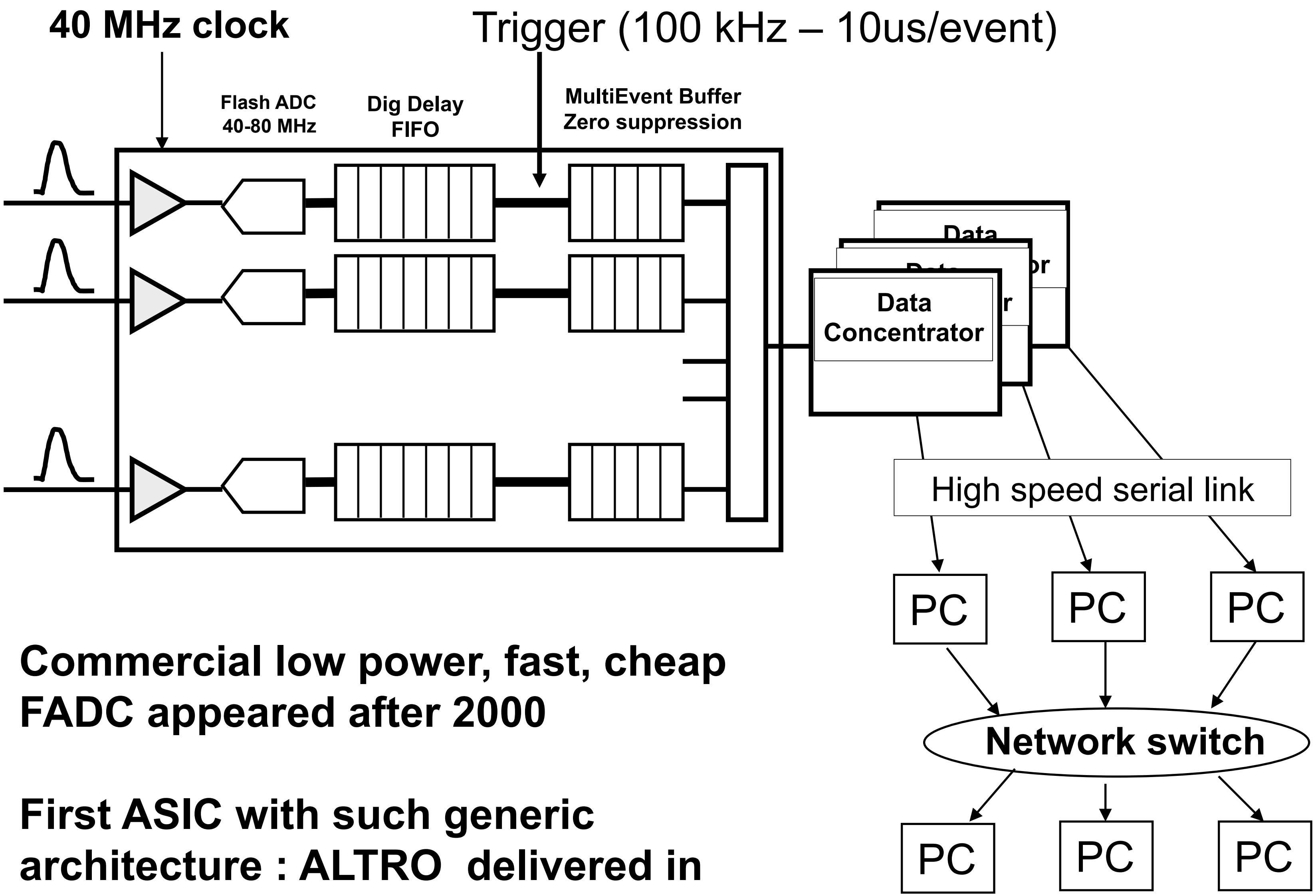

Commercial low power, fast, cheap FADC appeared after 2000

First ASIC with such generic architecture : ALTRO delivered in 2003

B. Ketzer

ALTRO EVOLUTION

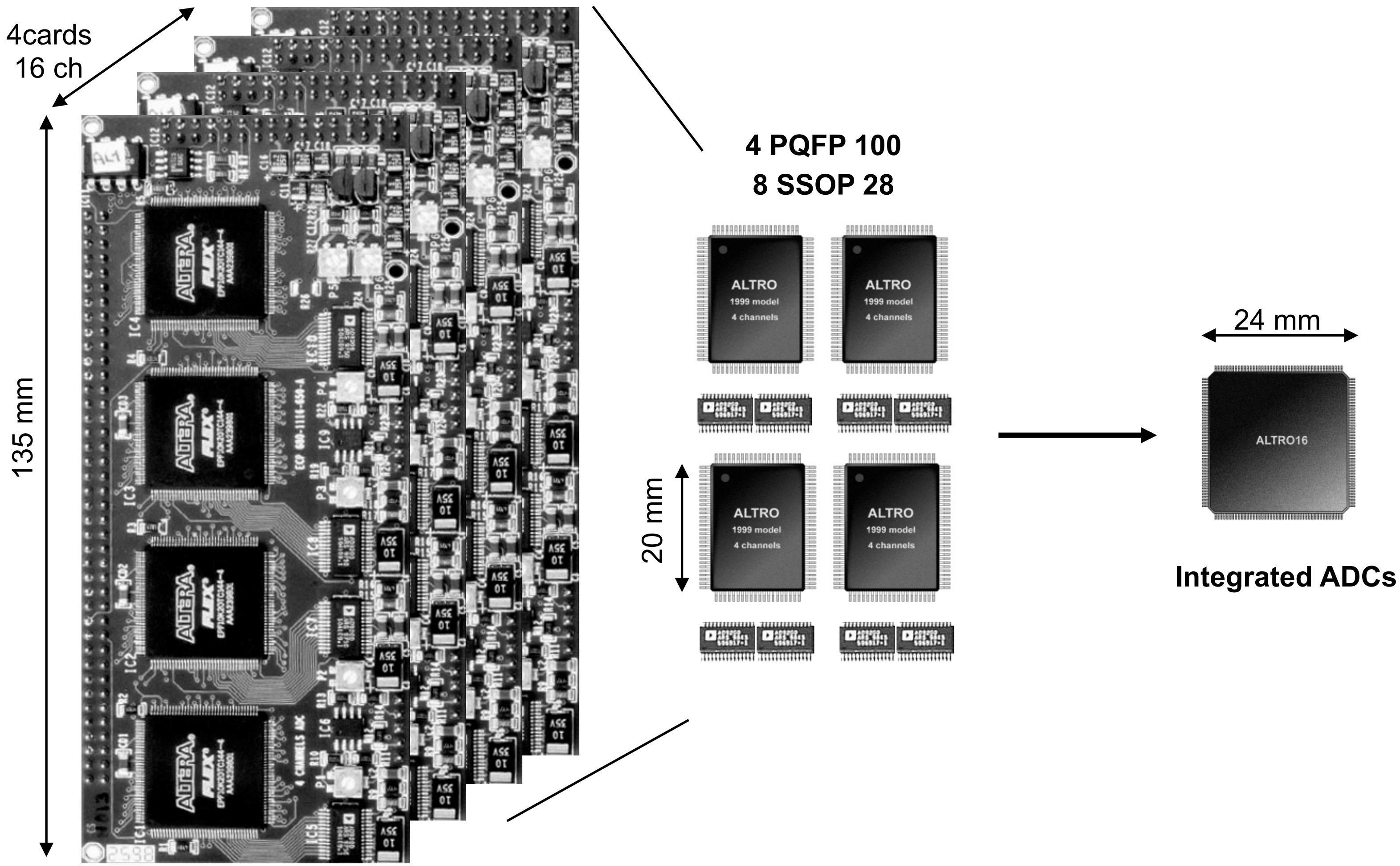

	1998	1999	2001
CHANNELS / CHIP:	1	4	1
POWER / CH:	120mW	80mW	16mW
PRICE / CH:	50CHF	8CHF	5CHF

Multi-Level Trigger

Level "0": Event rate: 10^9 Hz. Detector channels: 10^7 - 10^8
DAQ is running constantly at 40 MHz. Data flow ≈ 10^{16} bit/sec

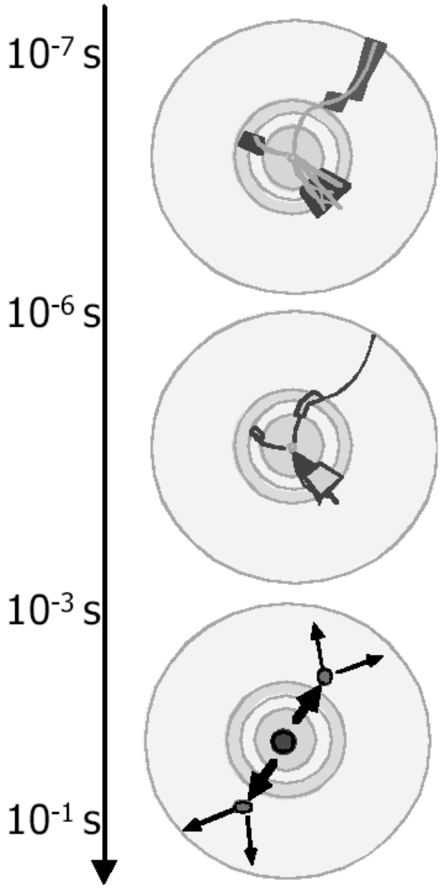

Level-1 trigger: coarse selection of interesting candidate events within a few μs. L1-rigger output rate ≈ 100 kHz
Implementation: specific hardware (ASICS, FPGA, DSP)

Level-2 trigger: refinement of selection criteria within ≈ 1 ms.
L2 output rate: ≈ 1 kHz
Implementation: fast processor farms.

Level-3 trigger: identification of the physical process. Writing data to storage medium.
L3- output rate: 10 - 100 Hz
Event size: ≈ 1 Mbyte.
Implementation: fast processor farms.

ATLAS, LHCb

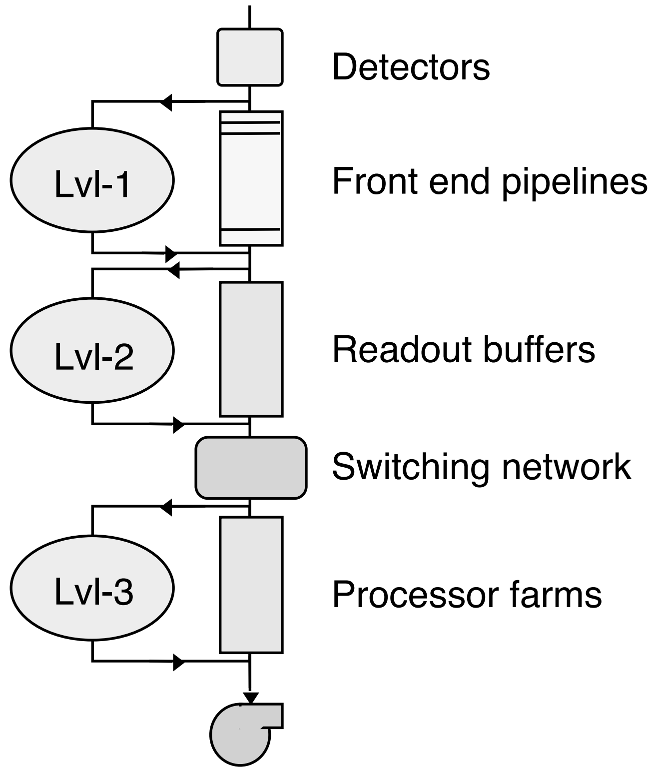

Trigger/DAQ parameters: summary

	No.Levels Trigger	Level-1 Rate (Hz)	Event Size (Byte)	Readout Bandw.(GB/s)	Filter Out MB/s (Event/s)
ATLAS 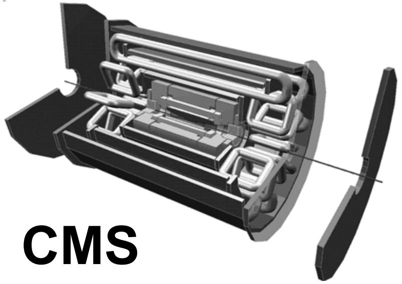	**3**	**10^5** LV-2 **10^3**	**10^6**	**10**	**100** (10^2)
CMS 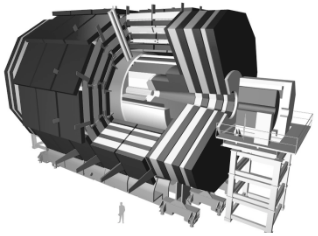	**2**	**10^5**	**10^6**	**100**	**100** (10^2)
LHCb 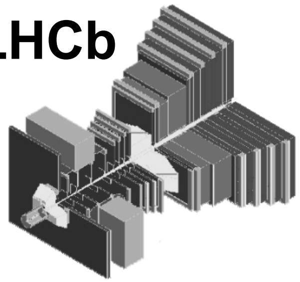	**3**	LV-0 **10^6** LV-1 **$4\ 10^4$**	**$2\text{x}10^5$**	**4**	**40** ($2\text{x}10^2$)
ALICE 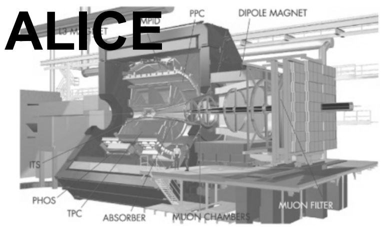	**4**	Pp-Pp **500** p-p **10^3**	**$5\text{x}10^7$** **$2\text{x}10^6$**	**5**	**1250** (10^2) **200** (10^2)

Trigger/DAQ systems: present & future

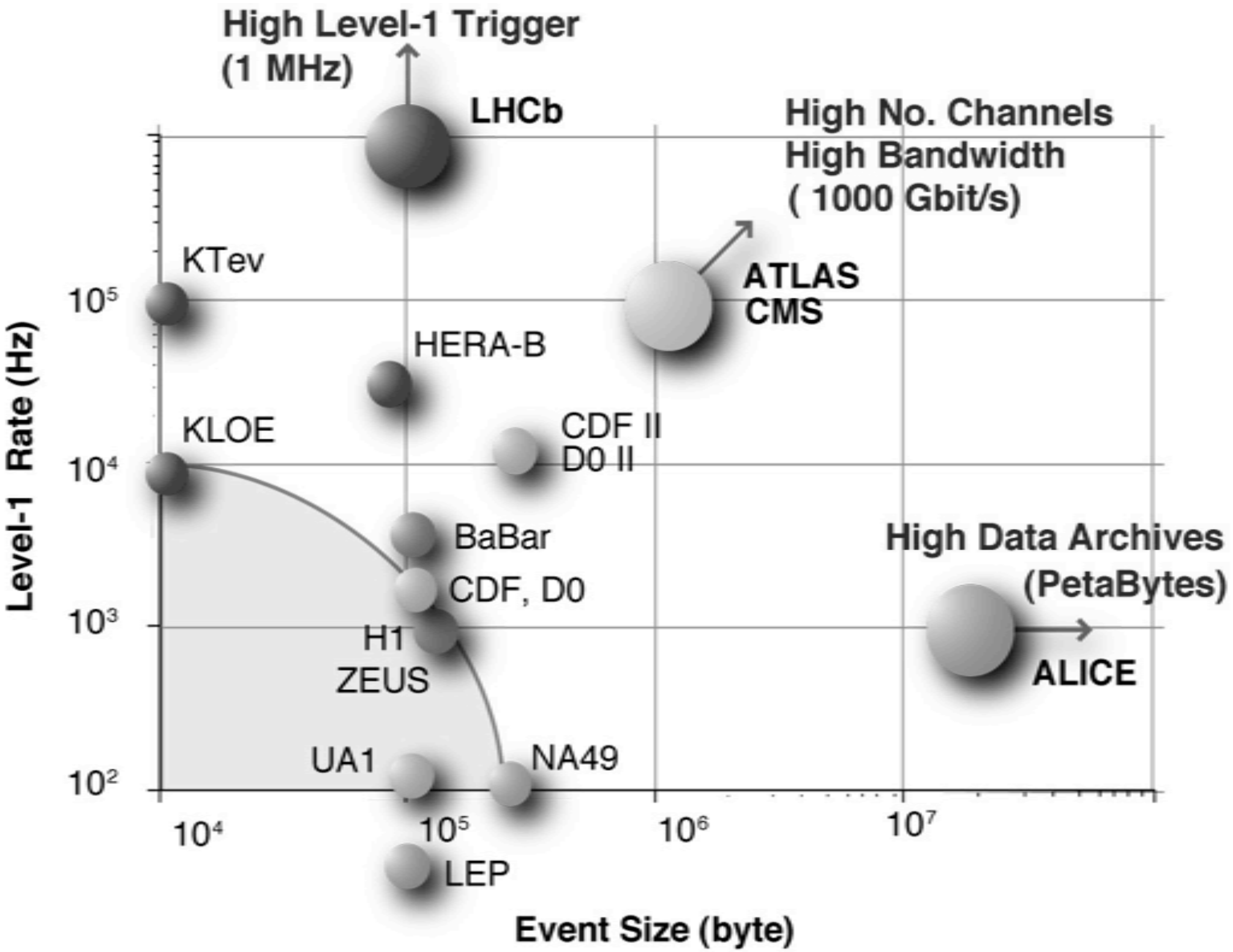

Future DAQ Architectures

Trigger-less DAQ: **PANDA, CBM, ILC**

- **no electrical or optical trigger signal to FEE**
- **each channel detects signal ⇨ time stamps it ⇨ sends it out**

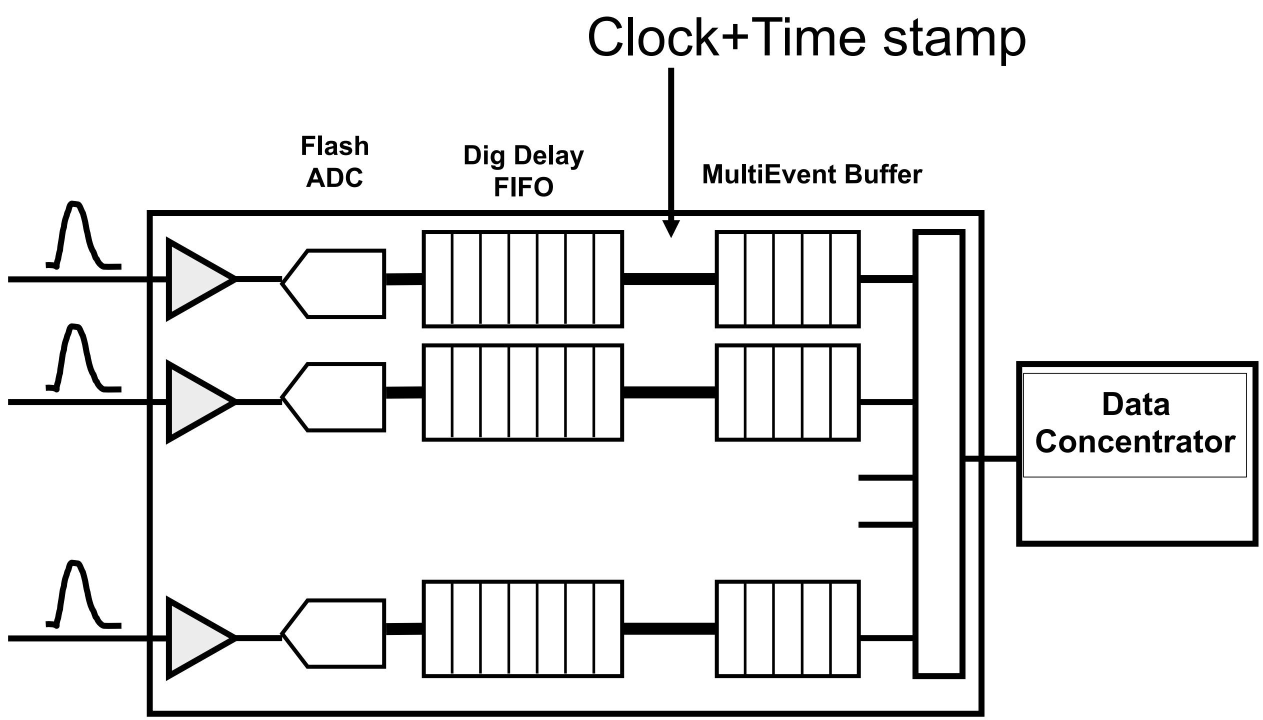

B. Ketzer

Future DAQ Architectures

Trigger-less DAQ: **PANDA, CBM, ILC**

- no electrical or optical trigger signal to FEE
- each channel detects signal ⇨ time stamps it ⇨ sends it out
- data are combined using time information
- definition of “event” only after full reconstruction!

⇨ complicated event selection criteria possible (e.g. displaced vertices)
⇨ wide physics cases – no common logic for trigger
⇨ software trigger algorithms: very flexible architecture
⇨ online data processing

Trigger/DAQ

The exponential evolution of electronics features has allowed the construction of particle detectors with >100 million channels that can measure particle interactions at 40MHz rate.

Only 1 in approx. 10^6 events can be written to tape at LHC.

The techniques to do this without losing information include pipelines (analog or digital) and de-randomizing buffers (FIFOs).

Interesting events are selected in several trigger levels using 'fast and easy' detector information.

Typical trigger signals are high pt events from the calorimeters and the muon systems.

Trigger and DAQ architectures are rapidly changing according to available electronics technology and computing power.

'Triggerless' time stamped readout systems using highly integrated frontends and massive switching networks and PC farms are proposed technologies for future experiments.